

**CHARACTERIZATION AND APPLICATION OF PEPTIDOGLYCAN *O*-
ACETYLTRANSFERASE B UTILIZING *N*-ACETYLCYSTEAMINE
DERIVATIVES**

by

Yiben Wang

A dissertation submitted to the Faculty of the University of Delaware in partial fulfillment of the requirements for the degree of Doctor of Philosophy in Chemistry & Biochemistry

Summer 2017

© 2017 Yiben Wang
All Rights Reserved

**CHARACTERIZATION AND APPLICATION OF PEPTIDOGLYCAN *O*-
ACETYLTRANSFERASE B UTILIZING *N*-ACETYLCYSTEAMINE
DERIVATIVES**

by

Yiben Wang

Approved: _____
Murray V. Johnston, Ph.D.
Chair of the Department of Chemistry & Biochemistry

Approved: _____
George H. Watson, Ph.D.
Dean of the College of Arts & Sciences

Approved: _____
Ann L. Ardis, Ph.D.
Senior Vice Provost for Graduate and Professional Education

I certify that I have read this dissertation and that in my opinion it meets the academic and professional standard required by the University as a dissertation for the degree of Doctor of Philosophy.

Signed:

Catherine Leimkuhler Grimes, Ph.D.
Professor in charge of dissertation

I certify that I have read this dissertation and that in my opinion it meets the academic and professional standard required by the University as a dissertation for the degree of Doctor of Philosophy.

Signed:

Joseph M. Fox, Ph.D.
Member of dissertation committee

I certify that I have read this dissertation and that in my opinion it meets the academic and professional standard required by the University as a dissertation for the degree of Doctor of Philosophy.

Signed:

Jennifer Gallo-Fox, Ph.D.
Member of dissertation committee

I certify that I have read this dissertation and that in my opinion it meets the academic and professional standard required by the University as a dissertation for the degree of Doctor of Philosophy.

Signed:

Xinqiao Jia, Ph.D.
Member of dissertation committee

I certify that I have read this dissertation and that in my opinion it meets the academic and professional standard required by the University as a dissertation for the degree of Doctor of Philosophy.

Signed:

Harold B. White, Ph.D.

Member of dissertation committee

ACKNOWLEDGMENTS

First and foremost, I would like to convey my sincerest thanks to my advisor, Dr. Catherine Leimkuhler Grimes. This dissertation would not have been possible without her continued guidance and support over the years. In addition to promoting my growth as a researcher, she has also cultivated my development as an educator. The confidence she has instilled in me has helped me to achieve my goal of joining the faculty rank.

I would also like to thank my committee members: Dr. Joseph M. Fox, Dr. Jennifer Gallo-Fox, Dr. Xinqiao Jia and Dr. Harold B. White, III for their advice throughout the progression of this dissertation. I also thank Dr. John T. Koh for introducing us to the short *N*-acetylcysteamine derivatives that was a vital part of this dissertation. Moreover, thanks to Dr. Brian Bahnson for all of the wisdom he has imparted to me. In addition, big thanks to the staff of the Department of Chemistry and Biochemistry: Eileen Burns, Linda Staib, Brenda Carboni, Jim Draper, John Famiglietti, Pat McMahon, Rick Bernard, Federico Cruz, Steve Bai, PapaNii Asare-Okai, Mark Schrader, Moiscell Robinson, Doug Nixon, Gary Lance and especially Susan Cheadle for all of their help.

Also, many thanks to all the past and present group members of the Grimes Lab. Vishnu, my co-champion in doubles racquetball, for his valuable insights, which has improved my problem solving skills. Sandy for her amazing friendship, inspiration and motivation that has pushed me to new limits. Mackenzie for her lifelong friendship, constructive feedback and enlightened conversation(s) that have helped me

evolve as a biochemist. Lauren for her awesome friendship, uplifting spirit and bubbly personality that always cheers me up. Klare and Kristen for their thoughtful inputs that helped expand the scope of this dissertation. Hai for his assistance with microscopy that helped elevate the project to a new level. Siavash for his illuminating life discussions that helped broaden my view of the world. Elizabeth for her willingness to be a team player and cheerful personality that help raise the energy of the group. Wally (the lucky one that gets to take over the best desk in the office when I leave) for his laid back attitude that brings calm to the group. Andrea for her role in taking over my group jobs which relieved me from maintaining the lyophilizer. Additional thanks to Jason, Jenna, Ashley, Matt and Ophelia for being an integral part of the Grimes lab. To all of my wonderful and dear friends: Beth, Hayden, Yegeun, Katie, Matt, Kasey, Jeff, Job, Laura, Tianhang, Kai and Shawn you have all enriched my life significantly. In particular, I want to thank my friend, Yehia, for his optimistic outlook on life and for introducing me to the love of my life, Joseph F. Brodie, Ph.D.

My family has been very supportive during my Ph.D. journey. Their constant encouragement has been much needed and appreciated over the years. Furthermore, special thanks to my brother, Yiwei, whose aid comes in the form of delicious home-cooked meals, which are a sight for sore eyes (and mouth) after a long day of work. Finally, my heartfelt gratitude to Joe, whose intelligence and passion has deeply influenced my work. In addition, Joe has been a pillar of strength since the day we met and I thank him for his unwavering support and encouragement throughout the dissertation process. We have gone on multiples adventures and shared so many precious memories of time spent together. I look forward to our future with bated breath.

TABLE OF CONTENTS

LIST OF TABLES	xii
LIST OF FIGURES	xiii
LIST OF ABBREVIATIONS	xxi
ABSTRACT	xxvi
Chapter	
1 INTRODUCTION	1
1.1 The Human Microbiome	1
1.2 Bacteria Sensing by the Immune System	3
1.3 Peptidoglycan	5
1.3.1 Bacterial Classification with Gram Staining	8
1.3.2 Peptidoglycan as a Labeling Target	10
1.3.3 Peptidoglycan as an Antibiotic Target	12
1.4 Bacterial Protection Strategies	13
1.5 Overview of Dissertation.....	17
REFERENCES	18
2 CHARACTERIZATION OF PEPTIDOGLYCAN O- ACETYLTRANSFERASE B (PatB)	29
2.1 Introduction	29
2.2 Materials and Methods	31
2.2.1 Materials and Instrumentation	31
2.2.2 Cloning of PatB Construct.....	32
2.2.3 Expression of PatB in <i>E. coli</i>	32
2.2.4 GST- and Nickel-Affinity Purification of PatB.....	33
2.2.5 Biochemical Characterization of PatB	33
2.2.5.1 SDS PAGE Analysis	33
2.2.5.2 Circular Dichroism	34
2.2.5.3 <i>p</i> -nitrophenyl acetate (<i>p</i> NP-Ac) Hydrolysis Assay	34

2.3	Results and Discussion	34
2.3.1	Expression and Purification of PatB.....	34
2.3.2	Biochemical Characterization of PatB	35
2.3.2.1	SDS PAGE Analysis	36
2.3.2.2	Circular Dichroism	37
2.3.2.3	<i>p</i> -nitrophenyl acetate (<i>p</i> NP-Ac) Hydrolysis Assay	38
2.4	Conclusions	40
	REFERENCES	41
3	EXPLORATION OF PatB'S DONOR PREFERENCE WITH <i>p</i> NP AND SNAC DERIVATIVES	43
3.1	Introduction	43
3.2	Materials and Methods	45
3.2.1	Materials and Instrumentation.....	45
3.2.2	Synthesis of <i>p</i> NP Derivatives.....	46
3.2.3	Synthesis of SNAc Derivatives	48
3.2.4	Analysis of Esterase Activity	51
3.2.4.1	<i>p</i> -nitrophenyl acetate (<i>p</i> NP-Ac) Hydrolysis Assay	51
3.2.4.2	Analysis of Hydrolysis Activity with Ellman's Reagent.....	51
3.3	Results and Discussion	52
3.3.1	Synthesis of <i>p</i> NP Derivatives.....	52
3.3.2	Synthesis of SNAc Derivatives	52
3.3.3	Analysis of Esterase Activity	52
3.3.3.1	<i>p</i> -nitrophenyl acetate (<i>p</i> NP-Ac) Hydrolysis Assay	53
3.3.3.2	Analysis of Hydrolysis Activity with Ellman's Reagent.....	54
3.4	Conclusions	55
	REFERENCES	57
4	EXPLORATION OF PatB'S ACCEPTOR SPECIFICITY	60
4.1	Introduction	60

4.2	Materials and Methods	62
4.2.1	Materials and Instrumentation.....	62
4.2.2	Analysis of PatB's Ability to Modify Mono- and Tri-saccharides.....	62
4.2.3	Analysis of Acetyltransferase Activity.....	63
4.2.3.1	<i>p</i> -nitrophenyl acetate (<i>p</i> NP-Ac) Transferase Assay	63
4.2.3.2	Analysis of Transferase Activity with Ellman's Reagent	63
4.2.4	Peptidoglycan, the Natural Acceptor.....	64
4.2.4.1	Isolation of Peptidoglycan.....	64
4.2.4.2	Confirmation of Peptidoglycan	66
4.2.4.2.1	Peptidoglycan Pull-Down Assay	66
4.2.4.2.2	Analysis of Peptidoglycan Fragments with MS	66
4.2.4.2.3	Nuclear Factor kappa-light-chain-enhancer of activated B cells (NF-κB) Activation Assay	66
4.2.4.2.4	Fluorescence-Assisted Carbohydrate Electrophoresis (FACE) Analysis	67
4.3	Results and Discussion	67
4.3.1	Analysis of PatB's Ability to Modify Mono- and Tri-saccharides.....	67
4.3.2	Analysis of Acetyltransferase Activity.....	70
4.3.2.1	<i>p</i> -nitrophenyl acetate (<i>p</i> NP-Ac) Transferase Assay	71
4.3.2.2	Analysis of Transferase Activity with Ellman's Reagent	72
4.3.3	Peptidoglycan, the Natural Acceptor.....	73
4.3.3.1	Isolation of Peptidoglycan.....	73
4.3.3.2	Confirmation of Peptidoglycan	74
4.3.3.2.1	Peptidoglycan Pull-Down Assay	75
4.3.3.2.2	Analysis of Peptidoglycan Fragments with MS	76

4.3.3.2.3	Nuclear Factor kappa-light-chain- enhancer of activated B cells (NF-κB) Activation Assay	77
4.3.3.2.4	Fluorescence-Assisted Carbohydrate Electrophoresis (FACE) Analysis	80
4.4	Conclusions	82
REFERENCES		84
5	<i>IN VITRO</i> AND <i>IN VIVO</i> APPLICATIONS OF PATB	86
5.1	Introduction	86
5.2	Materials and Methods	88
5.2.1	Materials and Instrumentation	88
5.2.2	Peptidoglycan Degradation Assay (<i>in vitro</i>)	88
5.2.3	Bacterial Cell Labeling (<i>in vivo</i>)	88
5.3	Results and Discussion	90
5.3.1	Peptidoglycan Degradation Assay (<i>in vitro</i>)	90
5.3.2	Bacterial Cell Labeling (<i>in vivo</i>)	94
5.4	Conclusions	103
REFERENCES		104
6	CONCLUSIONS AND FUTURE DIRECTIONS	108
6.1	Conclusions	108
6.1.1	Purification and Characterization of PatB Expression from an <i>E. coli</i> System	108
6.1.2	Donor and Acceptor Promiscuity of PatB	108
6.1.3	Applications of the PatB/SNAc System	109
6.2	Future Directions	109
6.2.1	Crystallization of PatB	109
6.2.2	Labeling of <i>B. subtilis</i> Spores	110
6.2.3	Direct Fluorophore Attachment	111
6.2.4	Bacteria and Peptidoglycan as Educational Tools	115
REFERENCES		120

Appendix

A	SPECTROSCOPIC DATA	122
A.1	NMR	122
A.1.1	NMR of <i>p</i> NP Derivatives	122
A.1.2	NMR of SNAc Derivatives	128
A.2	HRMS	134
A.2.1	HRMS of <i>p</i> NP Derivatives	134
A.2.2	HRMS of SNAc Derivatives	137
A.3	IR	140

LIST OF TABLES

Table 1.1: Overview of the ligands for TLRs and NLRs.	4
Table 3.1: Esterase activity of PatB (1 μ M) with <i>p</i> NP donors at pH 6.5 (sodium phosphate buffer) as monitored at 405 nm.	54
Table 3.2: Esterase activity of PatB (1 μ M) with acetyl-CoA and SNAc donors at pH 6.5 (sodium phosphate buffer) and pH 8.5 (tris buffer) as monitored at 412 nm.	55
Table 4.1: No detection of modified products was observed by high-resolution mass spectrometry when PatB was incubated with <i>p</i> NP-Ac and SNAc donors with monosaccharides (Glc, GlcN, NAG and NAM) and trisaccharide (GlcN) ₃	68
Table 4.2: Detection of modified (NAG) ₃ products using PatB with <i>p</i> NP and SNAc donors by high-resolution mass spectrometry.	69
Table 4.3: Acetyltransferase activity of PatB (1 μ M) with <i>p</i> NP donors and 1 mM (NAG) ₃ at pH 6.5 (sodium phosphate buffer) as monitored at 405 nm. .	71
Table 4.4: Acetyltransferase activity of PatB (1 μ M) with acetyl-CoA and SNAc donors and 1 mM (NAG) ₃ at pH 6.5 (sodium phosphate buffer) and pH 8.5 (tris buffer) as monitored at 412 nm.	73
Table 6.1: A selection of biochemical topics, concepts and techniques that students encounter in the articles they read for Chem342 Beer, Bugs & Drugs.	117

LIST OF FIGURES

- Figure 1.1: The various species of bacteria found at the different regions of the human body. (Image credit: Darryl Leja, National Human Genome Research Institute (NHGRI))..... 2
- Figure 1.2: A molecular view of the bacterial peptidoglycan composition. Structural differences between most Gram (+) and Gram (-) bacterial species are highlighted. Also shown are MDP (red) and iE-DAP (blue), ligands for Nod2 and Nod1, respectively. 6
- Figure 1.3: The peptidoglycan biosynthetic pathway. MurA and MurB convert UDP-NAG into UDP-NAM. MurC, MurD, MurE, and MurF add the pentapeptide chain. MraY attaches the precursor to the membrane via undecaprenyl pyrophosphate. MurG converts Lipid I to Lipid II by adding NAG. FemX, Fem A, and FemB synthesize the poly-glycine linkage. The molecule is then flipped from the cytoplasm to the periplasm by FtsW, where it is cross linked onto existing peptidoglycan through transglycosylases and transpeptidases. Figure reproduced from Veening et al. (2013).⁴⁰ 7
- Figure 1.4: Gram (-) bacteria have a thin layer of peptidoglycan that is sandwiched between the outer and inner membranes (A). Gram (+) bacteria have a thick layer of peptidoglycan on the exterior of the bacterial cell (B). The difference in peptidoglycan abundance and accessibility is the driving principle behind the Gram staining method. Figure adapted from Casadevall et al. (2015).⁵⁰ 8
- Figure 1.5: Diagram depicting the physical appearance of a mixed population of bacterial cells after each step (crystal violet addition (A), iodine treatment (B), alcohol wash (C), and safranin stain (D)) of the Gram staining method. Gram (+) cells (oval) are stained purple while Gram (-) cells (circle) are stained pink..... 9
- Figure 1.6: Review of select peptidoglycan labeling strategies found in literature. Three main strategies have been employed to label the peptidoglycan: the incorporation of unnatural amino acids (B-F), the use of fluorescent antibiotics (G), and the integration of unnatural sugar derivatives (A,H). A⁶¹ B⁵³ C⁵⁶ D⁵⁷ E⁵⁴ F⁵⁵ G^{58,59} H⁶⁰ 11

Figure 1.7: The class of β -lactam antibiotics such as penicillin is structurally similar to that of D-Ala-D-Ala, which allows them to bind to PBPs and inhibit their activity (top). Vancomycin binds directly to D-Ala-D-Ala, blocking the dipeptide from binding to PBPs. Vancomycin resistant bacteria have altered the dipeptide from D-Ala-D-Ala to D-Ala-D-Lac to disrupt the hydrogen bonding necessary for vancomycin's activity (bottom).	13
Figure 1.8: Post-synthetic modifications of the peptidoglycan such as <i>N</i> -deacetylation and <i>O</i> -acetylation prevent degradation by lytic enzymes, which usually results in the formation of a 1,6-anhydro ring. R: peptide chain.....	14
Figure 1.9: Comparison of the Oat proteins found in Gram (+) bacteria and the Pat proteins found in Gram (-) bacteria that is responsible for the <i>O</i> -acetylation of the peptidoglycan.....	16
Figure 2.1: A) An acetyl functional group (red) is translocated across the plasmic membrane by PatA, where it is subsequently transferred onto the sixth hydroxyl position of NAM by PatB. B) Unnatural SNAc donors are employed to install bioorthogonal functional groups (blue) onto the peptidoglycan through PatB.	30
Figure 2.2: Overview of the purification scheme. The dual-tagged PatB, present in the cell lysate is incubated with GST resin. Any non-specific proteins are washed off the column prior to the addition of PreScission Protease to the column. The PreScission Protease itself is tagged with GST, but it does not have a self-cleavage site in its sequence. After over-night incubation, the PreScission Protease will cleave the GST tag off of PatB. Free GST tag and PreScission Protease are left on the column while PatB is eluted. The resulting protein is further purified by incubation with a Nickel column that will bind to the His ₆ tag on PatB and allow any remaining purities to be washed away. PatB is eluted from the Nickel column with an imidazole buffer. The His ₆ tag is not cleaved from PatB.	35
Figure 2.3: SDS page gel of purified PatB (37 kDa). The purity of PatB increases from left to right. Post cell lysis (Pre GST), there are numerous protein bands present on the gel. After PatB was applied to a GST resin column (Post GST), the number of bands was reduced to a handful. Following further purification on a Ni column (Post Ni), the main band present is PatB with a couple of very faint bands. Upon concentration, PatB is the major band present and the other bands are still very faint.....	37

Figure 2.4: Experimental (blue) and theoretical (red) CD spectra of PatB. The two minimal points at 210 and 225 nm suggests that there are α -helices present in PatBs structure.	38
Figure 2.5: The release of <i>p</i> NP from <i>p</i> NP-Ac is used to monitor the rate of esterase (in the absence of an acceptor) or acetyltransferase (in the presence of an acceptor) activity of PatB (1 μ M).	39
Figure 2.6: Release of <i>p</i> NP from <i>p</i> NP-Ac over time in the presence (blue) and absence (red) of PatB (1 μ M). The slope of the blue line (0.0047) is ~2.5x higher than that of the red line (0.0019).	39
Figure 3.1: Two set of donors were synthesized to probe for PatB's donor specificity. The first set of donors retained the <i>p</i> NP moiety (top row) and the second set of donors were short <i>N</i> -acetyl cysteamine derivatives (bottom row) that resemble the natural substrate, acetyl-CoA (middle).	45
Figure 3.2: Determining the esterase activity of PatB with SNAc donors by measuring the production rate of TNB at 412 nm.	53
Figure 4.1: To assess PatB's acceptor specificity, various monosaccharide and trisaccharide acceptors were tested with PatB and <i>p</i> NP and SNAc donors.	61
Figure 4.2: A) HRMS spectrum of Alexa Fluor 488 labeled (NAG) ₃ via CUAAC. Exact mass of product: 1281.49249 Observed mass [M+H ⁺]: 1282.49741. B) HRMS/MS spectrum of the fragmentation pattern of the click product showing the loss of one and two NAG molecules from the trisaccharide product. Loss of a NAG: exact mass: 1078.41312 Observed mass [M+H ⁺]: 1079.41493. Loss of two NAG molecules: exact mass: 875.33375 Observed mass [M+H ⁺]: 876.33604.	70
Figure 4.3: Peptidoglycan was isolated from various Gram (+) (<i>B. subtilis</i>) and Gram (-) (<i>E. coli</i> , <i>V. parahaemolyticus</i> , and <i>P. putida</i>) bacterial species following literature precedence with modifications. ³	74
Figure 4.4: Prior to incubation with insoluble peptidoglycan (pellet), Nod2 was only found in the supernatant. Post incubation, Nod2 is observed in both lanes indicating that insoluble peptidoglycan was able to pull down Nod2. This binding was shown to be pH dependent as the pull down ability is lost at pH 8.5.	76

Figure 4.5: The structure of two proposed fragments of the peptidoglycan that corresponds with the two masses detected post lysozyme digestion via HRMS. M4: NAM with a tetrapeptide stem. G-M4: NAG-NAM with a tetrapeptide stem.	77
Figure 4.6: Upon binding of MDP or other peptidoglycan fragments to Nod2, the NF- κ B signaling pathway is activated. The NF- κ B transcription factor translocates from the cytoplasm to the nucleus. When the NF- κ B transcription factor binds to the promoter region of the DNA, it turns on the luciferase gene, which is placed downstream of the promoter. The activation level is quantified by measuring the production of luciferin.	78
Figure 4.7: The supernatant of lysozyme digested peptidoglycan is able to activate the NF- κ B pathway. CMV: control no Nod2. Nod2: over-expresses Nod2. Data is not statistically significant as the experiments were done in duplicates. However, the goal was to employ the NF- κ B assay as a qualitative method to verify peptidoglycan.	80
Figure 4.8: Scheme of carbohydrate labeling via reductive amination with ANDA. ..	81
Figure 4.9: Fluorescent detection of ANDA labeled peptidoglycan fragments (Pep) on a carbohydrate gel along with a homemade starch ladder (Starch) and reference controls (NAG, Mal (maltose), Glc, and Com (combined sample containing NAG, Mal and Glc)).	82
Figure 5.1: Unmodified peptidoglycan is susceptible to lysozyme degradation (top), forming a 1,6-anhydro-NAM product. However if the peptidoglycan is modified by PatB prior to lysozyme treatment, then the peptidoglycan is protected against lysozyme degradation.	87
Figure 5.2: PatB-modified PG, with <i>p</i> NP-Ac, from <i>B. subtilis</i> Δ Oat (green) was protected against lysozyme degradation as compared to no modification (blue) and no lysozyme control (red). Values plotted are average of three independent experiments as the mean+S.D.	91
Figure 5.3: PatB-modified PG, with 6 (purple), 7 (black) or 8 (orange), from <i>B. subtilis</i> Δ Oat was protected against lysozyme degradation. Unmodified peptidoglycan (green). Blank (blue). Peptidoglycan without lysozyme (red). Values plotted are average of three independent experiments as the mean+S.D.	91

Figure 5.4: PatB-modified PG, with 6 (purple), 7 (black) or 8 (orange), from <i>E. coli</i> was protected against lysozyme degradation. Unmodified peptidoglycan (green). Blank (blue). Peptidoglycan without lysozyme (red). Values plotted are average of three independent experiments as the mean+S.D.	92
Figure 5.5: PatB-modified PG, with 6 (purple), 7 (black) or 8 (orange), from <i>P. putida</i> was protected against lysozyme degradation. Unmodified peptidoglycan (green). Blank (blue). Peptidoglycan without lysozyme (red). Values plotted are average of three independent experiments as the mean+S.D.	93
Figure 5.6: PatB-modified PG, with 6 (purple), 7 (black) or 8 (orange), from <i>V. parahaemolyticus</i> was protected against lysozyme degradation. Unmodified peptidoglycan (green). Blank (blue). Peptidoglycan without lysozyme (red). Values plotted are average of three independent experiments as the mean+S.D.	93
Figure 5.7: SIM and corresponding DIC images of Alexa-Fluor 488 labeled <i>B. subtilis</i> Δ Oat cells post modification by PatB and SNAk, PatB and SNAc, or SNAk alone at the various time points indicated. Scale bar denotes 10 μ m.	95
Figure 5.8: SIM and corresponding DIC images of Alexa-Fluor 488 labeled <i>B. subtilis</i> WT cells post modification by PatB and SNAk, PatB and SNAc, or SNAk alone at the various time points indicated. Scale bar denotes 10 μ m.	96
Figure 5.9: Large field SIM and corresponding DIC images of Figure 5.11. Red arrows indicate the cells that are shown in Figure 5.11. Scale bar denotes 10 μ m.	98
Figure 5.10: Large field SIM and corresponding DIC images of Figure 5.12. Red arrows indicate the cells that are shown in Figure 5.12. Scale bar denotes 10 μ m.	99
Figure 5.11: SIM and corresponding DIC images of <i>B. subtilis</i> Δ Oat cells labeled with Alexa-Fluor 488 (top row) post modification by PatB and SNAc-Ak, PatB and SNAc, or SNAc-Ak alone for 240 min. The cell wall was also stained with a tetramethylrhodamine WGA conjugate (second row) to show colocalization of the fluorophores (third row). Images are representative of three biological replicates. Scale bar denotes 2 μ m.	101

Figure 5.12: SIM and corresponding DIC images of <i>B. subtilis</i> WT cells labeled with Alexa-Fluor 488 (top row) post modification by PatB and SNAc-Ak, PatB and SNAc, or SNAc-Ak alone for 240 min. The cell wall was also stained with a tetramethylrhodamine WGA conjugate (second row) to show colocalization of the fluorophores (third row). Images are representative of three biological replicates. Scale bar denotes 2 μm	102
Figure 6.1: Small crystals were observed during initial crystal screening conditions. However further optimizations are required to obtain a crystal suitable for X-ray diffraction. Due to instrumentation errors, no error bar is shown.....	110
Figure 6.2: A) <i>B. subtilis</i> spores were labeled with Alexa Fluor 488 after being modified by PatB with SNAk in PBS buffer. B) <i>B. subtilis</i> spores labeled with MalF-GFP and FM-4-64. Figure (part B) adapted from Rubio and Pogliano (2004). ⁷	111
Figure 6.3: SNAc-Bodipy was synthesized and installed onto (NAG) ₃ by PatB.	112
Figure 6.4: SIM and corresponding DIC images of <i>B. subtilis</i> ΔOat cells labeled with SNAc-Bodipy by PatB for 240mins (first row). The cell wall was also stained with a tetramethylrhodamine WGA conjugate (second row) to show colocalization of the fluorophores (third row). Images are representative of three biological replicates.	113
Figure 6.5: SIM and corresponding DIC images of <i>B. subtilis</i> WT cells labeled with SNAc-Bodipy by PatB for 240mins (first row). The cell wall was also stained with a tetramethylrhodamine WGA conjugate (second row) to show colocalization of the fluorophores (third row). Images are representative of three biological replicates.	114
Figure 6.6: Timeline of the ten primary literature articles that students in Chem342 Beer, Bugs & Drugs, will examine over the course of the semester.	115
Figure 6.7: Comparison of bacterial growth on a traditional LB-agar plate (left) and an alternative plate made with gelatin and chicken bouillon (right).	119
Figure A.1: ¹ H NMR Spectra (CDCl ₃) of <i>p</i> NP-Ak Compound (2). ¹ H NMR (400 MHz, Chloroform- <i>d</i>) δ 8.31 (d, 2H, benzyl), 7.36 (d, 2H, benzyl), 1.55 (s, 1H, CCH).....	122

Figure A.2: ^{13}C NMR Spectra (CDCl_3) of <i>p</i> NP-Ak Compound (2). ^{13}C NMR (151 MHz, Chloroform- <i>d</i>) δ 154.38, 149.81, 145.93, 125.53, 122.38, 78.26, 73.64.....	123
Figure A.3: ^1H NMR Spectra (CDCl_3) of <i>p</i> NP-Az Compound (3). ^1H NMR (400 MHz, Chloroform- <i>d</i>) δ 8.31 (d, 2H, benzyl), 7.36 (d, 2H, benzyl), 4.20 (s, 2H, CH_2N_3).....	124
Figure A.4: ^{13}C NMR Spectra (CDCl_3) of <i>p</i> NP-Az Compound (3). ^{13}C NMR (151 MHz, Chloroform- <i>d</i>) δ 166.17, 154.66, 145.88, 125.52, 122.28, 50.55.....	125
Figure A.5: ^1H NMR Spectra (CDCl_3) of <i>p</i> NP-Bn Compound (4). ^1H NMR (400 MHz, Chloroform- <i>d</i>) δ 8.35 (d, 2H, benzyl), 8.21 (d, 2H, benzyl), 7.68 (t, 1H, benzyl), 7.55 (t, 2H, benzyl), 7.43 (d, 2H, benzyl).	126
Figure A.6: ^{13}C NMR Spectra (CDCl_3) of <i>p</i> NP-Bn Compound (4). ^{13}C NMR (151 MHz, Chloroform- <i>d</i>) δ 164.37, 155.84, 145.51, 134.40, 130.46, 128.93, 128.62, 125.42, 122.79.	127
Figure A.7: ^1H NMR Spectra (CDCl_3) of SNAc Compound (6). ^1H NMR (600 MHz, Chloroform- <i>d</i>) δ 6.02 (s, 1H, NH), 3.43 (q, $J = 6.3$ Hz, 2H, CH_2NH), 3.03 (t, $J = 6.5$ Hz, 2H, CH_2S), 2.36 (s, 3H, acetyl), 1.97 (s, 3H, acetyl).	128
Figure A.8: ^{13}C NMR Spectra (CDCl_3) of SNAc Compound (6). ^{13}C NMR (151 MHz, Chloroform- <i>d</i>) δ 196.37, 170.30, 39.68, 30.72, 29.03, 23.28.	129
Figure A.9: ^1H NMR Spectra (MeOD) of SNAz Compound (7). ^1H NMR (400 MHz, Methanol- <i>d</i> 4) δ 4.15 (s, 2H, CH_2N_3), 3.37 (t, $J = 6.6$ Hz, 2H, $\text{HNCH}_2\text{CH}_2\text{S}$), 3.09 (t, $J = 6.6$ Hz, 2H, $\text{HNCH}_2\text{CH}_2\text{S}$), 1.93 (s, 3H, acetyl).	130
Figure A.10: ^{13}C NMR Spectra (CDCl_3) of SNAz Compound (7). ^{13}C NMR (101 MHz, Methanol- <i>d</i> 4) δ 195.55, 172.12, 57.45, 38.41, 27.72, 21.06.	131
Figure A.11: ^1H NMR Spectra (CDCl_3) of SNAk Compound (8). ^1H NMR (600 MHz, Chloroform- <i>d</i>) δ 5.81 (s, 1H, NH), 3.44 (q, $J = 6.1$ Hz, 2H, $\text{HNCH}_2\text{CH}_2\text{S}$), 3.06 (t, $J = 6.4$ Hz, 2H, $\text{HNCH}_2\text{CH}_2\text{S}$), 2.81 (t, $J = 7.2$ Hz, 2H, $\text{CH}_2\text{CH}_2\text{CCH}$), 2.54 (td, $J = 7.2, 2.6$ Hz, 2H, $\text{CH}_2\text{CH}_2\text{CCH}$), 1.99 (t, $J = 2.6$ Hz, 1H, $\text{CH}_2\text{CH}_2\text{CCH}$), 1.96 (s, 3H, acetyl).	132
Figure A.12: ^{13}C NMR Spectra (CDCl_3) of SNAk Compound (8). ^{13}C NMR (151 MHz, Chloroform- <i>d</i>) δ 198.01, 170.39, 81.90, 69.66, 42.55, 39.71, 28.80, 23.37, 14.83.	133

- Figure A.13: HRMS Spectra of *p*NP-Ak Compound (**2**). HRMS (ESI-pos) for $C_9H_6NO_4^+$ $[M+H]^+$: calculated 192.02913, observed 192.02921..... 134
- Figure A.14: HRMS Spectra of *p*NP-Az Compound (**3**). HRMS (ESI-pos) for $C_8H_7N_4O_4^+$ $[M+H]^+$: calculated 223.04618, observed 223.04630. 135
- Figure A.15: HRMS Spectra of *p*NP-Bn Compound (**4**). HRMS (ESI-pos) for $C_{13}H_{10}NO_4^+$ $[M+H]^+$: calculated 244.06043, observed 244.06064. 136
- Figure A.16: HRMS of SNAc Compound (**6**). HRMS (ESI-pos) for $C_6H_{12}NO_2S^+$ $[M+H]^+$: calculated 162.05833, observed 162.05845. 137
- Figure A.17: HRMS Spectra of SNAz Compound (**7**). HRMS (ESI-pos) for $C_6H_{11}N_4O_2S^+$ $[M+H]^+$: calculated 203.05972, observed 203.05939..... 138
- Figure A.18: HRMS Spectra of SNAk Compound (**8**). HRMS (ESI-pos) for $C_9H_{14}NO_2S^+$ $[M+H]^+$: calculated 200.07398, observed 200.07380. 139
- Figure A.19: IR Spectra of *p*NP-Az Compound (**3**). IR shift: 2105.73cm^{-1} (Azide).. 140
- Figure A.20: IR Spectra of SNAz Compound (**7**). IR shift: 2099.29cm^{-1} (Azide). 140

LIST OF ABBREVIATIONS

Ala: alanine

ANDA: 7-amino-1,3-naphthalenedisulfonic acid

ATCC: American Type Culture Collection

CD: Circular Dichroism

CMV: cytomegalovirus

CuAAC: copper catalyzed azide alkyne cycloaddition

CuSO₄: copper (II) sulfate

DCC: N,N'-dicyclohexylcarbodiimide

DCM: dichloromethane

DIC: differential interference contrast microscopy

DMAP: 4-dimethylaminopyridine

DMSO: dimethyl sulfoxide

DNA: deoxyribonucleic acid

DTNB: 5,5-dithio-bis-(2-nitrobenzoic) acid

DTT: dithiothreitol

EDTA: ethylenediaminetetraacetic acid

ESI: electrospray ionization

EtOAc: ethyl acetate

FACE: fluorescence-assisted carbohydrate electrophoresis

FemA: aminoacyltransferase A

FemB: aminoacyltransferase B

FemX: UDP-*N*-acetylmuramylpentapeptide-lysine-*N*-(6)-alanyltransferase

FM-4-64: *N*-(3-Triethylammoniumpropyl)-4-(6-(4-(Diethylamino) Phenyl) Hexatrienyl) Pyridinium Dibromide

FtsW: peptidoglycan glycosyltransferase

GFP: green fluorescent protein

Glc: glucose

GlcN: glucosamine

(GlcN)₃: tri-glucosamine

GST: glutathione S-transferase

HCl: hydrochloric acid

His: histidine

HMP: Human Microbiome Project

HPLC: high-performance liquid chromatography

HRLC/MS: high-resolution liquid chromatography mass spectrometry

HRMS: high-resolution mass spectrometry

iE-DAP: γ -D-glutamyl-meso-diaminopimelic acid

IPTG: isopropyl β -D-1-thiogalactopyranoside

IR: infrared spectroscopy

KOH: potassium hydroxide

Lac: lactate

LB: Lysogeny broth

LPG: lysylphosphatidylglycerol

LPS: lipopolysaccharide

Lys: lysine

Mal: maltose

MalF: maltose transport system permease protein

MAMPs: microbe-associated molecular patterns

MDP: muramyl dipeptide

MeOH: methanol

meso-A₂pm: *meso*-diaminopimelic acid

MraY: phosphor-*N*-acetylmuramyl-pentapeptide transferase

MS: mass spectrometry

MurA: UDP-*N*-acetylglucosamine enolpyruvyl transferase

MurB: UDP-*N*-acetylenolpyruvoylglucosamine reductase

MurC: UDP-*N*-acetylmuramic acid-*L*-alanine ligase

MurD: UDP-*N*-acetylmuramylalanine-*D*-glutamate ligase

MurE: UDP-*N*-acetylmuramyl-*L*-alanyl-*D*-glutamate-2,6-diaminopimelate ligase

MurF: UDP-*N*-acetylmuramyl-tripeptide-*D*-alanyl-*D*-alanine ligase

MurG: UDP-*N*-acetylglucosamine-*N*-acetylmuramyl-(pentapeptide)
pyrophosphoryl-undecaprenol *N*-acetylglucosamine transferase

MWCO: molecular weight cut off

NaCNBH₃: sodium cyanoborohydride

NAG: *N*-acetylglucosamine

(NAG)₃/(GlcNAc)₃: tri-*N*-acetylglucosamine

NAM: *N*-acetylmuramic acid

NF- κ B: Nuclear Factor kappa-light-chain-enhancer of activated B cells

NHGRI: National Human Genome Research Institute

NIH: National Institute of Health

NLR: Nod-like receptors

NMR: nuclear magnetic resonance spectroscopy

Nod1: nucleotide-binding and oligomerization domain-containing 1

Nod2: nucleotide-binding and oligomerization domain-containing 2

OatA: *O*-acetyltransferase A

OatB: *O*-acetyltransferase B

OD: optical density

PatA: peptidoglycan *O*-acetyltransferase A

PatB: peptidoglycan *O*-acetyltransferase B

PBL: Problem-Based Learning

PBPs: penicillin-binding proteins

PBS: phosphate-buffered saline

PCR: polymerase chain reaction

PdaA: peptidoglycan *N*-acetylmuramic acid deacetylase A

PG: peptidoglycan

PgdA: peptidoglycan *N*-acetylglucosamine deacetylase A

*p*NP: *p*-nitrophenol

*p*NP-Ac: *p*-nitrophenyl acetate

*p*NP-Ak: *p*-nitrophenyl alkyne; 4-nitrophenyl propiolate

*p*NP-Az: *p*-nitrophenyl azide; 4-nitrophenyl 2-azidoacetate

*p*NP-Bn: *p*-nitrophenyl benzoyl; 4-nitrophenyl benzoate

POGIL: Process Oriented Guided Inquiry Learning

RNA: ribonucleic acid

rRNA: ribosomal RNA

S.D.: standard deviation

SDS: sodium dodecyl sulfate

SEEK: STEM Early Education Kinship

SIM: structured illumination microscopy

SNAc: short *N*-acetylcysteamine; *S*-(2-acetamidoethyl) ethanethioate

SNAk: *S*-(2-(pent-4-ynamido)ethyl ethanethioate

SNAz: *S*-(2-(2-azidoacetamido)ethyl ethanethioate

SUMO: small ubiquitin-like modifier

TBTA: tris[(1-benzyl-1*H*-1,2,3-triazol-4-yl)methyl]amine

TLC: thin-layer chromatography

TLR: Toll-like receptors

TNB: 2-nitro-5-thiobenzoate

UDP: uridine diphosphate

WGA: wheat germ agglutinin

WT: wild type

WTA: wall teichoic acids

ABSTRACT

Bacteria have the natural ability to install protective post-synthetic modifications onto its bacterial peptidoglycan (PG); the coat that is woven into bacterial cell wall. Peptidoglycan *O*-acetyltransferase B (PatB) catalyzes the *O*-acetylation of peptidoglycan in Gram (–) bacteria, which aids in bacterial survival, as it prevents autolysins such as lysozyme from cleaving the peptidoglycan at the β -1,4-glycosidic bond between *N*-acetylmuramic acid (NAM) and *N*-acetylglucosamine (NAG). In this dissertation, the substrate promiscuity and mechanistic details of PatB's acetylation function was explored and it was determined that PatB has substrate tolerance for bioorthogonal short *N*-acetylcysteamine (SNAc) donors. Exploiting this lax specificity, a variety of functionality including azides and alkynes were installed on tri-*N*-acetylglucosamine (NAG)₃, a peptidoglycan mimic, as well as peptidoglycan isolated from various Gram (+) (*Bacillus subtilis*) and Gram (–) (*Escherichia coli*, *Vibrio parahaemolyticus*, and *Pseudomonas putida*) bacterial species. The bioorthogonal modifications were shown to protect the isolated peptidoglycan against lysozyme degradation *in vitro*. We further demonstrate that this post-synthetic modification of peptidoglycan can be extended to use click chemistry to fluorescently label the carbohydrate backbone of mature peptidoglycan in whole bacterial cells of *Bacillus subtilis*. Modifying peptidoglycan post-synthetically can aid in the development of antibiotics and immune modulators by expanding on the current understanding of how the bacterial peptidoglycan is processed by lytic enzymes presented in the innate immune system.

Chapter 1

INTRODUCTION

1.1 The Human Microbiome

Over the past decade, the interest in the human microbiome has exploded. This relates to the collection of microorganisms that live in/on the human body. In 2008, the National Institute of Health (NIH) launched the Human Microbiome Project (HMP) with the specific aims of elucidating the composition of the human microbiome and defining the relationship between the human microbiome and diseases.^{1,2,3} The program gathered data regarding the various types of microbes present on five different parts of the body (mouth, nose, gut, urogenital tract, and skin) using 16S ribosomal RNA (rRNA) sequencing (Figure 1.1). The results indicate that there are more than 10,000 microbial species in a healthy microbiome from various domains (archaea, bacteria, eukaryotes, and viruses).⁴ Many of the organisms remained uncharacterized, but it was concluded that bacteria constitutes an overwhelming majority of the microbes of the human microbiome.⁵

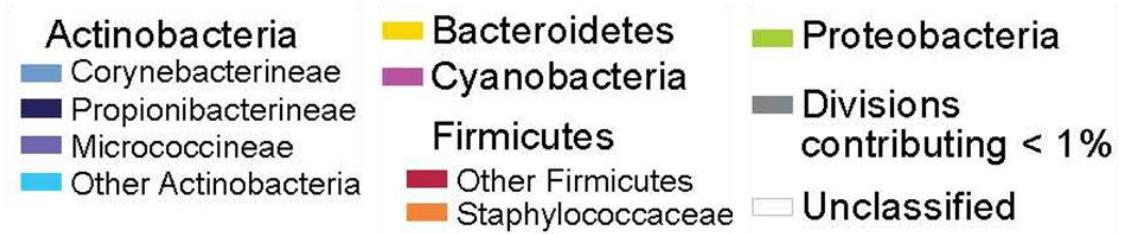
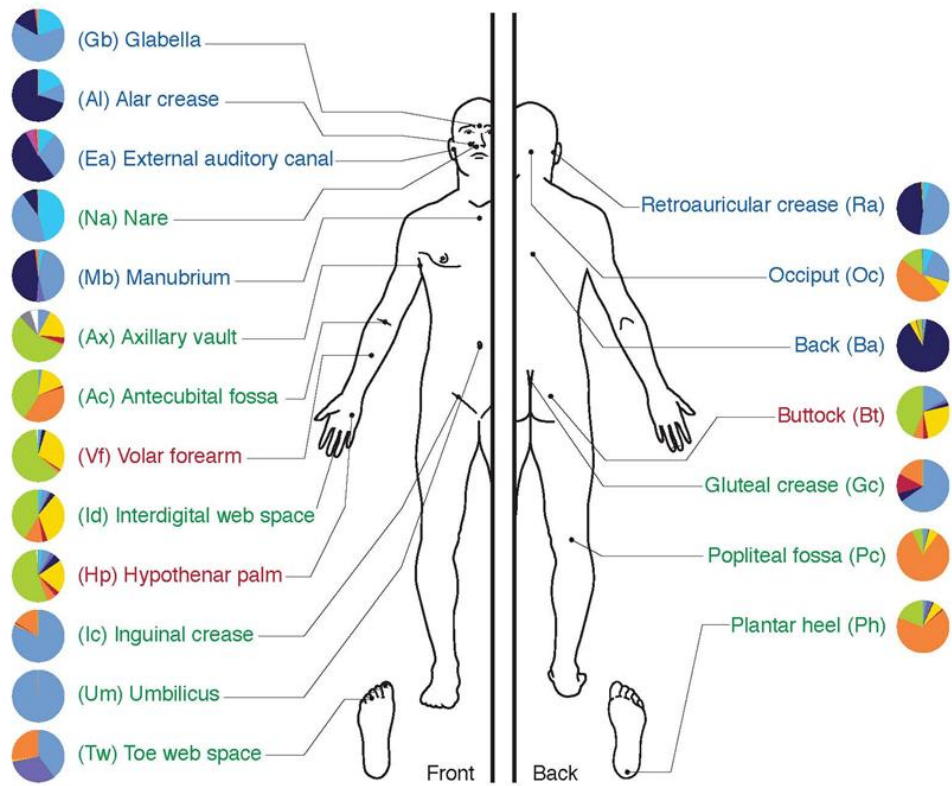


Figure 1.1: The various species of bacteria found at the different regions of the human body. (Image credit: Darryl Leja, National Human Genome Research Institute (NHGRI))

It is currently estimated that there are as many bacterial cells as human cells.⁶ However given the smaller size of bacterial cells, the number of bacterial genes (~3.3 million) far outnumbers the number of human genes (~22,000).⁷ It is known that some of the bacteria are commensal by helping to synthesize vitamins and aiding with

digestion.⁸ However, there are pathogenic bacteria present in the microbiome as well, and an unbalanced regulation of commensal and pathogenic bacteria can lead to diseases such as obesity, mental illness, and chronic inflammation.^{9,10,11} Therefore it is of critical importance to understand the intricate dynamics of the bacterial composition and the resulting impact on our body.

1.2 Bacteria Sensing by the Immune System

The amount of bacteria (~30-50 trillion) living on and in the human body at any given moment is simply astonishing. So how does our body sense and respond to these passengers? In 1996, Hoffman and coworkers identified a type of receptors called Toll-like receptors (TLRs) and showed that *Drosophila* are able to sense fungal infections using TLRs.¹² A couple of years later, Beutler and coworkers demonstrated that TLR4 specificity was capable of sensing the presence of bacterial lipopolysaccharide (LPS).¹³ For their work, Hoffman and Beutler won the Nobel Prize for physiology or medicine along with Steinman in 2011. However it is worth to note that prior to Beutler's paper on TLR4 in 1998, Charles Janeway had laid the groundwork that linked TLR 4 to immunity back in 1989. Sadly, Janeway passed away in 2003 and was not eligible for the 2011 Nobel Prize. Since then other types of receptors such as the Nod-like receptors (NLRs) have been discovered.¹⁴ TLRs are usually found on cell surfaces while NLRs are cytosolic. With the help of both TLRs and NLRs, the innate immune system is able to recognize conserved microbe-associated molecular patterns (MAMPs) (Table 1.1).¹⁵

Table 1.1: Overview of the ligands for TLRs and NLRs.

Receptor	Ligand (Source)	Reference
TLR1	Lipopeptides (Bacteria)	16
TLR2	Peptidoglycan and Lipoteichoic acid (Gram (+) Bacteria)	17
TLR3	dsDNA (Viruses)	18
TLR4	Lipopolysaccharide (Gram (-) Bacteria)	19
TLR5	Flagellin (Bacteria)	20
TLR6	Lipoteichoic acid (Gram (+) Bacteria)	17
TLR7	sDNA (Viruses)	21
TLR8	sDNA (Viruses)	22
TLR9	CpG-containing DNA (Bacteria and Viruses)	23
Nod1	Peptidoglycan – iE-DAP (Gram (-) Bacteria)	24, 25, 26
Nod2	Peptidoglycan – MDP (Bacteria)	27, 28

Upon recognition, both types of receptors activate various pathways to produce inflammatory cytokines and chemokines to combat the invading microbes.²⁹ However the question then becomes if our body is responding to the presence of MAMPs, then can we distinguish the MAMPs from commensal bacteria and the MAMPs from pathogenic bacteria? One hypothesis is that the human innate immune system has evolved over the years to detect MAMPs that are specifically produced by pathogenic bacteria. This hypothesis is supported by the fact that different bacterial families will have different peptidoglycan (PG) composition and that the various receptors respond to different ligands.^{30,31} Unlike TLR4, the nucleotide-binding and oligomerization domain-containing 2 (Nod2) receptor senses a small fragment of the

peptidoglycan, such as muramyl dipeptide (MDP), and Nod1 senses a different peptidoglycan fragment, γ -D-glutamyl-meso-diaminopimelic acid (iE-DAP). The release of different immunostimulatory peptidoglycan fragments could help the innate immune system distinguish between commensal and pathogenic bacteria. However as with all things biological, it is presumably much more complicated, and additional experiments and methodology are needed in order to illuminate the processes through which MAMPs are generated.

1.3 Peptidoglycan

Bacterial cell wall, also known as peptidoglycan, is unique to bacteria^{32,33,34} and is composed of a polymeric network of alternating units of *N*-acetylglucosamine (NAG) and *N*-acetylmuramic acid (NAM)-pentapeptide carbohydrates that are further cross-linked (Figure 1.2).

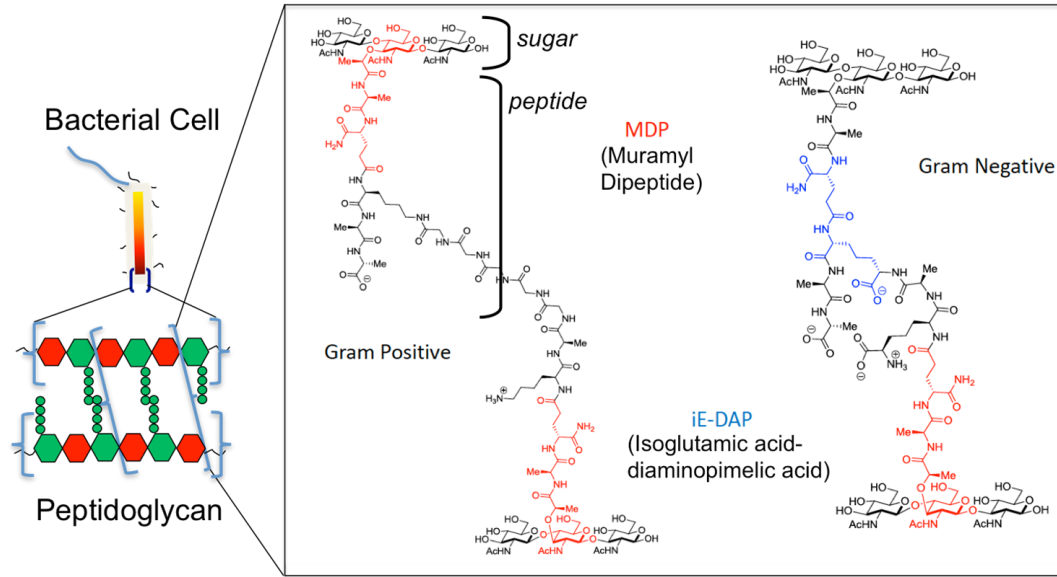


Figure 1.2: A molecular view of the bacterial peptidoglycan composition. Structural differences between most Gram (+) and Gram (-) bacterial species are highlighted. Also shown are MDP (red) and iE-DAP (blue), ligands for Nod2 and Nod1, respectively.

However there are some subtle variations in the peptide stems, as well as cross-linking patterns across different bacterial species.³⁵ For example, most Gram (+) bacterial species have a lysine at the third amino acid position of the pentapeptide chain with the exception of Bacilli, which have *meso*-A₂pm at the third position similar to that of Gram (-) bacterial species.³⁶ Yet the fourth amino acid in the chain is always an alanine regardless of the type of bacteria.^{37,38} These subtle differences are attributed to the specificity of the Mur enzymes, which are involved in peptidoglycan biosynthesis (Figure 1.3).^{39,40}

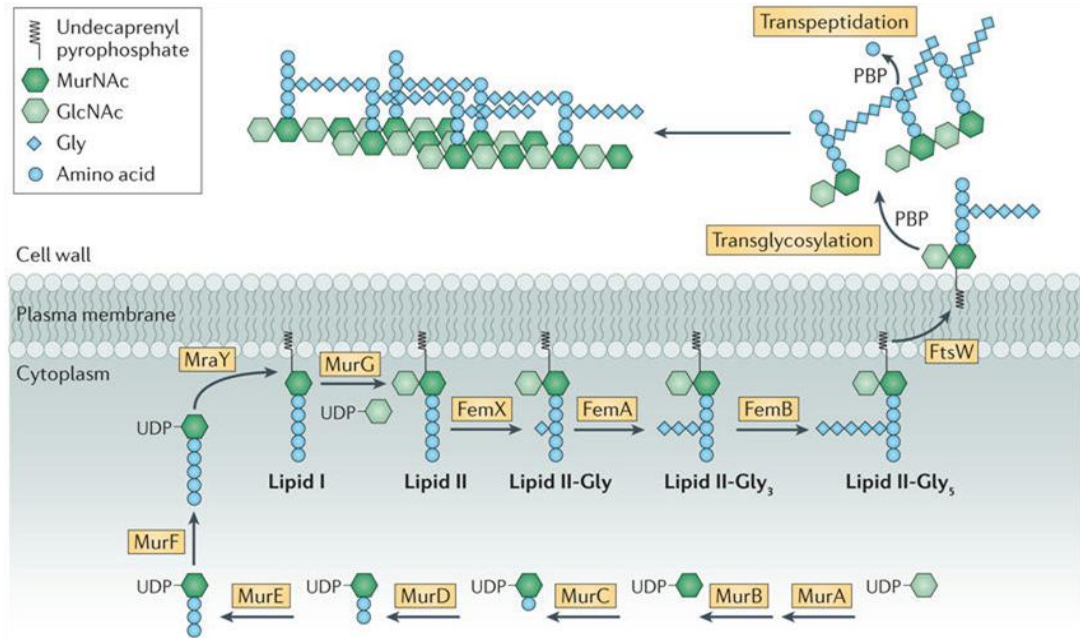


Figure 1.3: The peptidoglycan biosynthetic pathway. MurA and MurB convert UDP-NAG into UDP-NAM. MurC, MurD, MurE, and MurF add the pentapeptide chain. MraY attaches the precursor to the membrane via undecaprenyl pyrophosphate. MurG converts Lipid I to Lipid II by adding NAG. FemX, Fem A, and FemB synthesize the poly-glycine linkage. The molecule is then flipped from the cytoplasm to the periplasm by FtsW, where it is cross linked onto existing peptidoglycan though transglycosylases and transpeptidases. Figure reproduced from Veening et al. (2013).⁴⁰

Peptidoglycan is a key component in bacterial cell survival, regulating the osmotic pressure, temperature and pH.^{41,42,43} It also contributes to the bacterial cell shape, and serves as the anchoring point for wall teichoic acids (WTA) and extracellular proteins.⁴⁴ Given the varied roles of the peptidoglycan, it is not surprising that biochemists have exploited the polymer for a number of applications. The Gram staining method is used to classify a bacteria either as Gram (+) or Gram (-) based on the accessibility of the peptidoglycan.⁴⁵ Since the peptidoglycan is unique to bacteria,

numerous researchers have targeted it as a means to fluorescently label the bacteria.⁴⁶ In addition, many antibiotics target the biosynthesis of this bacterial calling card in order to kill the bacterium.⁴⁷

1.3.1 Bacterial Classification with Gram Staining

Gram staining is a widely used method to distinguish between two groups of bacteria.^{48,49} The main principle of the method is that Gram (+) bacteria have a much thicker layer of peptidoglycan as compared to Gram (-) bacteria (Figure 1.4).⁵⁰ The difference in peptidoglycan abundance allows researchers to stain the cells with different dyes in order to distinguish the various bacterial species present in a mix population.

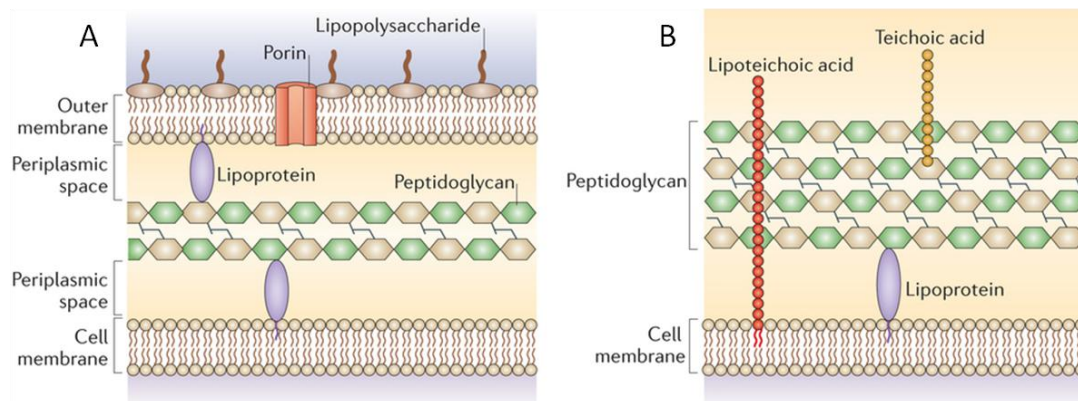


Figure 1.4: Gram (-) bacteria have a thin layer of peptidoglycan that is sandwiched between the outer and inner membranes (A). Gram (+) bacteria have a thick layer of peptidoglycan on the exterior of the bacterial cell (B). The difference in peptidoglycan abundance and accessibility is the driving principle behind the Gram staining method. Figure adapted from Casadevall et al. (2015).⁵⁰

The bacterial cells are first treated with a solution of crystal violet dye. Both Gram (+) and Gram (-) cells are stained purple after the initial treatment. Next an iodine solution is added to form a complex with the crystal violet dye. Then the bacterial cells are washed with alcohol. During this step, the Gram (+) cells retained the purple color due to the iodine-crystal violet complex being trapped within the thick layer of peptidoglycan. In contrast, the purple color is washed away in Gram (-) cells because the thin layer of peptidoglycan is unable to trap the iodine-crystal violet complex. Lastly the bacterial cells are treated with safranin. Gram (+) cells are unable to uptake this second dye, so they remained a purple color. Gram (-) cells are stained by safranin resulting in a pink color (Figure 1.5).⁵¹

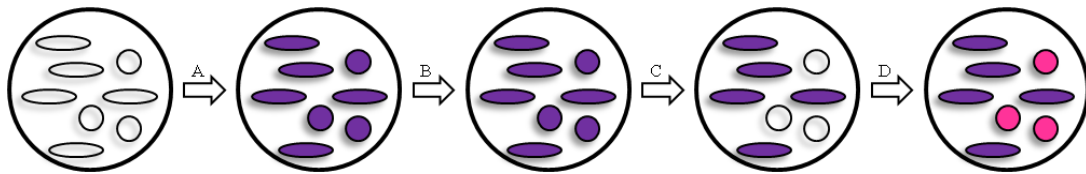


Figure 1.5: Diagram depicting the physical appearance of a mixed population of bacterial cells after each step (crystal violet addition (A), iodine treatment (B), alcohol wash (C), and safranin stain (D)) of the Gram staining method. Gram (+) cells (oval) are stained purple while Gram (-) cells (circle) are stained pink.

This powerful technique often serves as a starting point to differentiate bacterial species present in a mix population.⁵² Gram staining also illustrates one of the many important utilities of the peptidoglycan.

1.3.2 Peptidoglycan as a Labeling Target

The peptidoglycan has also been the target of numerous labeling strategies. A majority of the strategies have relied on the incorporation of unnatural derivatives of either amino acids or sugar building blocks. For example, Maurelli and coworkers used unnatural D-Ala-D-Ala derivatives to include an azido handle on the peptide stem (Figure 1.6b).⁵³ Likewise, the Bertozzi group also used a D-Ala derivative to install an alkyne⁵⁴ or a cyclooctyne⁵⁵ on the peptide stem (Figure 1.6e and 1.6f). Similarly, Kuru et al. used fluorescent D-Ala derivatives to directly attach a fluorophore onto the peptide stem (Figure 1.6c).⁵⁶ In 2014, the Walker and Kahne labs labeled the peptidoglycan in an analogous manner using unnatural lysine derivatives containing fluorescein (Figure 1.6d).⁵⁷ Although successful, these strategies to fluorescently label the peptidoglycan on the peptide stem has a major drawback. The pentapeptide stem is trimmed in the cross-linking process, and for MDP to be produced, both the Ala and Lys amino acids would be cleaved.

Therefore other groups, such as the Errington lab, have used fluorescent antibiotics as another means to label the peptidoglycan (Figure 1.6g).^{58,59} This method is advantageous because it labels existing peptidoglycan and does not rely on the enzymes present in the peptidoglycan biosynthesis pathway. While the labeling is successful, antibiotic treated cells are unhealthy and thus are not suitable for additional *in vivo* studies. Another strategy is to incorporate fluorescence through the carbohydrate backbone of peptidoglycan. In 2008, the Nishimura group was able to label the peptidoglycan through glucosamine derivatives (Figure 1.6h).⁶⁰ The downside to this approach is the glucosamine is found throughout the cell, hence there is a high level of background fluorescence that is not localized to the peptidoglycan. Recently, the Grimes lab mitigated both of these issues by labeling the peptidoglycan

with unnatural NAM derivatives,⁶¹ which is specific to the peptidoglycan and not harmful to the bacteria (Figure 1.6a). The disadvantage of this method is that it also relies on the bacteria for the assimilation of the derivatives.

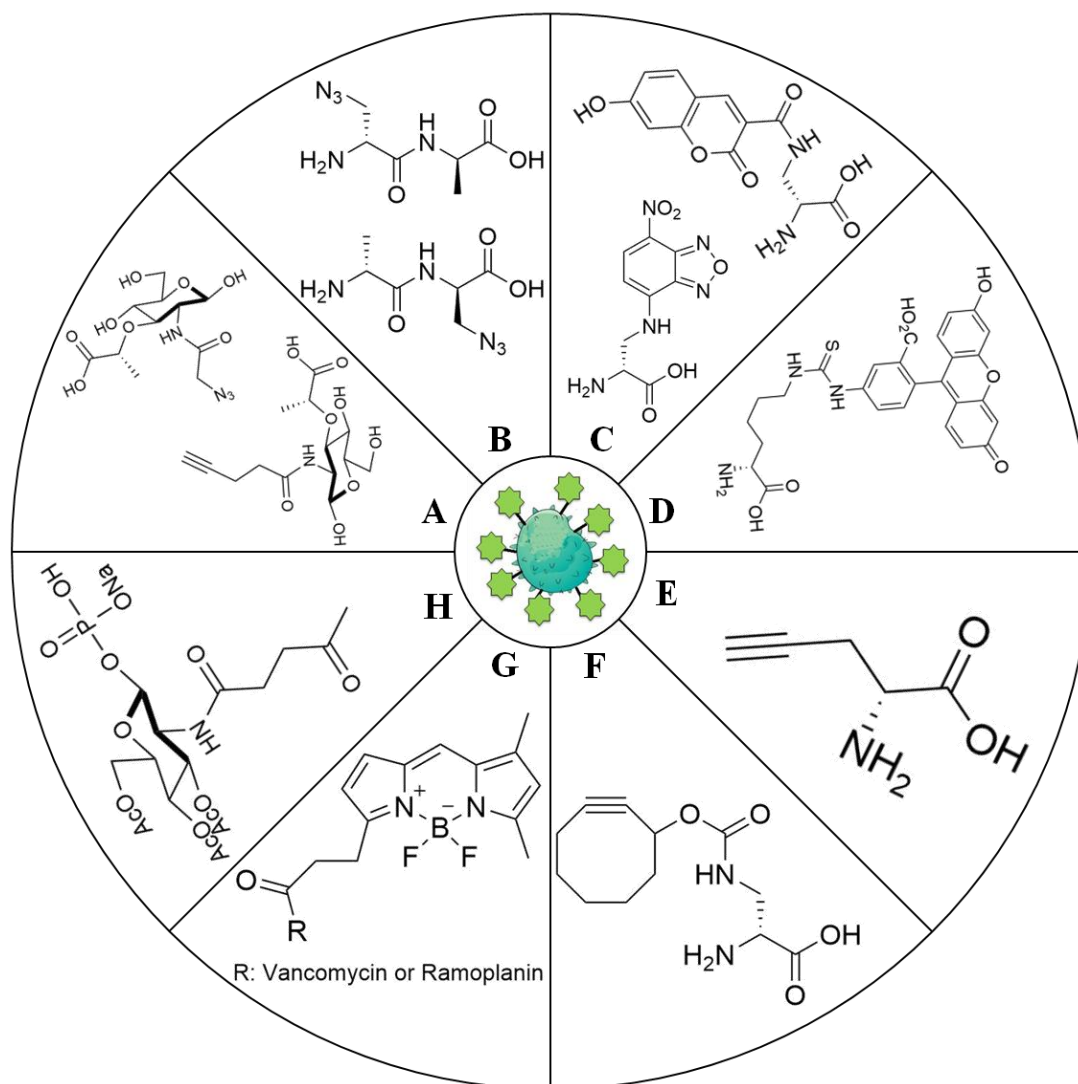


Figure 1.6: Review of select peptidoglycan labeling strategies found in literature. Three main strategies have been employed to label the peptidoglycan: the incorporation of unnatural amino acids (B-F), the use of fluorescent antibiotics (G), and the integration of unnatural sugar derivatives (A,H).
A⁶¹ B⁵³ C⁵⁶ D⁵⁷ E⁵⁴ F⁵⁵ G^{58,59} H⁶⁰

1.3.3 Peptidoglycan as an Antibiotic Target

Several components of the peptidoglycan biosynthetic pathway are also the targets of many antibiotics.⁶² A common mechanism of action include inactivation of the enzymes involved in peptidoglycan biosynthesis either through direct binding of the antibiotic to the enzyme or by blocking the interaction between the enzyme and its substrate. For example, one of the well known antibiotic, penicillin works by blocking the transpeptidases that are responsible for peptidoglycan cross-linking.⁶³ As a result, the transpeptidases are often referred to as penicillin-binding proteins (PBPs). Penicillin was first discovered by Alexander Fleming in 1928⁶⁴ and is a member of the β -lactam class of antibiotics. The structure of penicillin mimics that of the D-Ala-D-Ala, so the transpeptidase binds to penicillin and is rendered inactive (Figure 1.7).⁶⁵ The lack of cross-linking results in structural instability of the peptidoglycan, which eventually leads to cell lysis.

Interestingly, another well known antibiotic, vancomycin, also interferes with the binding of transpeptidases to D-Ala-D-Ala. Vancomycin binds directly to D-Ala-D-Ala (Figure 1.7), and as a consequence of its size, it blocks the binding of transpeptidases to D-Ala-D-Ala.⁶⁶ Antibiotics that target the peptidoglycan further demonstrates the utility of this unique feature of bacterial cells.

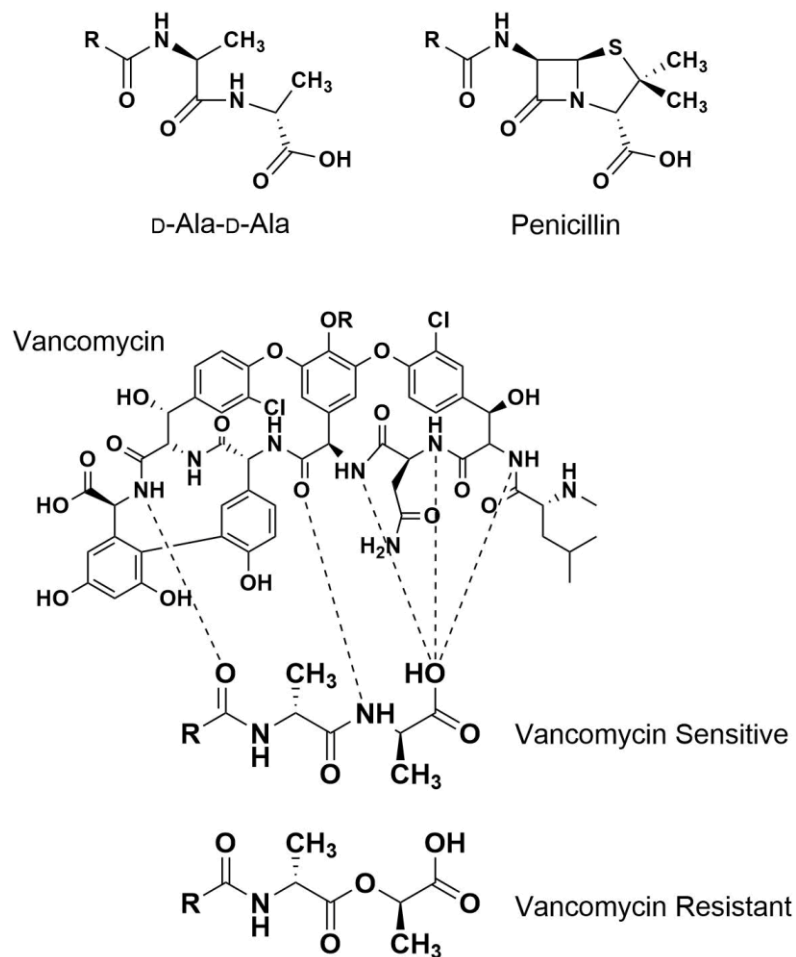


Figure 1.7: The class of β -lactam antibiotics such as penicillin is structurally similar to that of D-Ala-D-Ala, which allows them to bind to PBPs and inhibit their activity (top). Vancomycin binds directly to D-Ala-D-Ala, blocking the dipeptide from binding to PBPs. Vancomycin resistant bacteria have altered the dipeptide from D-Ala-D-Ala to D-Ala-D-Lac to disrupt the hydrogen bonding necessary for vancomycin's activity (bottom).

1.4 Bacterial Protection Strategies

Due to the widespread misuse of antibiotics, bacteria have developed resistance mechanisms.⁶⁷ Bacteria that are resistant to penicillin or other members of the β -lactam family of antibiotics produced enzymes that catalyze the opening of the

β -lactam ring rendering the antibiotic harmless.⁶⁸ In addition, some *Lactobacillus* species have altered the composition of the peptide stem to incorporate D-Ala-D-Lac instead of D-Ala-D-Ala to prevent the binding of vancomycin (Figure 1.7).⁶⁹ This protection strategy was initially discovered in *Enterococcus faecium*.⁷⁰ VanA makes the D-Ala-D-Lac dipeptide and VanX specifically hydrolyzes the D-Ala-D-Ala dipeptide.⁷¹ The accumulating of D-Ala-D-Lac forces MurF to add the dipeptide to the existing tripeptide chain on NAM. The presence of D-Ala-D-Lac in the pentapeptide results in the loss of a hydrogen bond between vancomycin and its substrate.⁷²

In addition to these resistance mechanisms, bacteria also utilize other broad, survival mechanisms involving the post-synthetic modification of its peptidoglycan in order to combat other threats. Lysozyme, a mammalian antimicrobial enzyme, acts on the peptidoglycan by cleaving the β -1,4-glycosidic bond between NAG and NAM.⁷³ As a defense mechanism against degradation, bacteria often modify their mature peptidoglycan via multiple pathways such as *N*-deacetylation and *O*-acetylation to block such cleavage (Figure 1.8).⁷⁴

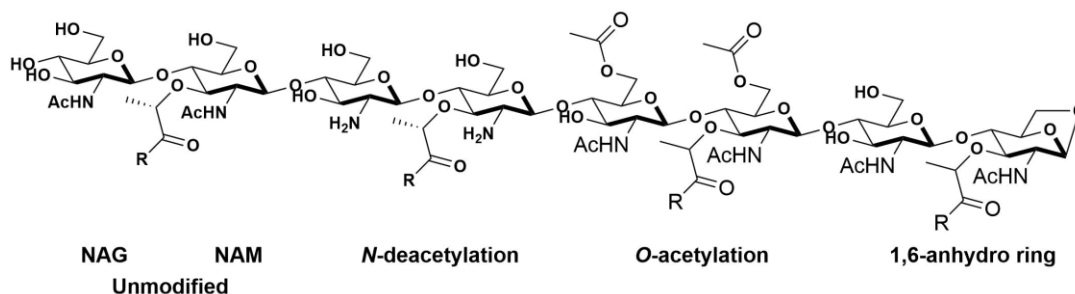


Figure 1.8: Post-synthetic modifications of the peptidoglycan such as *N*-deacetylation and *O*-acetylation prevent degradation by lytic enzymes, which usually results in the formation of a 1,6-anhydro ring. R: peptide chain.

N-deacetylation has been observed in several pathogenic bacterial species including *Bacillus anthracis* and *Streptococcus pneumoniae*.^{75,76} The process is catalyzed by two enzymes: PdaA,⁷⁷ which deacetylates NAM, and PgdA,⁷⁸ which deacetylates NAG. It has been shown that lysozyme has poor affinity for deacetylated peptidoglycan⁷⁹ as the acetyl groups are necessary to interact with the amino acids present in the binding pocket of lysozyme. Moreover, the lytic activity of lysozyme can be restored acetylating the peptidoglycan chemically. In addition, the peptidoglycan becomes more positively charged due to the free amino groups that form as a result of deacetylation, which could confer resistance to cationic antimicrobial peptides produced by the innate immune system similar to how *Staphylococcus aureus* resist cationic host defense factors by modifying their lysylphosphatidylglycerol (LPG) with L-Lys.⁸⁰

O-acetylation of peptidoglycan has also been found in numerous pathogenic bacterial species including *S. aureus* and *N. gonorrhoeae*,^{81,82} leading to resistance of lysozyme degradation.⁸³ Thus it is not surprising that the level of *O*-acetylation can be as high as 70% in certain bacterial species.⁸⁴ Despite the prevalence of *O*-acetylation, the source and delivery mechanism of the acetate is debated; it is hypothesized that the natural source of the acetate group is from acetyl-CoA. However given that *O*-acetyl groups are not found on Lipid II, a precursor in the PG biosynthetic pathway, *O*-acetylation is considered to occur post synthetically on either nascent or mature PG.^{85,86,87,88} Therefore a mechanism through which the acetate derived from acetyl-CoA is translocated from the cytoplasm to the periplasmic space via a transporter has been proposed.⁸⁹

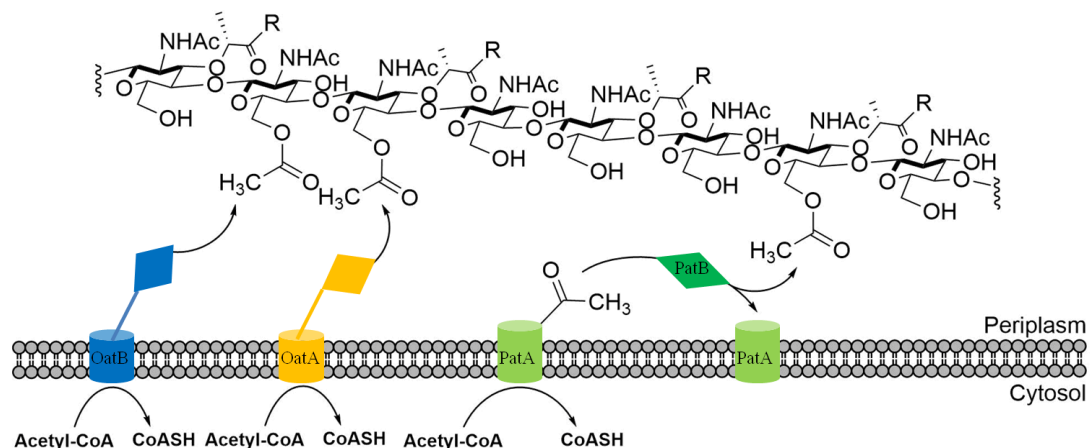


Figure 1.9: Comparison of the Oat proteins found in Gram (+) bacteria and the Pat proteins found in Gram (-) bacteria that is responsible for the *O*-acetylation of the peptidoglycan.

In Gram (+) bacteria, there exist two enzymes that are responsible for *O*-acetylating the carbohydrate backbone of peptidoglycan. *O*-acetyltransferase A (OatA) was first identified in *S. aureus* and shown to acetylate the 6-OH position of NAM,⁹⁰ while OatB, which was identified in *Lactobacillus sakei*, is responsible for the acetylation of the 6-OH position of NAG (Figure 1.9).⁹¹ Both proteins have yet to be characterized due to the difficulties associated with the expression and purification of transmembrane proteins. However sequence analysis predicts that both proteins have eleven transmembrane regions that are proposed to be responsible for the transport of an acetyl group from the cytoplasm into the periplasm.⁹² Both OatA and OatB also have a second component that is responsible for the transfer of the acetyl group onto the peptidoglycan. In Gram (-) bacteria, the enzymes responsible for *O*-acetylation are peptidoglycan *O*-acetyltransferase A (PatA)⁹³ and B (PatB)⁹⁴ (Figure 1.9). Unlike the Oat proteins, the Pat proteins are not bilobal. PatA is a transmembrane protein, while PatB resides freely in the periplasm. Similar to the transmembrane portion of the Oat

proteins, PatA is presumed to translocate the acetyl group that PatB puts on the peptidoglycan in order to protect the bacteria against exogenous autolysins.

1.5 Overview of Dissertation

PatB is an important part of the bacterial survival mechanism. However despite that significance, we have limited knowledge on its biochemistry. This dissertation aims to improve upon the current purification and characterization of PatB, to elucidate PatB's substrate specificity using a wide range of synthetic donors, and demonstrate the versatility of PatB modification pathway. Chapter 2 details the development of the use of the *E. coli* system for the over-expression and purification of dual tagged PatB along with characterization of the purified PatB with biochemical assays. Chapter 3 details the synthesis of two sets of possible donors to probe for PatB's substrate specificity. Chapter 4 describes the exploration for suitable small molecule acceptors for PatB including the isolation of the natural acceptor, peptidoglycan. Chapter 5 details the application of PatB to confer lysozyme resistance to isolated peptidoglycan. Also detailed is the application of PatB to fluorescently label whole bacterial cells. Chapter 6 discusses the significance of the dissertation and additional directions for the future.

REFERENCES

1. Peterson, J.; Garges, S.; Giovanni, M.; McInnes, P.; Wang, L.; Schloss, J. A.; Bonazzi, V.; McEwen, J. E.; Wetterstrand, K. A.; Deal, C.; Baker, C. C.; Di Francesco, V.; Howcroft, T. K.; Karp, R. W.; Lunsford, R. D.; Wellington, C. R.; Belachew, T.; Wright, M.; Giblin, C.; David, H.; Mills, M.; Salomon, R.; Mullins, C.; Akolkar, B.; Begg, L.; Davis, C.; Grandison, L.; Humble, M.; Khalsa, J.; Little, A. R.; Peavy, H.; Pontzer, C.; Portnoy, M.; Sayre, M. H.; Starke-Reed, P.; Zakhari, S.; Read, J.; Watson, B.; Guyer, M.; Grp, N. H. W. The NIH Human Microbiome Project. *Genome Research*, **2009**, *19* (12), 2317-2323. doi: 10.1101/gr.096651.109.
2. Thaiss, C. A.; Zmora, N.; Levy, M.; Elinav, E. The microbiome and innate immunity. *Nature*, **2016**, *535* (7610), 65-74. doi: 10.1038/nature18847.
3. Lozupone, C. A.; Stombaugh, J. I.; Gordon, J. I.; Jansson, J. K.; Knight, R. Diversity, stability and resilience of the human gut microbiota. *Nature*, **2012**, *489* (7415), 220-230. doi: 10.1038/nature11550.
4. The Human Microbiome Project Consortium. A framework for human microbiome research. *Nature*, **2012**, *486*, 215-221. doi: 10.1038/nature11209.
5. The Human Microbiome Project Consortium. Structure, function and diversity of the healthy human microbiome. *Nature*, **2012**, *486*, 207-214. doi:10.1038/nature11234.
6. Sender, R.; Fuchs, S.; Milo, R. Revised Estimates for the Number of Human and Bacteria Cells in the Body. *Plos Biology*, **2016**, *14* (8), 14. doi: 10.1371/journal.pbio.1002533.

7. Qin, J.; Li, R.; Raes, J.; Arumugam, M.; Burgdorf, K.S.; Manichanh, C.; Nielsen, T.; Pons, N.; Levenez, F.; Yamada, T.; Mende, D.R.; Li, J.; Xu, J.; Li, S.; Li, D.; Cao, J.; Wang, B.; Liang, H.; Zheng, H.; Xie, Y.; Tap, J.; Lepage, P.; Bertalan, M.; Batto, J.M.; Hansen, T.; Le Paslier, D.; Linneberg, A.; Nielsen, B.; Pelletier, E.; Renault, P.; Sicheritz-Ponten, T.; Turner, K.; Zhu, H.; Yu, C.; Li, S.; Jian, M.; Zhou, Y.; Li, Y.; Zhang, X.; Li, S.; Qin, N.; Yang, H.; Wang, J.; Brunak, S.; Dore, J.; Guarner, F.; Kristiansen, K.; Pedersen, O.; Parkhill, J.; Weissenbach, J.; MetaHIT Consortium; Bork, P.; Ehrlich, S.D.; Wang, J. A human gut microbial gene catalog established by metagenomic sequencing. *Nature*, **2010**, *464*(7285), 59-65. doi: 10.1038/nature08821.
8. Tlaskalova-Hogenova, H.; Stepankova, R.; Hudcovic, T.; Tuckova, L.; Cukrowska, B.; Lodinova-Zadnikova, R.; Kozakova, H.; Rossmann, P.; Bartova, J.; Sokol, D. Commensal bacteria (normal microflora), mucosal immunity and chronic inflammatory and autoimmune diseases. *Immunology Letters*, **2004**, *93* (2-3), 97-108. doi: 10.1016/j.imlet.2004.02.005.
9. Le Chatelier, E.; Nielsen, T.; Qin, J. J.; Prifti, E.; Hildebrand, F.; Falony, G.; Almeida, M.; Arumugam, M.; Batto, J. M.; Kennedy, S.; Leonard, P.; Li, J. H.; Burgdorf, K.; Grarup, N.; Jorgensen, T.; Brandslund, I.; Nielsen, H. B.; Juncker, A. S.; Bertalan, M.; Levenez, F.; Pons, N.; Rasmussen, S.; Sunagawa, S.; Tap, J.; Tims, S.; Zoetendal, E. G.; Brunak, S.; Clement, K.; Dore, J.; Kleerebezem, M.; Kristiansen, K.; Renault, P.; Sicheritz-Ponten, T.; de Vos, W. M.; Zucker, J. D.; Raes, J.; Hansen, T.; Bork, P.; Wang, J.; Ehrlich, S. D.; Pedersen, O.; Meta, H. I. T. C. Richness of human gut microbiome correlates with metabolic markers. *Nature*, **2013**, *500* (7464), 541-+. doi: 10.1038/nature12506.
10. Rogers, G. B.; Keating, D. J.; Young, R. L.; Wong, M. L.; Licinio, J.; Wesselingh, S. From gut dysbiosis to altered brain function and mental illness: mechanisms and pathways. *Molecular Psychiatry*, **2016**, *21* (6), 738-748. doi: 10.1038/mp.2016.50.
11. Belkaid, Y.; Hand, T. Role of the microbiota in immunity and inflammation. *Cell*, **2014**, *157* (1), 121-141. doi: 10.1016/j.cell.2014.03.011.
12. Lemaitre, B.; Nicolas, E.; Michaut, L.; Reichhart, J. M.; Hoffmann, J. A. The dorsoventral regulatory gene cassette spatzle/Toll/cactus controls the potent antifungal response in *Drosophila* adults. *Cell*, **1996**, *86* (6), 973-983. doi: 10.1016/s0092-8674(00)80172-5.

13. Poltorak, A.; Smirnova, I.; He, X. L.; Liu, M. Y.; Van Huffel, C.; Birdwell, D.; Alejos, E.; Silva, M.; Du, X.; Thompson, P.; Chan, E. K. L.; Ledesma, J.; Roe, B.; Clifton, S.; Vogel, S.; Beutler, B. Genetic and physical mapping of the Lps locus: Identification of the Toll-4 receptor as a candidate gene in the critical region. *Blood Cells Molecules and Diseases*, **1998**, *24* (17), 340-355. doi: 10.1006/bcmd.1998.0201.
14. Geddes, K.; Magalhaes, JG.; Girardin, SE. Unleashing the therapeutic potential of NOD-like receptors. *Nature Reviews Drug Discovery*, **2009**, *8*, 465-479. doi: 10.1038/nrd2783.
15. Mackey, D.; McFall, A. J. MAMPs and MIMPs: proposed classifications for inducers of innate immunity. *Molecular microbiology*, **2006**, *61* (6), 1365-71. doi: 10.1111/j.1365-2958.2006.05311.
16. Takeuchi, O.; Sato, S.; Horiuchi, T.; Hoshino, K.; Takeda, K.; Dong, Z.; Modlin, RL.; Akira, S. Cutting edge: Role of Toll-like receptor 1 in mediating immune response to microbial lipoproteins. *J. Immunology*, **2002**, *169* (1), 10–14. doi: 10.4049/jimmunol.169.1.10.
17. Schwadner, R.; Dziarski, R.; Wesche, H.; Rothe, M.; Kirschning, CJ. Peptidoglycan- and lipoteichoic acid-induced cell activation is mediated by Toll-like receptor 2. *J. Biol. Chem.*, **1999**, *274* (25), 17406–17409. doi: 10.1074/jbc.274.25.17406.
18. Alexopoulou, L., Holt, AC., Medzhitov, R.; Flavell, RA. Recognition of double-stranded RNA and activation of NF- κ B by Toll-like receptor 3. *Nature*, **2001**, *413*, 732–738. doi: 10.1038/35099560.
19. Poltorak, A.; He, X.; Smirnova, I.; Liu, MY.; Van Huffel, C.; Du, X.; Birdwell, D.; Alejos, E.; Silva, M.; Galanos, C.; Freudenberg, M.; Ricciardi-Castagnoli, P.; Layton, B.; Beutler, B. Defective LPS signaling in C3H/HeJ and C57BL/10ScCr mice: mutations in Tlr4 gene. *Science*, **1998**, *282* (5396), 2085–2088. doi: 10.1126/science.282.5396.2085.
20. Hayashi, F.; Smith, KD.; Ozinsky, A.; Hawn, TR.; Yi, EC.; Goodlett, DR.; Eng, JK.; Akira, S.; Underhill, DM.; Aderem, A. The innate immune response to bacterial flagellin is mediated by Toll-like receptor-5. *Nature*, **2001**, *410* (6832), 1099–1103. doi:10.1038/35074106.
21. Diebold, SS.; Kaisho, T.; Hemmi, H.; Akira, S.; Reis e Sousa, C. Innate antiviral responses by means of TLR7 mediated recognition of single-stranded RNA. *Science*, **2004**, *303* (5663), 1529–1531. doi: 10.1126/science.1093616.

22. Heil, F.; Hemmi, H.; Hochrein, H.; Ampenberger, F.; Kirschning, C.; Akira, S.; Lipford, G.; Wagner, H.; Bauer, S. Species-specific recognition of single-stranded RNA via Toll-like receptor 7 and 8. *Science*, **2004**, *303* (5663), 1526–1529. doi: 10.1126/science.1093620.
23. Hemmi, H.; Takeuchi, O.; Kawai, T.; Kaisho, T.; Sato, S.; Sanjo, H.; Matsumoto, M.; Hoshino, K.; Wagner, H.; Takeda, K.; Akira, S. A Toll-like receptor recognizes bacterial DNA. *Nature*, **2000**, *408*, 740–745. doi: 10.1038/35047123.
24. Chamaillard, M.; Hashimoto, M.; Horie, Y.; Masumoto, J.; Qiu, S.; Saab, L.; Ogura, Y.; Kawasaki, A.; Fukase, K.; Kusumoto, S.; Valvano, MA.; Foster, SJ.; Mak, TW.; Nunez, G.; Inohara, N. An essential role for NOD1 in host recognition of bacterial peptidoglycan containing diaminopimelic acid. *Nature Immunology*, **2003**, *4*, 702–707. doi: 10.1038/ni945.
25. Girardin, SE.; Travassos, LH.; Herve, M.; Blanot, D.; Boneca, IG.; Philpott, DJ.; Sansonetti, PJ.; Mengin-Lecreulx, D. Peptidoglycan molecular requirements allowing detection by Nod1 and Nod2. *J. Biol. Chem.*, **2003**, *278* (43), 41702–41708. doi: 10.1074/jbc.M307198200.
26. Kim, JG.; Lee, SJ.; Kagnoff, MF. Nod1 is an essential signal transducer in intestinal epithelial cells infected with bacteria that avoid recognition by toll-like receptors. *Infect Immun.*, **2004**, *72* (3), 1487–1495. doi: 10.1128/IAI.72.3.1487-1495.2004.
27. Girardin, SE.; Boneca, IG.; Viala, J.; Chamaillard, M.; Labigne, A.; Thomas, G.; Philpott, DJ.; Sansonetti, PJ. Nod2 is a general sensor of peptidoglycan through muramyl dipeptide (MDP) detection. *J. Biol. Chem.*, **2003**, *278* (11), 8869–8872. doi: 10.1074/jbc.C200651200.
28. Kobayashi, KS.; Chamaillard, M.; Ogura, Y.; Henegariu, O.; Inohara, N.; Nunez, G.; Flavell, RA. Nod2-dependent regulation of innate and adaptive immunity in the intestinal tract. *Science*, **2005**, *307* (5710), 731–734. doi: 10.1126/science.1104911.
29. Turner, MD.; Nedjai, B.; Hurst, T.; Pennington, DJ. Cytokines and chemokines: at the crossroads of cell signaling and inflammatory disease. *Biochimica et Biophysica Acta*, **2014**, *1843* (11), 2563–2582. doi: 10.1016/j.bbamcr.2014.05.014.
30. Akira, S.; Takeda, K. Toll-like receptor signaling. *Nature*, **2004**, *4*, 499–511. doi: 10.1038/nri1391.

31. Wilmanski, JM.; Petnicki-Ocwieja, T.; Kobayashi, KS. NLR proteins: integral members of innate immunity and mediators of inflammatory diseases. *J. Leukoc. Biol.*, **2008**, 83 (1), 13-30. doi: 10.1189/jlb.0607402.
32. Rogers, HJ. Bacterial growth and the cell envelope. *Bacteriol. Rev.*, **1970**, 34 (2), 194-214. PMID: PMC408316.
33. Nanninga, N. Morphogenesis of *Escherichia coli*. *Microbiol. Mol. Biol. Rev.*, **1998**, 62 (1), 110-129. PMID: PMC98908.
34. Mengin-Lecreulx, D.; Lemaitre, B. Structure and metabolism of peptidoglycan and molecular requirements allowing its detection by the *Drosophila* innate immune system. *J. Endotoxin. Res.*, **2005**, 11 (2), 105-111. doi: 10.1179/096805105X35233.
35. Vollmer, W.; Blanot, D.; de Pedro, MA. Peptidoglycan structure and architecture. *FEMS Microbiol. Rev.*, **2008**, 32 (2), 149-167. doi: 10.1111/j.1574-6976.2007.00094.
36. Boniface, A.; Bouhss, A.; Mengin-Lecreulx, D.; Blanot, D. The MurE synthetase from *Thermotoga maritima* is endowed with an unusual D-lysine adding activity. *J. Biol. Chem.*, **2006**, 281 (23), 15680-15686. doi: 10.1074/jbc.M506311200.
37. Duncan, K.; Heijenoort, JV.; Walsh, CT. Purification and characterization of the D-alanyl-D-alanine-adding enzyme from *Escherichia coli*. *Biochemistry*, **1990**, 29 (9), 2379-2386. doi: 10.1021/bi00461a023.
38. Bugg, TDH.; Wright, GD.; Dutka-Malen, S.; Arthur, M.; Courvalin, P.; Walsh, CT. Molecular basis for vancomycin resistance in *Enterococcus faecium* BM4147: biosynthesis of a depsipeptide peptidoglycan precursor by vancomycin resistance proteins VanH and VanA. *Biochemistry*, **1991**, 30 (43), 10408-10415. doi: 10.1021/bi00107a007.
39. El Zoeiby, A.; Sanschagrin, F.; Levesque, RC. Structure and function of the Mur enzymes: development of novel inhibitors. *Mol. Microbiol.*, **2003**, 47 (1), 1-12. doi: 10.1046/j.1365-2958.2003.03289.
40. Pinho, MG.; Kjos, M.; Veening, JW. How to get (a)round: mechanisms controlling growth and division of coccoid bacteria. *Nature Reviews Microbiology*, **2013**, 11, 601-614. doi: 10.1038/nrmicro3088.
41. Wood, JM. Bacterial responses to osmotic challenges. *J. Gen. Physiol.*, **2015**, 145 (5), 381-388. doi: 10.1085/jgp.201411296.

42. Kremer, L.; Guerardel, Y.; Gurcha, SS.; Locht, C.; Besra, GS. Temperature-induced changes in the cell-wall components of *Mycobacterium thermoresistibile*. *Microbiol.*, **2002**, *148* (10), 3145-3154. doi: 10.1099/00221287-148-10-3145.
43. Booth, IR. Regulation of cytoplasmic pH in bacteria. *Microbiol. Rev.*, **1985**, *49* (4), 359-378. PMID: PMC373043.
44. Brown, S.; Santa Maria, JP.; Walker, S. Wall teichoic acids of Gram-positive bacteria. *Annu. Rev. Microbiol.*, **2013**, *67*, 313-336. doi: 10.1146/annurev-micro-092412-155620.
45. Bartholomew, JW.; Mittwer, T. The Gram Stain. *Bacteriol. Rev.*, **1952**, *16* (1), 1-29. PMID: PMC180726.
46. Van Dam, V.; Orlachs, N.; Breukink, E. Specific labeling of peptidoglycan precursors as a tool for bacterial cell wall studies. *Chembiochem*, **2009**, *10* (4), 617-624. doi: 10.1002/cbic.200800678.
47. Kohanski, MA.; Dwyer, DJ.; Collins, JJ. How antibiotics kill bacteria: from targets to networks. *Nat. Rev. Microbiol.*, **2010**, *8* (6), 423-435. doi: 10.1038/nrmicro2333.
48. Srinivasan, U.; Ponnaluri, S.; Villareal, L.; Gillespie, B.; Wen, A.; Miles, A.; Bucholz, B.; Marrs, CF.; Iyer, RK.; Misra, D.; Foxman, B. Gram stains: a resource for retrospective analysis of bacterial pathogens in clinical studies. *PLoS ONE*, **2012**, *7* (10), 1-7. doi: 10.1371/journal.pone.0042898.
49. Wilhelm, MJ.; Sheffield, JB.; Gh, MS.; Wu, Y.; Spahr, C.; Gonella, G.; Xu, B.; Dai, HL. Gram's stain does not cross the bacterial cytoplasmic membrane. *ACS Chem. Biol.*, **2015**, *10* (7), 1711-1717. doi: 10.1021/acscchembio.5b00042.
50. Brown, L.; Wolf, JM.; Prados-Rosales, R.; Casadevall A. Through the wall: extracellular vesicles in Gram-positive bacteria, mycobacteria and fungi. *Nat. Rev. Microbiol.*, **2015**, *13*, 620-630. doi: 10.1038/nrmicro3480.
51. Beveridge, TJ. Use of the Gram stain in microbiology. *Biotech. Histochem.*, **2001**, *76* (3), 111-118. PMID: PMC11475313.

52. Yazdankhah, SP.; Sorum, H.; Larsen, HJS.; Gogstad, G. Rapid method for detection of Gram-positive and –negative bacteria in milk from cows with moderate or severe clinical mastitis. *J. Clin. Microbiol.*, **2001**, *39* (9), 3228-3233. doi: 10.1128/JCM.39.9.3228-3233.2001.
53. Liechti, GW.; Kuru, E.; Hall, E.; Kalinda, A.; Brun, YV.; VanNieuwenhze, M.; Maurelli, AT. A new metabolic cell-wall labeling method reveals peptidoglycan in *Chlamydia trachomatis*. *Nature*, **2014**, *506*, 507-510. doi: 10.1038/nature12892.
54. Siegrist, MS.; Whiteside, S.; Jewett, JC.; Aditham, A.; Cava, F.; Bertozzi, CR. D-amino acid chemical reporters reveal peptidoglycan dynamics of an intracellular pathogen. *ACS Chem. Biol.*, **2013**, *8*, 500-505. doi: 10.1021/cb3004995.
55. Shieh, P.; Siegrist, MS.; Cullen, AJ.; Bertozzi, CR. Imaging bacterial peptidoglycan with near-infrared fluorogenic azide probes. *Proc. Natl. Acad. Sci. USA*, **2014**, *111* (15), 5456-5461. doi: 10.1073/pnas.1322727111.
56. Kuru, E.; Hughes, HV.; Brown, PJ.; Hall, E.; Tekkam, S.; Cava, F.; de Pedro, MA.; Brun, YV.; VanNieuwenhze, MS. In situ probing of newly synthesized peptidoglycan in live bacteria with fluorescent D-amino acids. *Angew. Chem. Int. Ed. Engl.*, **2012**, *51*, 12519-12523. doi: 10.1002/anie.201206749.
57. Lebar, MD.; May, JM.; Meeske, AJ.; Leiman, SA.; Lupoli, TJ.; Tsukamoto, H.; Losick, R.; Rudner, DZ.; Walker, S.; Kahne, D. Reconstitution of peptidoglycan cross-linking leads to improved fluorescent probes of cell wall synthesis. *J. Am. Chem. Soc.*, **2014**, *136*, 10874-10877. doi: 10.1021/ja505668f.
58. Daniel, RA.; Errington, J. Control of cell morphogenesis in bacteria: two distinct ways to make a rod-shaped cell. *Cell*, **2003**, *113*, 767-776. PMID: PMC12809607.
59. Tiyanont, K.; Doan, T.; Lazarus, MB.; Fang, X.; Rudner, D.; Walker, S. Imaging peptidoglycan biosynthesis in *Bacillus subtilis* with fluorescent antibiotics. *Proc. Natl. Acad. Sci. USA*, **2006**, *103*, 11033-11038. doi: 10.1073/pnas.0600829103.

60. Sadamoto, R.; Matsubayashi, T.; Shimizu, M.; Ueda, T.; Koshida, S.; Koda, T.; Nishimura, S. Bacterial surface engineering utilizing glucosamine phosphate derivatives as cell wall precursor surrogates. *Chemistry*, **2008**, *14*, 10192-10195. doi: 10.1002/chem..200801734.
61. Liang, H.; DeMeester, KE.; Hou, C.; Parent, MA.; Caplan, JL.; Grimes, CL. Metabolic labeling of the carbohydrate core in bacterial peptidoglycan and its applications. *Nat. Commun.*, **2017**, *8*, 15015. doi: 10.1038/ncomms15015.
62. Bush, K. Antimicrobial agents targeting bacterial cell walls and cell membranes. *Rev. Sci. Tech.*, **2012**, *31* (1), 43-56. PMID: PMC22849267.
63. Glauner, B.; Keck, W.; Schwarz, U. Analysis of penicillin-binding sites with a micro method – the binding site of PBP 5 from *Escherichia coli*. *FEMS Microbiol. Lett.*, **1984**, *23* (2-3), 151-155. doi: 10.1111/j.1574-6968.1984.tb01052.
64. Fleming, A., On a remarkable bacteriolytic element found in tissues and secretions. *Proceedings of the Royal Society of London Series B-Containing Papers of a Biological Character*, **1922**, *93* (653), 306-317. doi: 10.1098/rspb.1922.0023.
65. Yocum, RR.; Rasmussen, JR.; Strominger, JL. The mechanism of action of penicillin: penicillin acylates the active site of *Bacillus stearothermophilus* D-alanine carboxypeptidase. *J. Biol. Chem.*, **1980**, *255* (9), 3977-3986. PMID: PMC7372662.
66. Hammes, WP.; Neuhaus, FC. On the mechanism of action of vancomycin: inhibition of peptidoglycan synthesis in *Gaffkya homari*. *Antimicrob. Agents Chemother.*, **1974**, *6* (6), 722-728. doi: 10.1128/AAC.6.6.722.
67. Blair, JMA.; Webber, MA.; Baylay, AJ.; Ogbolu, DO. Piddock, LJV. Molecular mechanisms of antibiotic resistance. *Nature Rev. Microbiol.*, **2015**, *13*, 42-51. doi: 10.1038/nrmicro3380.
68. Davies, J.; Davies, D. Origins and evolution of antibiotic resistance. *Microbiol. Mol. Biol. Rev.*, **2010**, *74* (3), 417-433. doi: 10.1128/MMBR.00016-10.
69. Roper, DI.; Huyton, T.; Vagin, A.; Dodson, G. The molecular basis of vancomycin resistance in clinically relevant *Enterococci*: crystal structure of D-alanyl-D-lactate ligase (VanA). *Proc. Natl. Acad. Sci. USA*, **2000**, *97* (16), 8921-8925. doi: 10.1073/pnas.150116497.

70. Bugg, TD.; Wright, GD.; Dutka-Malen, S.; Arthur, M.; Courvalin, P.; Walsh, CT. Molecular basis for vancomycin resistance in *Enterococcus faecium* BM4147: biosynthesis of a depsipeptide peptidoglycan precursor by vancomycin resistance proteins VanH and VanA. *Biochem.*, **1991**, *30* (43), 10408-10415. PMID: PMC1931965.
71. Kahne, D.; Leimkuhler, C.; Lu, W.; Walsh, C. Glycopeptide and lipoglycopeptide antibiotics. *Chem. Rev.*, **2005**, *105* (2), 425-448. doi: 10.1021/cr030103a.
72. Walsh, CT.; Fisher, SL.; Park, IS.; Prahalad, M.; Wu, Z. Bacterial resistance to vancomycin: five genes and one missing hydrogen bond tell the story. *Chem. & Biol.*, **1996**, *3* (1), 21-28. doi: 10.1016/S1074-5521(96)90079-4.
73. Chung, W.; Hancock, REW. Action of lysozyme and nisin mixtures against lactic acid bacteria. *Intl. J. Food Microbiol.*, **2000**, *60* (1), 25-32. doi: 10.1016/S0168-1605(00)00330-5.
74. Davis, KM.; Weiser, JN. Modifications to the peptidoglycan backbone help bacteria to establish infection. *Infection and Immunity*, **2011**, *79* (2), 562-570. doi: 10.1128/IAI.00651-10.
75. Zipperle, GF. Jr; Ezzell, JW. Jr; Doyle, RJ. Glucosamine substitution and muramidase susceptibility in *Bacillus anthracis*. *Can. J. Microbiol.*, **1984**, *30* (5), 553-559. PMID: PMC6430537.
76. Ohno, N.; Yadomae, T. Miyazaki, T. Identification of 2-amino-2-deoxyglucose residues in the peptidoglycan of *Streptococcus pneumonia*. *Carbohydr. Res.*, **1982**, *107* (1), 152-155. doi: 10.1016/S0008-6215(00)80785-5.
77. Fukushima, T. Kitajima, T.; Sekiguchi, J. A polysaccharide deacetylase homologue, PdaA, in *Bacillus subtilis* acts as an *N*-acetylmuramic acid deacetylase in vitro. *J. Bacteriol.*, **2005**, *187* (4), 1287-1292. doi: 10.1128/JB.187.4.1287-1292.2005.
78. Vollmer, W.; Tomasz, A. The *pgdA* gene encodes for a peptidoglycan *N*-acetylglucosamine deacetylase in *Streptococcus pneumonia*. *J. Biol. Chem.*, **2000**, *275* (27), 20496-20501. doi: 10.1074/jbc.M910189199.

79. Amano, K.; Hayashi, H.; Araki, Y.; Ito, E. The action of lysozyme on peptidoglycan with *N*-unsubstituted glucosamine residues, isolation of glycan fragments and their susceptibility to lysozyme. *Eur. J. Biochem.*, **1977**, *76*, 299–307. doi: 10.1111/j.1432-1033.1977.tb11596.
80. Peschel, A. How do bacteria resist human antimicrobial peptides? *Trends Microbiol.*, **2002**, *10* (4), 179-186. doi: 10.1016/S0966-842X(02)02333-8.
81. Ghuysen, M.; Strominger, JL. Structure of the cell wall of *Staphylococcus aureus*, strain Copenhagen. II. Separation and structure of disaccharides. *Biochemistry*, **1963**, *2*, 1119-1125. PMID: PMC14087370.
82. Blundell, JK.; Perkins, HR. Effects of β -lactam antibiotics on peptidoglycan synthesis in growing *Neisseria gonorrhoeae*, including changes in the degree of *O*-acetylation. *J. Bacteriol.*, **1981**, *147*, 633-641. PMID: PMC216084.
83. Brumfitt, W.; Wardlaw, AC.; Park, JT. Development of lysozyme-resistance in *Micrococcus lysodieticus* and its association with an increased *O*-acetyl content of the cell wall. *Nature*, **1958**, *181*, 1783-1784. doi: 10.1038/1811783a0.
84. Vollmer, W. Structural variation in the glycan strands of bacterial peptidoglycan. *FEMS Microbiol. Rev.*, **2008**, *32* (2), 287-306. doi: 10.1111/j.1574-6976.2007.00088.
85. Gmeiner, J.; Kroll, HP. Murein biosynthesis and *O*-acetylation of *N*-acetylmuramic acid during the cell-division cycle of *Proteus mirabilis*. *Eur. J. Biochem.*, **1981**, *117*, 171-177. doi: 10.1111/j.1432-1033.1981.tb06317.
86. Dougherty, TJ. Analysis of *Neisseria gonorrhoeae* peptidoglycan by reverse-phase, high-pressure liquid chromatography. *J. Bacteriol.*, **1983**, *163* (1), 69-74. PMID: PMC219081.
87. Lear, AL.; Perkins, HR. Degrees of *O*-acetylation and cross-linking of the peptidoglycan of *Neisseria gonorrhoeae* during growth. *J. Gen. Microbiol.*, **1983**, *129* (3), 885-888. doi: 10.1099/00221287-129-3-885.
88. Snowden, MA.; Perkins, HR.; Wyke, AW.; Hayes, MV.; Ward, JB. Cross-linking and *O*-acetylation of newly synthesized peptidoglycan in *Staphylococcus aureus* H. *J. Gen. Microbiol.*, **1989**, *135* (11), 3015-3022. doi: 10.1099/00221287-135-11-3015.

89. Moynihan, P.J.; Clarke, A.J. Mechanism of action of peptidoglycan *O*-acetyltransferase B involves a Ser-His-Asp catalytic triad. *Biochemistry* **2014**, *53*, 6243-6251. doi: 10.1021/bi501002d.
90. Bera, A.; Herbert, S.; Jakob, A.; Vollmer, W.; Gotz, F. Why are pathogenic staphylococci so lysozyme resistant? The peptidoglycan *O*-acetyltransferase OatA is the major determinant for lysozyme resistance of *Staphylococcus aureus*. *Mol. Microbiol.*, **2005**, *55*, 778-787.
91. Bernard, E.; Rolain, T.; Courtin, P.; Guillot, A.; Langella, P.; Hols, P.; Chapot-Chartier, M.P. Characterization of *O*-acetylation of *N*-acetylglucosamine: a novel structural variation of bacterial peptidoglycan. *J. Biol. Chem.*, **2011**, *286* (27), 23950-23958. doi: 10.1074/jbc.M111.241414.
92. Bera, A.; Biswas, R.; Herbert, S.; Gotz, F. The presence of peptidoglycan *O*-acetyltransferase in various Staphylococcal species correlates with lysozyme resistance and pathogenicity. *Infection and Immunity*, **2006**, *74* (8), 4598-4604. doi: 10.1128/IAI.00301-06.
93. Weadge, J.T.; Pfeffer, J.M.; Clarke, A.J. Identification of a new family of enzymes with potential *O*-acetylpeptidoglycan esterase activity in both Gram-positive and Gram-negative bacteria. *BMC Microbiol.*, **2005**, *5*, 49. doi: 10.1186/1471-2180-5-49.
94. Moynihan, P.J.; Clarke, A.J. *O*-acetylation of peptidoglycan in Gram-negative bacteria: identification and characterization of peptidoglycan *O*-acetyltransferase in *Neisseria gonorrhoeae*. *J. Biol. Chem.*, **2010**, *285*, 13264-13273. doi: 10.1074/jbc.M110.107086.

Chapter 2

CHARACTERIZATION OF PEPTIDOGLYCAN *O*-ACETYLTRANSFERASE B (PatB)

2.1 Introduction

The bacterial enzyme, peptidoglycan *O*-acetyltransferase B (PatB), was first identified in Gram-negative bacteria by Clarke and coworkers.¹ PatB is a periplasmic enzyme with a molecular mass of ~37,000 Da. Prior to its identification as an acetyltransferase, the hypothetical protein was originally considered to be an esterase based on sequence alignment with other esterase enzymes.² However, Clarke and coworkers demonstrated in 2010 that when PatB was incubated with *O*-acetylated peptidoglycan, no acetate release was observed.¹ In addition, they showed that when they expressed PatB in *E. coli*, which does not acetylate its peptidoglycan, the resulting peptidoglycan is acetylated. Therefore they concluded that PatB is indeed an *O*-acetyltransferase.

It is believed that PatB functions in conjunction with peptidoglycan *O*-acetyltransferase A (PatA), a transmembrane protein (Figure 2.1a) that is believed to be responsible for the translocation of an acetate functional group from the cytosol to the periplasm. To date, PatA remains uncharacterized. Thus the exact mechanism through which the acetyl group is translocated is not known. However, once the acetate is in the periplasm, PatB catalyzes the transfer of an acetyl group onto the 6-hydroxyl position of NAM embedded in the peptidoglycan (Figure 2.1a).³ This means that PatB is a critical component of a bacteria's survival mechanism as acetylated

peptidoglycan is highly resistant to lysozyme degradation and the subsequent immune response.⁴ Therefore we believe that it is of critical importance to characterize PatB in order to gain a better understanding of the acetylation modification, a widely used defense mechanism by many bacterial species.

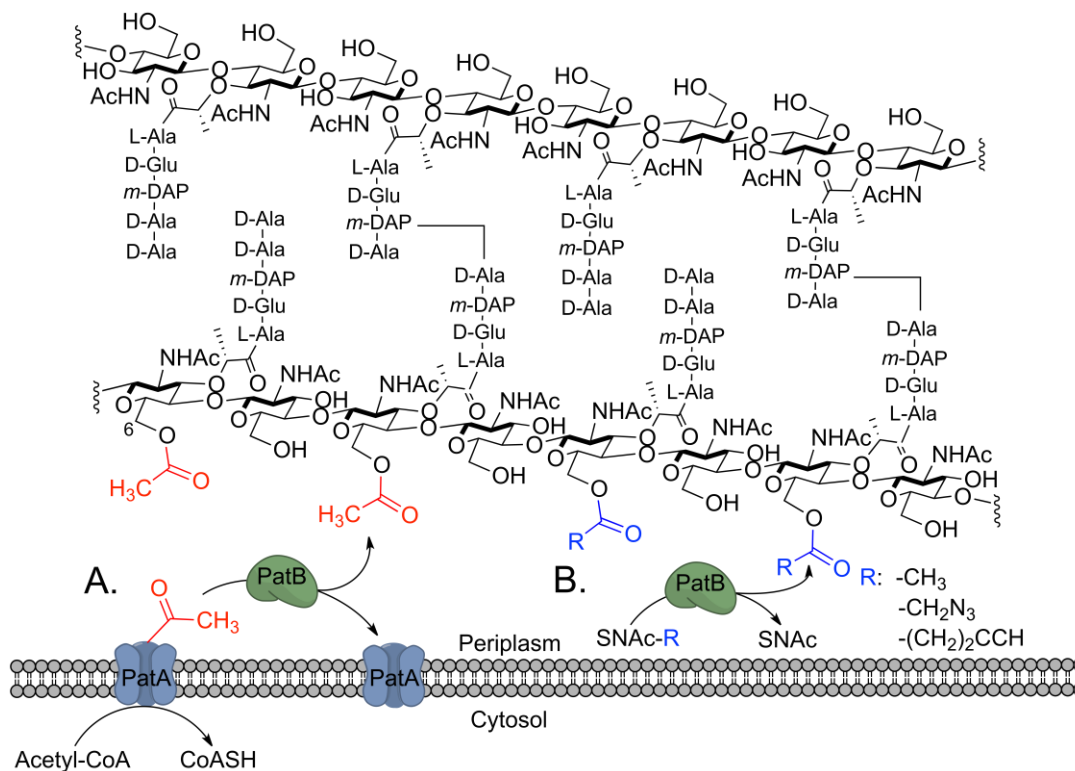


Figure 2.1: A) An acetyl functional group (red) is translocated across the plasmic membrane by PatA, where it is subsequently transferred onto the sixth hydroxyl position of NAM by PatB. B) Unnatural SNAc donors are employed to install bioorthogonal functional groups (blue) onto the peptidoglycan through PatB.

In order to study PatB, we first needed to express and purify the protein. Several attempts have been made to purify PatB with limited success. First, Clarke and coworkers chose to use the pBAD vector system to express and purify PatB.¹

However, they encountered many difficulties including mis-localization and degradation of the expressed PatB. In 2013, Clarke reported the first successful purification of a small ubiquitin-like modifier (SUMO)-tagged PatB using the pET-SUMO expression system.⁵ An attempt was made to remove the SUMO tag, but the resulting protein became highly unstable and degraded rapidly. Thus the SUMO tag was left on PatB for the characterization studies. Although a tagged protein can be used for characterization studies, a valid concern with this approach was the uncertainty of how the tag would influence the protein. The SUMO tag is roughly one third the size of PatB,⁶ so it could impact the protein folding and lead to mis-characterization of its activities. Given the importance of PatB, is it unsettling that the only biochemical information available regarding its structure and mechanism of action has been obtained with a SUMO-tagged protein. Therefore we set out to express and purify PatB without the large tag.

In this chapter, we report the expression and purification of a dual tagged PatB using Glutathione S-transferase (GST) and His₆ tags. Both tags aid in the stability and purification of PatB, but only the GST tag is cleaved post purification. Unlike the SUMO tag, the remaining small His₆ tag should not affect protein folding or function.⁷

2.2 Materials and Methods

2.2.1 Materials and Instrumentation

All chemicals were purchased from Sigma and ThermoFisher Scientific and used without further purification unless otherwise noted. GST and Ni Sepharose 6 Fast Flow beads were purchased from GE LifeSciences. IPTG and antibiotics were purchased from Gold Biotechnology. *E. coli* DH5 α and BL21 (DE3) cells were grown

from laboratory stocks. *B. subtilis* Δ Oat strain (BKE27140) was purchased from BGSC at Ohio State University. Centrifugation was performed with Eppendorf Centrifuge 5424, Sorvall RC5C Plus, or Beckman Coulter Optima L-100 XP Ultracentrifuge depending on speed and sample size. All absorbance spectra were taken with Eppendorf Bio Spectrometer.

2.2.2 Cloning of PatB Construct

The coding sequence for full-length PatB with 5'-BamHI and 3'-XhoI restriction sites was amplified by PCR from *N. gonorrhoeae* genome DNA (purchased from ATCC (#700825D-5)) using the primers PatB forward pGEX (5-CGC GGA TCC ATG TAC TGG CAG CAG ACC TAC CAC CGC-3) and PatB reverse pGEX (5-CCG CTC GAG TCA TGG CTG TGT ACT TGA TGG TTG CGT-3). The PCR product was digested with BamHI and XhoI and ligated into a pGEX-6P-1 vector to generate plasmids, which were sequenced through GENEWIZ for validation. The plasmids were transformed into *E. coli* BL21 (DE3) cells for protein expression.

2.2.3 Expression of PatB in *E. coli*

Dual-tagged PatB was expressed in 1.5 L cultures of LB media with the necessary antibiotics (carbenicillin 100 μ g/mL) at 37°C until an OD₆₀₀ of ~0.5. Protein expression was induced by the addition of 1 mM IPTG. After the addition of IPTG, the temperature was lowered to 18°C and the culture was shaken overnight. Cells were pelleted at 11,000 g for 15 min. The supernatant was discarded and the pellets were stored at -80°C until use.

2.2.4 GST- and Nickel-Affinity Purification of PatB

Cells were lysed by sonication on ice (50 Amp, 1 min total with pulsing every 2 sec) in a lysis buffer (50 mM Tris, 150 mM NaCl, 1 mM EDTA, 1 mM DTT at pH 7) containing a protease inhibitor tablet and cellular debris was collected by centrifugation at 27,000 g for 20 min. A second round of centrifugation was done on the supernatant to ensure the complete removal of cellular debris. PatB was purified using GST affinity chromatography. Briefly, the supernatant was added to a GST resin (5 mL) and incubated for 1 h. The bound PatB was eluted from the column with precision protease. Following elution, the sample was dialyzed against 50 mM Tris, 150 mM NaCl buffer at pH 7 to remove the EDTA and DTT. Post dialysis, PatB underwent a second round of purification using Ni affinity chromatography. The bound PatB was eluted with a high imidazole buffer (50 mM Tris, 500 mM Imidazole, 150 mM NaCl at pH 7). The eluted protein was dialyzed against tris buffer (50 mM Tris, 150 mM NaCl at pH 7) with a gradient of decreasing Imidazole concentrations (375 mM Imidazole, 250 mM Imidazole, 125 mM Imidazole, and 0 mM Imidazole) and purified PatB was stored at -80°C in 10% glycerol until use.

2.2.5 Biochemical Characterization of PatB

2.2.5.1 SDS PAGE Analysis

A 4-16% Bis-Tris gel (ThermoFisher Scientific) was run in a 50 mM bis-tris buffer (pH 7.5). PatB was diluted with 5x loading dye and 20 µL of the protein solution was loaded into each well. Protein ladder (10 µL) was loaded as a control. The gel was run at 200 V for 45 min at room temperature. The resulting gel was

stained with Commassie Blue dye and then destained prior to analysis on BioRad Gel Doc EZ Imager.

2.2.5.2 Circular Dichroism

The CD spectrum of PatB was taken with a JASCO J810 Spectropolarimeter with the protein solution in a cell with a pathlength of 0.1 cm. The spectrum is an average of three scans which were collected at 0.2 nm intervals over the wavelength range of 200-240 nm. Molar ellipticity ($[\theta]$) was calculated using $[\theta] = \theta / (n * C * l)$ where n is the number of residues, C is the molar concentration and l is the path length (cm). The ellipticity of the sample was corrected by a background subtraction of the buffer.

2.2.5.3 *p*-nitrophenyl acetate (*p*NP-Ac) Hydrolysis Assay

The absorbance (at 405 nm) of a 1 mM solution of *p*-nitrophenyl acetate (*p*NP-Ac) was monitored over 200 sec in the absence or presence of PatB (1 μ M) for the production of *p*-nitrophenol (*p*NP).

2.3 Results and Discussion

2.3.1 Expression and Purification of PatB

Previous purification of PatB has involved the use of a SUMO tag, which was left on the protein post purification.⁵ However, a tagged protein could lead to a misrepresentation of the protein. Therefore PatB was expressed with GST and His₆ tags on the N-terminal and C-terminal, respectively to improve stability and purification (Figure 2.2).⁸ As a part of the purification, the GST tag is cleaved from PatB. On the other hand, the His₆ tag, which was used to further purify PatB after the

initial GST purification, was left on the protein. Using this new purification system, PatB was purified with an estimated concentration of 100 $\mu\text{g/mL}$ or 0.1 mg/mL (2.70 μM) as determined by the Bradford Assay and the overall yield was $\sim 1 \text{ mg/L}$. Following purification, PatB was characterized with several biochemical techniques to confirm proper folding and activity.

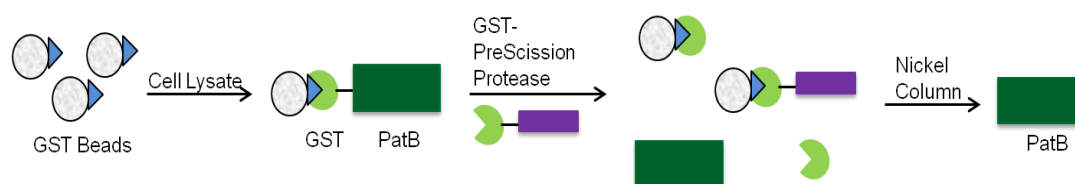


Figure 2.2: Overview of the purification scheme. The dual-tagged PatB, present in the cell lysate is incubated with GST resin. Any non-specific proteins are washed off the column prior to the addition of PreScission Protease to the column. The PreScission Protease itself is tagged with GST, but it does not have a self-cleavage site in its sequence. After over-night incubation, the PreScission Protease will cleave the GST tag off of PatB. Free GST tag and PreScission Protease are left on the column while PatB is eluted. The resulting protein is further purified by incubation with a Nickel column that will bind to the His₆ tag on PatB and allow any remaining purities to be washed away. PatB is eluted from the Nickel column with an imidazole buffer. The His₆ tag is not cleaved from PatB.

2.3.2 Biochemical Characterization of PatB

To confirm that the PatB protein was pure, properly folded and active, several analyses were performed. First the protein was analyzed on a protein gel to assess purity by the presence or absence of contaminating bands and the size of the bands as compared to the PatB band. Next a CD spectrum was obtained for PatB to determine if the purified protein was properly folded. A theoretical CD spectrum was also obtained using the amino acid sequence of PatB to use as a comparison for the experimental CD

spectrum. Lastly, PatB's esterase activity in the absence of an acceptor was tested with the established *p*NP-Ac assay to ensure that the protein is functional.

2.3.2.1 SDS PAGE Analysis

Denaturing gel electrophoresis is a standard technique that is used to separate proteins and DNA based on size and isoelectric point.⁹ Separation is accomplished with the help of an electric field that is applied as the charged proteins migrate through a porous gel matrix. Smaller proteins are able to move through the gel faster than larger proteins towards the positive electrode allowing for separation of protein mixtures. PatB was applied to a protein gel to assess purity after each purification step (Figure 2.3). In lane 1, various proteins bands can be observed in the cell lysate. Post purification with the GST column, only three bands are observed (lane 2). After additional purification with a nickel column, only the PatB band is visible (lane 3). In lane 4, there are a few faint bands on the gel in addition to the main band at 37 kDa, which corresponds to the PatB protein. The faint band at ~26 kDa is the cleaved GST tag. The faint band at ~60 kDa indicates GST tagged PatB, which was not cleaved by the GST tagged PreScission Protease (faint band around ~72 kDa) treatment. Overall, the purity of PatB was determined to be >95%.

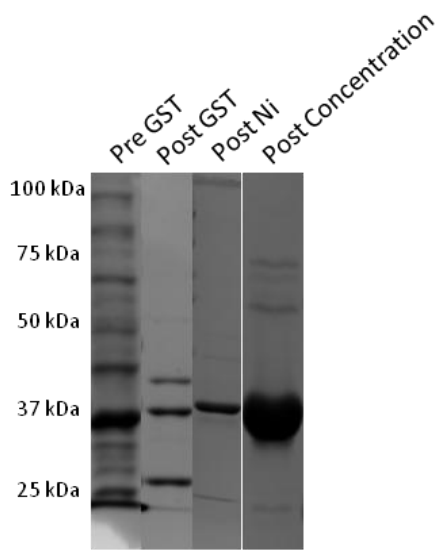


Figure 2.3: SDS page gel of purified PatB (37 kDa). The purity of PatB increases from left to right. Post cell lysis (Pre GST), there are numerous protein bands present on the gel. After PatB was applied to a GST resin column (Post GST), the number of bands was reduced to a handful. Following further purification on a Ni column (Post Ni), the main band present is PatB with a couple of very faint bands. Upon concentration, PatB is the major band present and the other bands are still very faint.

2.3.2.2 Circular Dichroism

Circular Dichroism (CD) is a classical method in biochemistry that is used to examine the structure of proteins and peptides.¹⁰ The spectra obtained with CD gives a glimpse into the secondary structure of the protein of interest because it measures the interactions of the amide bonds present in the polypeptide backbone.¹¹ Although the spectra can be complicated when there are multiple secondary structures (α -helices and β -sheets) present in the 3D structure of the protein. However using proteins that have had their crystal structures solved as references, there are certain characteristics of a spectrum that correspond to each secondary structure. For example, a β -sheet has a minimal point ~ 220 nm while a random coil has a minimal point ~ 195 nm.

The CD spectra of PatB confirmed that it was properly folded (Figure 2.4). The two minimal points at 210 and 225 nm are characteristic of a protein with α -helices in its 3D structure. In addition the experimentally obtained spectrum overlaps very well with the predicted spectrum. This supports the reasoning that the His₆ tag does not affect PatB's folding as the theoretical spectra was predicted using the full length sequence of PatB without the His₆ tag.

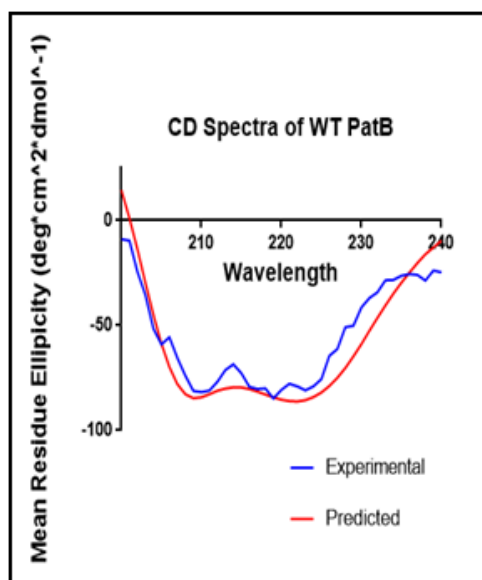


Figure 2.4: Experimental (blue) and theoretical (red) CD spectra of PatB. The two minimal points at 210 and 225 nm suggests that there are α -helices present in PatBs structure.

2.3.2.3 *p*-nitrophenyl acetate (*p*NP-Ac) Hydrolysis Assay

The *p*NP-Ac assay is a well established assay dating back to the 1940s, when it was first introduced by Huggins and Lapides.¹² They reasoned that the rate of esterase activity can be calculated by measuring the release of *p*NP ($\epsilon = 14,760 \text{ M}^{-1} \text{ cm}^{-1}$), which in solution yields a bright yellow color, over time (Figure 2.5). As shown in

figure 2.6, the rate of *p*NP release from *p*NP-Ac was 2.5x faster in the presence of PatB (blue). This indicates that the purified PatB is functional and was able to remove the acetate group from *p*NP-Ac.

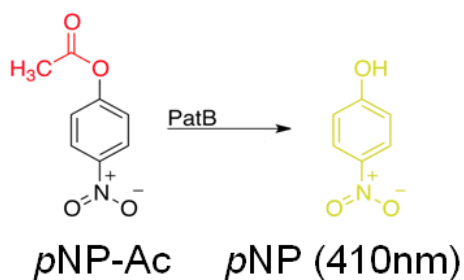


Figure 2.5: The release of *p*NP from *p*NP-Ac is used to monitor the rate of esterase (in the absence of an acceptor) or acetyltransferase (in the presence of an acceptor) activity of PatB (1 μ M).

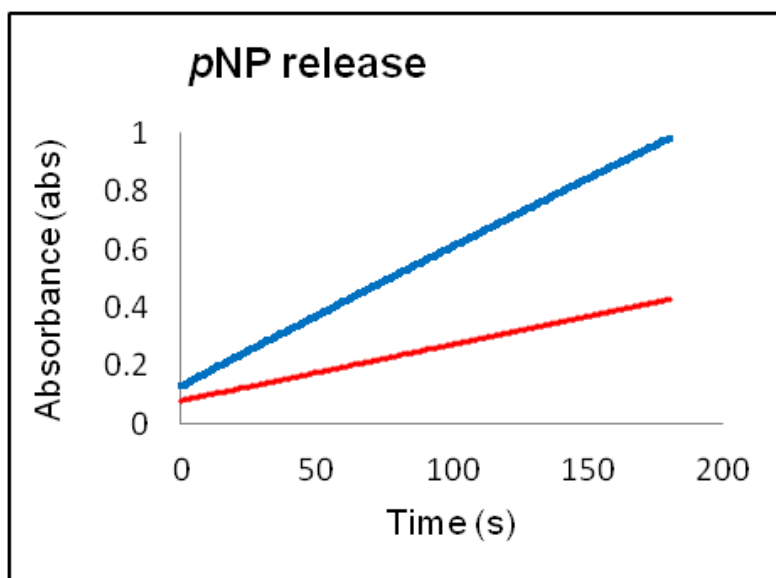


Figure 2.6: Release of *p*NP from *p*NP-Ac over time in the presence (blue) and absence (red) of PatB (1 μ M). The slope of the blue line (0.0047) is ~2.5x higher than that of the red line (0.0019).

2.4 Conclusions

This chapter detailed the development of an improved expression and purification system for a dual tagged PatB that ultimately yields a PatB without a bulky tag. The purified PatB was biochemically characterized through established biochemical techniques such as gel electrophoresis, circular dichroism, and *p*NP-Ac activity assay to ensure proper folding and function. Now that we have functional PatB in hand, we aimed to gain a better understanding of its substrate specificity.

REFERENCES

1. Moynihan, PJ.; Clarke, AJ. *O*-acetylation of peptidoglycan in Gram-negative bacteria: identification and characterization of peptidoglycan *O*-acetyltransferase in *Neisseria gonorrhoeae*. *J. Biol. Chem.*, **2010**, *285*, 13264-13273. doi: 10.1074/jbc.M110.107086.
2. Weadge, JT.; Clarke, AJ. Identification and characterization of *O*-acetylpeptidoglycan esterase: a novel enzyme discovered in *Neisseria gonorrhoeae*. *Biochemistry*, **2006**, *45* (3), 839-851. doi: 10.1021/bi051679s.
3. Moynihan, PJ.; Clarke, AJ. *O*-acetylated peptidoglycan: controlling the activity of bacterial autolysins and lytic enzymes of innate immune systems. *Intl. J. of Biochem. & Cell Biol.*, **2011**, *43* (12), 1655-1659. doi: 10.1016/j.biocel.2011.08.007.
4. Pushkaran, AC.; Nataraj, N.; Nair, N.; Gotz, F.; Biswas, R.; Mohan, CG. Understanding the structure-function relationship of lysozyme resistance in *Staphylococcus aureus* by peptidoglycan *O*-acetylation using molecular docking, dynamics, and lysis assay. *J. Chem. Inf. Model.*, **2015**, *55* (4), 760-770. doi: 10.1021/ci500734k.
5. Moynihan, PJ.; Clarke, AJ. Assay for peptidoglycan *O*-acetyltransferase: a potential ne antibacterial target. *Anal. Biochem.*, **2013**, *439* (2), 73-79. doi: 10.1016/j.ab.2013.04.022.
6. Panavas, T.; Sanders, C.; Butt, TR. SUMO fusion technology for enhanced protein production in prokaryotic and eukaryotic expression systems. *Methods Mol. Biol.*, **2009**, *497*, 303-317. doi: 10.1007/978-1-59745-566-4_20.
7. Carson, M.; Johnson, DH.; McDonald, H.; Brouillette, C.; DeLucas, LJ. His-tag impact on structure. *Acta. Cryst.*, **2007**, *D63*, 295-301. doi: 10.1107/S09074444906052024.

8. Esposito, D.; Chatterjee, DK. Enhancement of soluble protein expression through the use of fusion tags. *Curr. Opin. Biotechnol.*, **2006**, *17* (4), 353-358. doi: 10.1016/j.copbio.2006.06.003.
9. Laemmli, UK. Cleavage of structural proteins during the assembly of the head of bacteriophage T4. *Nature*, **1970**, *227* (5259), 680-685. PMID: PMC5432063.
10. Woody, RW. Circular Dichroism. *Methods Enzymol.*, **1995**, *246*, 34-71. doi: 10.1016/0076-6879(95)46006-3.
11. Micsonai, A.; Wien, F.; Kernya, L.; Lee, YH.; Goto, Y.; Refregiers, M.; Kardos, J. Accurate secondary structure prediction and fold recognition for circular Dichroism spectroscopy. *Proc. Natl. Acad. Sci. USA*, **2015**, *112* (24), E3095-3103. doi: 10.1073/pnas.1500851112.
12. Huggins, C. & Lapides, J. Chromogenic substrates: IV. Acyl esters of *p*-nitrophenol as substrates for the colorimetric determination of esterase. (1947). *J. Biol. Chem.*, **1947**, *170*, 467-482.

Chapter 3

EXPLORATION OF PatB'S DONOR PREFERENCE WITH *p*NP AND SNAC DERIVATIVES

3.1 Introduction

The proposed natural source of the acetate functional group utilized by PatB is acetyl-CoA (**5**, Figure 3.1).¹ However PatB does not directly interact with acetyl-CoA as **5** is not found in the periplasm. Therefore it is believed that PatB functions in tandem with PatA to modify peptidoglycan. PatA moves the acetate group across the membrane where it then hands it off to PatB. It is reasonable to hypothesize that the acetyl group is likely linked to either a serine/threonine or cysteine residue of PatA through an ester or thio ester bond respectively. When exploring the substrate specificity of PatB, donors that contain both types of bonds were considered.

The Clarke group has elegantly demonstrated that purified PatB accepts *p*NP-Ac (**1**, Figure 3.1), an acetyl-coA mimic, to label small molecule PG fragments *in vitro*. In addition, they demonstrated that PatB hydrolyzes propionyl CoA.² Intrigued by PatB's promiscuity, we set out to determine if the enzyme could be used to install bioorthogonal functionality onto the peptidoglycan (Figure 2.1b), which could help to illuminate the mechanism and extent of modification of *O*-acetylation.

To that end, a variety of *p*NP based acetyl donors, containing alkyne, azido, and phenyl functionalities, were synthesized (**2-4**, Figure 3.1) and assayed for compatibility with PatB through the *p*NP-Ac hydrolysis assay. In addition, it was hypothesized that smaller variants of acetyl-CoA (**5**) could be used as potential donors

as a variety of CoA ester-utilizing enzymes have been reported to accept truncated CoA thioesters known as short *N*-acetylcysteamine thioesters (SNAc) (Figure 3.1).^{3,4,5,6}

In 2005, Pohl and coworkers used SNAc analogues to prepare labeled sugar nucleotides with bioorthogonal functionality,⁷ noting that SNAcs are advantageous compared to their CoA derivatives due to their synthetic simplicity.^{8,9} To assess the possibility of using these short acetyl-CoA compounds as donors for PatB, *S*-(2-acetamidoethyl)-ethanethioate (SNAc, **6**),⁸ a novel azido SNAc derivative, *S*-(2-acetamidoethyl)-2-azidoethanethioate (SNAz, **7**) along with an alkynyl form, *S*-(2-acetamidoethyl)-2-alkynylethanethioate (SNAk, **8**)⁹ were synthesized (Figure 2c). Following synthesis and characterization of all the donors, they were assayed for suitability as substrates for PatB.

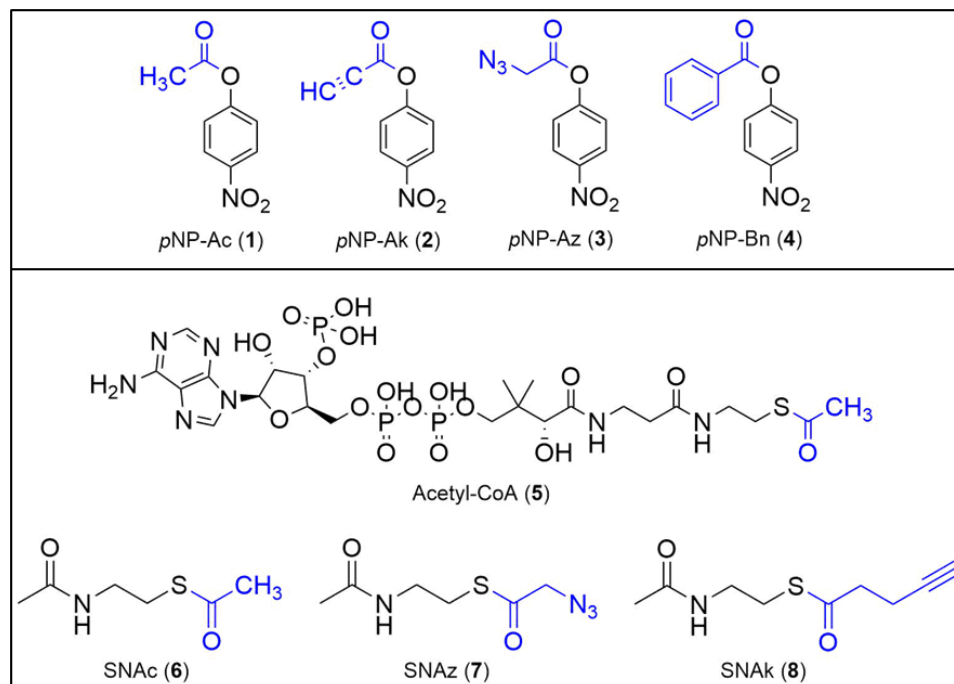


Figure 3.1: Two set of donors were synthesized to probe for PatB's donor specificity. The first set of donors retained the *p*NP moiety (top row) and the second set of donors were short *N*-acetyl cysteamine derivatives (bottom row) that resemble the natural substrate, acetyl-CoA (middle).

3.2 Materials and Methods

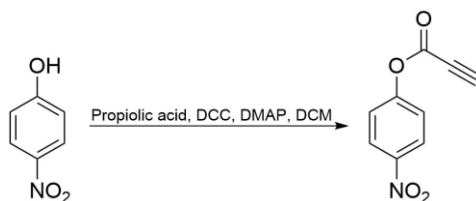
3.2.1 Materials and Instrumentation

All chemicals were purchased from Sigma and ThermoFisher Scientific and used without further purification unless otherwise noted. All solvents were reagent grade anhydrous purchased from Sigma. (NAG)₃ was purchased from TCI America. Deuterated NMR solvents were purchased from Cambridge Isotope Laboratories.

NMR spectra were recorded on either a Bruker AVIII 400 MHz or AV III 600 MHz spectrometers. High Res Mass spectra (ESI) were obtained at the Department of Chemistry, University of Delaware Mass Spectrometry Facility (Thermo Q-Exactive

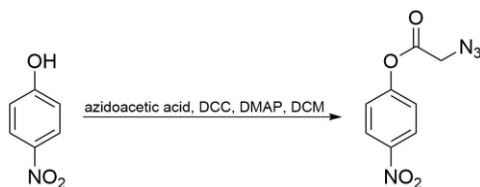
Orbitrap). Mass Spectra were obtained using an ACQUITY UPLC H-Class/SQD2 at the Department of Chemistry, University of Delaware Mass Spectrometry Facility. IR spectra were obtained with Thermo Nicolet IR 100 Spectrometer. All absorbance spectra were taken with Eppendorf BioSpectrometer. All reactions were performed under nitrogen unless specified otherwise. Analytical thin-layer chromatography was performed on silica gel glass plates (250 μm , Sorbent Technologies) and visualized via UV and para-anisaldehyde stain. Flash chromatography was carried out on silica gel (60 \AA , 40-63 μm), purchased from Sorbent Technologies. Chemical shifts are reported in units of parts per million (ppm). Multiplicities are reported with following abbreviations: bs= broad singlet, s = singlet, d = doublet, t = triplet, td= triplet of doublets, q = quartet, m = multiplet, J = coupling constant in Hertz.

3.2.2 Synthesis of *p*NP Derivatives

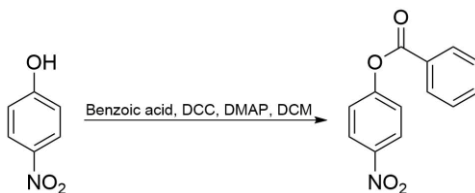


4-nitrophenyl propiolate (*p*NP-Ak) (2): para-nitrophenol (0.952 g, 7 mmol, 1 eq), propiolic acid (0.560 g, 8 mmol, 1.1 eq) and DCC (2.0 g, 10 mmol, 1.25 eq) were stirred together in 10 mL of anhydrous DCM for 1 h at 0°C under nitrogen. DMAP (0.002 g, 0.02 mmol, 0.025 eq) was then added and the solution was allowed to warm to room temperature overnight. The solution was then filtered and condensed. The crude compound was then purified by column chromatography, 100% chloroform, to yield a colorless solid (1.05 g, 81%). NMR data matched previously reported data.¹⁰ ¹H NMR (400 MHz, Chloroform-*d*) δ 8.31 (d, 2H, benzyl), 7.36 (d, 2H, benzyl), 1.55

(s, 1H, CCH). ^{13}C NMR (151 MHz, Chloroform-*d*) δ 154.38, 149.81, 145.93, 125.53, 122.38, 78.26, 73.64. HRMS (ESI-pos) for $\text{C}_9\text{H}_6\text{NO}_4^+$ $[\text{M}+\text{H}]^+$: calculated 192.02913, observed 192.02921.

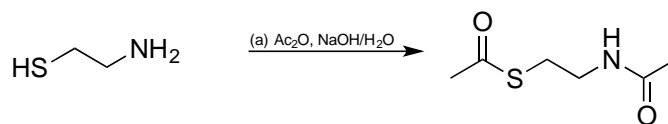


4-nitrophenyl 2-azidoacetate (*p*NP-Az) (**3**): para-nitrophenol (1.00 g, 7.18 mmol, 1 eq), azidoacetic acid (0.808 g, 8 mmol, 1.1 eq) and DCC (2.0 g, 10 mmol, 1.25 eq) were stirred together in 10 mL of anhydrous DCM for 1 h at 0°C under nitrogen. DMAP (0.002 g, 0.02 mmol, 0.025 eq) was then added and the solution was allowed to warm to room temperature overnight. The solution was then filtered and condensed. The crude compound was then purified by column chromatography, 100% chloroform, to yield a colorless solid (1.37 g, 86%). NMR data matched previously reported data.¹¹ ^1H NMR (400 MHz, Chloroform-*d*) δ 8.31 (d, 2H, benzyl), 7.36 (d, 2H, benzyl), 4.20 (s, 2H, CH_2N_3). ^{13}C NMR (151 MHz, Chloroform-*d*) δ 166.17, 154.66, 145.88, 125.52, 122.28, 50.55. Additional peaks from DMAP present in proton and carbon NMR. HRMS (ESI-pos) for $\text{C}_8\text{H}_7\text{N}_4\text{O}_4^+$ $[\text{M}+\text{H}]^+$: calculated 223.04618, observed 223.04630. IR shift: 2105.73 cm^{-1} (Azide).



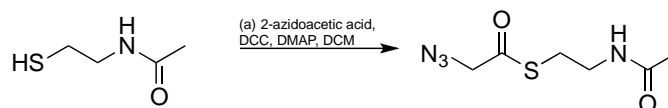
4-nitrophenyl benzoate (*p*NP-Bn) (4): para-nitrophenol (0.142 g, 1.02 mmol, 1.25 eq), benzoic acid (0.100 g, 0.819 mmol, 1 eq) and DCC (0.211 g, 1.02 mmol, 1.25 eq) were stirred together in 1 mL of anhydrous DCM for 1 h at 0°C under nitrogen. DMAP (0.002 g, 0.02 mmol, 0.025 eq) were then added and the solution was allowed to warm to room temperature overnight. The solution was then filtered and condensed. The crude compound was then purified by column chromatography, 100% chloroform, to yield a colorless solid (0.179 g, 90%). NMR data matched previously reported data.¹² ¹H NMR (400 MHz, Chloroform-*d*) δ 8.35 (d, 2H, benzyl), 8.21 (d, 2H, benzyl), 7.68 (t, 1H, benzyl), 7.55 (t, 2H, benzyl), 7.43 (d, 2H, benzyl). ¹³C NMR (151 MHz, Chloroform-*d*) δ 164.37, 155.84, 145.51, 134.40, 130.46, 128.93, 128.62, 125.42, 122.79. Additional peaks from DMAP present in proton and carbon NMR. HRMS (ESI-pos) for C₁₃H₁₀NO₄⁺ [M+H]⁺: calculated 244.06043, observed 244.06064.

3.2.3 Synthesis of SNAc Derivatives



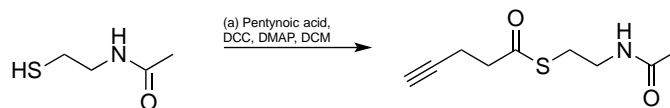
S-(2-acetamidoethyl) ethanethioate (SNAc) (6): Cysteamine HCl (1.00 g, 8.8 mmols) was dissolved in 8 mL of water. The pH was adjusted to 8 on ice with 4 N KOH. Acetic anhydride (2.5 mL, 24.5 mmols, 3 eq) was added dropwise, while maintaining the pH at 8 by the addition of 4 N KOH periodically. Following acetic

anhydride addition, 1 N HCl was added to adjust the pH to 7. The reaction mixture stirred at 0°C for 1.5 h until completion which was determined by TLC (TLC=20%MeOH in DCM, R_f = 0.6). Saturated NaCl was added and the product was extracted with DCM. The organic layer was dried with sodium sulfate and condensed. The resulting oil was purified using column chromatography (100% ethyl acetate) to yield a colorless oil (0.750 g, 43%). NMR data matched previously reported data.⁸ ¹H NMR (600 MHz, Chloroform-*d*) δ 6.02 (s, 1H, NH), 3.43 (q, J = 6.3 Hz, 2H, CH₂NH), 3.03 (t, J = 6.5 Hz, 2H, CH₂S), 2.36 (s, 3H, acetyl), 1.97 (s, 3H, acetyl). ¹³C NMR (151 MHz, Chloroform-*d*) δ 196.37, 170.30, 39.68, 30.72, 29.03, 23.28. HRMS (ESI-pos) for C₆H₁₂NO₂S⁺ [M+H]⁺: calculated 162.05833, observed 162.05845.



S-(2-(2-azidoacetamido)ethyl) ethanethioate (SNAz) (7): Azidoacetic acid (0.057 mls, 0.77 mmol) and DCC (0.173 g, 0.84 mmols, 1.1 eq) were stirred together in 11 mL of anhydrous DCM for 5 min at 0°C. *N*-acetylcysteamine (0.089 mls, 0.84 mmol, 1.1 eq) and DMAP (0.093 g, 0.76 mmol, 1 eq) were then added and the solution was allowed to warm to room temperature overnight. The solution was filtered and condensed, then dissolved in ethyl acetate. The ethyl acetate solution was filtered into a separatory funnel through filter paper. The organic layer was washed with brine, dried with sodium sulfate and condensed. The crude oil was then purified by column chromatography, 25-100% EtOAc in hexanes, to yield a colorless oil (0.078 g, 51%). R_f =0.25 in EtOAc. ¹H NMR (400 MHz, Methanol-*d*₄) δ 4.15 (s, 2H, CH₂N₃), 3.37 (t, J = 6.6 Hz, 2H, HNCH₂CH₂S), 3.09 (t, J = 6.6 Hz, 2H, HNCH₂CH₂S), 1.93 (s, 3H, acetyl). ¹³C NMR (101 MHz, Methanol-*d*₄) δ 195.55,

172.12, 57.45, 38.41, 27.72, 21.06. HRMS (ESI-pos) for $C_6H_{11}N_4O_2S^+$ $[M+H]^+$: calculated 203.05972, observed 203.05939. IR shift: 2099.29cm^{-1} (Azide).



S-(2-(pent-4-ynamido)ethyl ethanethioate (SNAk) (8): Pentynoic acid (0.123 g, 1.25 mmol) and DCC (0.234 g, 1.38 mmols, 1.1 eq) were stirred together in 17 mL of anhydrous DCM for 5 min at 0°C . *N*-acetylcysteamine (0.134 mL, 1.38 mmol, 1.1 eq) and DMAP (0.153 g, 1.25 mmol, 1 eq) were then added and the solution was allowed to warm to room temperature overnight. The solution was then filtered and condensed, then dissolved in ethyl acetate. The ethyl acetate solution was then filtered through filter paper into a separatory funnel. The organic layer was washed with brine, dried with sodium sulfate and condensed. The crude oil was then purified by column chromatography, 20-80% EtOAc in hexanes, to yield a colorless oil (0.096 g, 39%). NMR data matched previously reported data.⁹ ^1H NMR (600 MHz, Chloroform-*d*) δ 5.81 (s, 1H, *NH*), 3.44 (q, $J = 6.1$ Hz, 2H, $\text{HNCH}_2\text{CH}_2\text{S}$), 3.06 (t, $J = 6.4$ Hz, 2H, $\text{HNCH}_2\text{CH}_2\text{S}$), 2.81 (t, $J = 7.2$ Hz, 2H, $\text{CH}_2\text{CH}_2\text{CCH}$), 2.54 (td, $J = 7.2, 2.6$ Hz, 2H, $\text{CH}_2\text{CH}_2\text{CCH}$), 1.99 (t, $J = 2.6$ Hz, 1H, $\text{CH}_2\text{CH}_2\text{CCH}$), 1.96 (s, 3H, acetyl). ^{13}C NMR (151 MHz, Chloroform-*d*) δ 198.01, 170.39, 81.90, 69.66, 42.55, 39.71, 28.80, 23.37, 14.83. HRMS (ESI-pos) for $C_9H_{14}NO_2S^+$ $[M+H]^+$: calculated 200.07398, observed 200.07380.

3.2.4 Analysis of Esterase Activity

3.2.4.1 *p*-nitrophenyl acetate (*p*NP-Ac) Hydrolysis Assay

PatB (1 μ M) was incubated with varying concentrations of donors to determine the esterase kinetics of the donors. For the *p*NP-R donors, the absorbance at 405 nm was monitored over 8 min at room temp for the release of *p*NP. The absorbance of controls (Buffer only, Buffer with PatB, Buffer with donors, and Buffer with PatB and donors) were plotted to obtain the initial velocity of each control. The control with the highest initial velocity (Buffer with donors) was subtracted from the samples (Buffer with PatB and donors) prior to graphing the sample (i.e. Background was subtracted from control that contained all components of the reaction except PatB). The initial velocity data for each of the donor concentrations were plotted and the K_m and k_{cat} values were calculated using nonlinear regression analysis. Each kinetic analysis was done in triplicates.

3.2.4.2 Analysis of Hydrolysis Activity with Ellman's Reagent

PatB (1 μ M) was incubated with varying concentrations of donors to determine the esterase kinetics of the donors. For the SNAc donors, Ellman's reagent (5,5-dithio-bis-(2-nitrobenzoic acid) (DTNB) (1 mM)) was added to the reaction mixture and the absorbance at 412 nm was monitored over time at room temp for the presence of a free thiol. The absorbance of controls (Buffer only, Buffer with DTNB, Buffer with DTNB and PatB, Buffer with DTNB and donors, and Buffer with DTNB and PatB and donors) were plotted to obtain the initial velocity of each control. The control with the highest initial velocity (Buffer with DTNB and donors) was subtracted from the samples (Buffer with DTNB and PatB and donors) prior to graphing the sample (ie. Background was subtracted from control that contained all components of the reaction

except PatB). The initial velocity data for each of the donor concentrations were plotted and the K_m and k_{cat} values were calculated using nonlinear regression analysis. Each kinetic analysis was done in triplicates.

3.3 Results and Discussion

3.3.1 Synthesis of *p*NP Derivatives

Three different derivatives (*p*NP-Ak, *p*NP-Az, and *p*NP-Bn) of *p*NP containing different functional groups (alkyne, azide, and phenyl) were synthesized to assess PatB's versatility in donors. All three compounds were synthesized through the Steglich esterification¹³ method using DCC as a coupling reagent and DMAP as a catalyst. NMR (proton and carbon), HRMS, and IR (for *p*NP-Az) were obtained for all the compounds to ensure identity and purity. See appendix for spectroscopic data.

3.3.2 Synthesis of SNAc Derivatives

Three different SNAc derivatives (SNAc, SNAz, and SNAk) containing different functional groups were synthesized to further assess PatB's versatility in utilizing short acetyl-CoA donors. SNAc and SNAk were synthesized according to literature precedence.^{8,9} SNAz is a novel compound reported here for the first time. NMR (proton and carbon), HRMS, and IR (for *p*NP-Az) were obtained for all the compounds to ensure identity and purity. See appendix for spectroscopic data.

3.3.3 Analysis of Esterase Activity

The ability of PatB to utilize the *p*NP and SNAc donors were assessed through esterase activities. For the *p*NP donors, *p*NP-Ac assay (described in Chapter 2) was repeated.¹⁴ For the SNAc donors, we turned to another established assay using

Ellman's Reagent, DTNB.¹⁵ If PatB is able to utilize the SNAc donors, then the thioester bond would be broken generating in a free thiol, which would attack the disulfide bond present in DTNB. As a result 2-nitro-5-thiobenzoate (TNB) would be produced giving the solution a bright yellow color that can be measured spectroscopically (Figure 3.2).

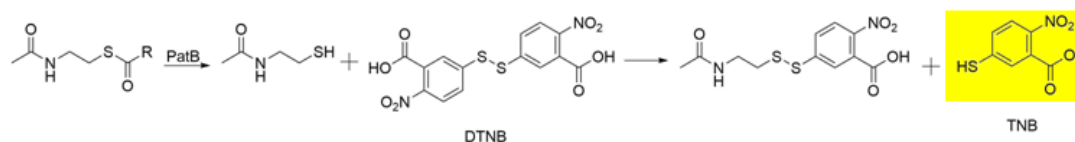


Figure 3.2: Determining the esterase activity of PatB with SNAc donors by measuring the production rate of TNB at 412 nm.

3.3.3.1 *p*-nitrophenyl acetate (*p*NP-Ac) Hydrolysis Assay

Under conditions reported in literature, the kinetic parameters for PatB's esterase activity with *p*NP donors were calculated (Table 3.1). Both the K_m and the overall K_{cat}/K_m value for all the *p*NP donors were similar to those that have been published (*p*NP-Ac: $K_m = 0.96$ mM and $K_{cat}/K_m = 797$ M⁻¹ sec⁻¹) indicating that the PatB used in this study is as efficient as the previously expressed SUMO-tagged PatB at hydrolyzing the *p*NP donors.²

Table 3.1: Esterase activity of PatB (1 μ M) with *p*NP donors at pH 6.5 (sodium phosphate buffer) as monitored at 405 nm.

Substrate	Esterase Activity		
	K_m (mM)	K_{cat} (sec^{-1})	K_{cat}/K_m ($\text{M}^{-1}\text{sec}^{-1}$)
<i>p</i> NP-Ac	0.91	0.741	814
<i>p</i> NP-Ak	0.83	0.524	631
<i>p</i> NP-Az	0.87	0.626	719
<i>p</i> NP-Bn	0.86	0.581	675

3.3.3.2 Analysis of Hydrolysis Activity with Ellman's Reagent

Using the established DTNB assay, the kinetic parameters for PatB's esterase activity with SNAc donors as well as acetyl-CoA were calculated (Table 3.2). Despite the fact that the K_m values were slightly higher than those of *p*NP donors, the overall K_{cat}/K_m value for all the SNAc donors were approximately four times lower than those of *p*NP donors. In order to optimize the transfer, we reasoned that pH of the reaction could be important, as the natural environment (the periplasm of *N. gonorrhoeae*) in which PatB resides in is slightly basic.^{16,17} The kinetic analysis was repeated in a tris buffer (pH 8.5) and the overall K_{cat}/K_m value for all the SNAc donors were approximately eight to ten times higher at pH 8.5 than at pH 6.5. Moreover, the K_{cat}/K_m values for SNAc donors at pH 8.5 are approximately twice as high as the K_{cat}/K_m values for *p*NP donors at pH 6.5. It is noted that at either pH, PatB is not very efficient at using acetyl-CoA as a donor. On the other hand, this is not surprising since

PatA is the enzyme proposed to be responsible for interacting with acetyl-CoA directly, not PatB.

Table 3.2: Esterase activity of PatB (1 μ M) with acetyl-CoA and SNAc donors at pH 6.5 (sodium phosphate buffer) and pH 8.5 (tris buffer) as monitored at 412 nm.

Substrate	Esterase Activity					
	pH = 6.5			pH = 8.5		
	K_m (mM)	K_{cat} (sec^{-1})	K_{cat}/K_m ($\text{M}^{-1}\text{sec}^{-1}$)	K_m (mM)	K_{cat} (sec^{-1})	K_{cat}/K_m ($\text{M}^{-1}\text{sec}^{-1}$)
Acetyl-CoA	0.90	0.016	18.0	0.88	0.092	104.5
SNAc	1.14	0.238	208.8	1.08	1.82	1,685
SNAz	1.03	0.148	143.7	1.01	1.22	1,208
SNAk	1.27	0.209	164.6	1.09	1.76	1,614

3.4 Conclusions

This chapter detailed the synthesis and enzymatic utilization of two sets of donors for PatB. PatB was able to use all of the donors as determined through esterase assays. We also found that our PatB has higher activity at a pH of 8.5, which is in contrast with previous studies that had suggested that PatB would have maximal activity at pH 7.0.¹⁸ However, those results were again obtained with a SUMO-tagged PatB, which leads to us to doubt their validity. The results presented here indicate that PatB has higher activity at a more basic pH, which is representative of its natural

environment. Now that we have donors that PatB can utilize, we set our sights on studying the acceptor specificity of PatB.

REFERENCES

1. Moynihan, PJ.; Clarke, AJ. *O*-acetylated peptidoglycan: controlling the activity of bacterial autolysins and lytic enzymes of innate immune systems. *Intl. J. of Biochem. & Cell Biol.*, **2011**, *43* (12), 1655-1659. doi: 10.1016/j.biocel.2011.08.007.
2. Moynihan, PJ.; Clarke, AJ. Substrate specificity and kinetic characterization of peptidoglycan *O*-acetyltransferase B from *Neisseria gonorrhoeae*. *J. Biol. Chem.*, **2014**, *289* (24), 16748-16760. doi: 10.1074/jbc.M114.567388.
3. Gerstein, J.; Jencks, WP. Equilibria and rates for acetyl transfer among substituted phenyl acetates, acetylimidazole, *O*-acylhydroxamic acids and thiol esters. *J. Am. Chem. Soc.*, **1964**, *86* (21), 4655-4663. doi: 10.101/ja01075a027.
4. Jacobsen, JR.; Hutchinson, CR.; Cane, DE.; Khosla, C. Precursor-directed biosynthesis of erythromycin analogs by an engineered polyketide synthase. *Science*, **1997**, *277*(5324), 367-369. doi: 10.1126/science.277.5324.367.
5. Mishra, PK.; Drucekhammer, DG. Coenzyme A analogues and derivatives: synthesis and applications as mechanistic probes of Coenzyme A ester-utilizing enzymes. *Chem. Rev.*, **2000**, *100* (9), 3283-3310. doi: 10.1021/cr990010m.
6. Xie, X.; Watanabe, K.; Wojcicki, WA.; Wang, CC.; Tang, Y. Biosynthesis of iostatatin analogs with a broadly specific acyltransferase. *Chem. & Biol.*, **2006**, *13* (11), 1161-1169. doi: 10.1016/j.chembiol.2006.09.008.
7. Mizanur, RM.; Jaipuri, FA.; Pohl, NL. One-step synthesis of labeled sugar nucleotides for protein *O*-GlcNAc modification studies by chemical function analysis of an Archaeal protein. *J. Am. Chem. Soc.*, **2005**, *127* (3), 836-837. doi: 10.1021/ja044117p.

8. Schwab, JM.; Klassen, JB. Steric course of the allylic rearrangement catalyzed by β -hydroxydecanoylthioester dehydrase. Mechanistic implications. *J. Am. Chem. Soc.*, **1984**, *106* (23), 7217-7227. doi: 10.1021/ja00335a060.
9. Sandy, M.; Zhu, X.; Rui, Z.; Zhang, W. Characterization of AntB, a promiscuous acyltransferase involved in antimycin biosynthesis. *Org. Lett.*, **2013**, *15* (13), 3396-3399. doi: 10.1021/ol4014365.
10. Bialecka-Florjanczyk, E. A simple method for the preparation of substituted phenoxyacrylic acid phenyl esters. *Syn. Comm.*, **2000**, *30* (24), 4417-4424. doi: 10.1080/00397910008087068.
11. Ortiz Barbosa, YA.; Hart, DJ.; Magomedov, NA. Spiroquinazoline support studies: methods for the preparation of imidazoloindolines from oxindoles. *Tetrahedron*, **2006**, *62* (37), 8748-8754. doi: 10.1016/j.tet.2006.06.103.
12. Ueda, M.; Mori, H. Diphenyl (2,3-dihydro-2-thioxo-3-benzoxazolyl)phosphonate: a new, reactive condensing agent for the synthesis of amides, esters, peptides, and β -lactams via condensation. *Bull. Chem. Soc. Jpn.*, **1992**, *65* (6), 1636-1641. doi: 10.1246/bcsj.65.1636.
13. Neises, B.; Steglich, W. Simple method for the esterification of carboxylic acids. *Angew. Chem. Int. Ed. Engl.*, **1978**, *17*, 522-524. doi: 10.1002/anie.197805221.
14. Huggins, C. & Lapides, J. Chromogenic substrates: IV. Acyl esters of *p*-nitrophenol as substrates for the colorimetric determination of esterase. (1947). *J. Biol. Chem.*, **1947**, *170*, 467-482.
15. Riddles, PW.; Blakeley, RL.; Zenner, B. Ellman's reagent: 5,5'-dithiobis(2-nitrobenzoic acid)-a reexamination. *Anal. Biochem.*, **1979**, *94* (1), 75-81. doi: 10.1016/0003-2697(79)90792-9.
16. Brookes, R.; Sikyta, B. Influence of pH on the growth characteristics of *Neisseria gonorrhoeae* in continuous culture. *Appl. Microbiol.*, **1967**, *15* (2), 224-227. PMID: PMC546882.
17. Morse, SA.; Hebel, BH. Effect of pH on the growth and glucose metabolism of *Neisseria gonorrhoeae*. *Infect. Immun.* **1978**, *21* (1), 87-95. PMID: PMC421961.

18. Moynihan, PJ.; Clarke, AJ. Mechanism of action of peptidoglycan *O*-acetyltransferase B involves a Ser-His-Asp catalytic triad. *Biochemistry* **2014**, *53*, 6243-6251. doi: 10.1021/bi501002d.

Chapter 4

EXPLORATION OF PatB'S ACCEPTOR SPECIFICITY

4.1 Introduction

In order to get a more complete mechanistic picture of PatB, we aimed to study its acceptor specificity. Given that PatB modifies the carbohydrate backbone of peptidoglycan, we know that it prefers oligosaccharides. However, we wanted to determine if PatB is able to modify smaller molecules. We explored mono- and trisaccharides as potential acceptors. In addition we isolated peptidoglycan from both Gram (+) and Gram (-) bacterial species to determine if PatB is capable of modifying both types of peptidoglycan. Although there are subtle differences (described in Chapter 1) between the two types of bacteria,¹ those differences are typically in the peptide stem, not the carbohydrate backbone. Therefore we believe that PatB should be able to modify isolated peptidoglycan from both Gram (+) and Gram (-) bacterial species despite the fact that PatB itself is only found in Gram (-) bacteria.

The Clarke group has shed some light on the acceptor requirements of PatB. They demonstrated that SUMO-tagged PatB will only modify an oligosaccharide that is at least three sugars (trisaccharide) in length. Also they observed that the acetylation of the 2-amino group of NAG and NAM is necessary for PatBs activity.² Given that our donor data was in contrast with the published data, we were interested in how our acceptor data would compare.

Moreover, we were interested in finding a small molecule acceptor for PatB so that we can assess its acetyltransferase activity. Although the kinetics data for PatB's

esterase activity informed us that PatB was able to take the functional group of interest from the donors, we needed an appropriate acceptor in order to determine if PatB is able transfer the functional group.

The acceptors tested (Figure 4.1) were readily available mono- and trisaccharides. Peptidoglycan is available for purchase through companies such as Sigma. However the selection is small and expensive. In addition, there is incredible batch to batch variation. Therefore we decided to isolate peptidoglycan following literature precedence with slight modifications.³ Following isolation, the peptidoglycan was characterized using several methods in order to confirm identity prior to analysis with PatB.

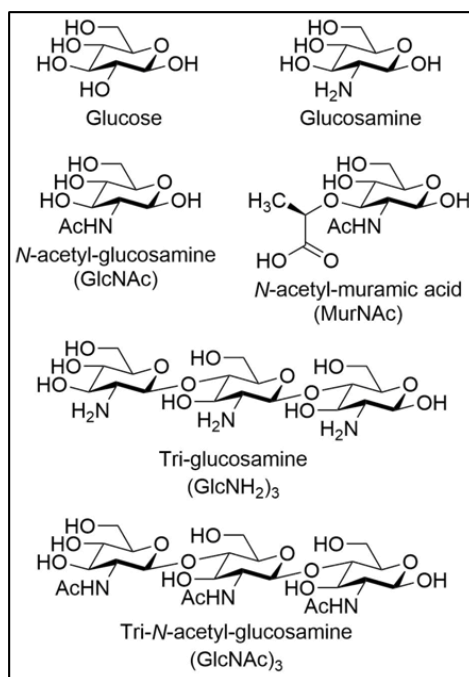


Figure 4.1: To assess PatB's acceptor specificity, various monosaccharide and trisaccharide acceptors were tested with PatB and *p*NP and SNAc donors.

4.2 Materials and Methods

4.2.1 Materials and Instrumentation

All chemicals were purchased from Sigma and ThermoFisher Scientific and used without further purification unless otherwise noted. High Res Mass spectra (ESI) were obtained at the Department of Chemistry, University of Delaware Mass Spectrometry Facility (Thermo Q-Exactive Orbitrap). Mass Spectra were obtained using an ACQUITY UPLC H-Class/SQD2 at the Department of Chemistry, University of Delaware Mass Spectrometry Facility. All absorbance spectra were taken with Eppendorf BioSpectrometer. *E. coli* DH5 α and BL21 (DE3) cells were grown from laboratory stocks. *B. subtilis* Δ Oat strain (BKE27140) was purchased from BGSC at Ohio State University. *P. putida* strain KT2440 was purchased from ATCC (#47054). *V. parahaemolyticus* strain RIMD2210633 was obtained from Dr. Boyd's lab in the Biology department at the University of Delaware.

4.2.2 Analysis of PatB's Ability to Modify Mono- and Tri-saccharides

Purified PatB (1 μ M) was incubated with acceptors (1 mM) and the corresponding donor (4 mM) in Tris buffer (90 mM Tris, 250 mM NaCl at pH=9) at 37°C for 2 h. Post incubation, the solution was passed through a 3,000 MWCO filter to remove PatB. Excess donor was extracted with ethyl acetate and the resulting aqueous layer was lyophilized. The modified product was analyzed and confirmed via high resolution mass spectrometry.

(NAG)₃ was incubated with PatB (1 μ M) and SNAk (4 mM) at 37°C. Subsequently, 100 μ M CuSO₄, 12.8 μ M tris[(1-benzyl-1H-1,2,3-triazol-4-yl)methyl]amine (TBTA), 1.2 mM sodium ascorbate, and 20 μ M of Alexa-Fluor 488 was added to the solution and incubated at room temp for 30 min prior to MS analysis.

4.2.3 Analysis of Acetyltransferase Activity

4.2.3.1 *p*-nitrophenyl acetate (*p*NP-Ac) Transferase Assay

PatB (1 μ M) was incubated with varying concentrations of donors in the presence of 1 mM (NAG)₃ to determine the acetyltransferase kinetics of the donors. For the *p*NP-R donors, the absorbance at 405 nm was monitored over 8 min at room temp for the release of *p*NP.⁴ The absorbance of controls (Buffer only, Buffer with PatB, Buffer with donors, Buffer with (NAG)₃, Buffer with PatB and donors, Buffer with PatB and (NAG)₃, and Buffer with donors with (NAG)₃) were plotted to obtain the initial velocity of each control. The control with the highest initial velocity (Buffer with donors with (NAG)₃) was subtracted from the samples (Buffer with PatB and donors with (NAG)₃) prior to graphing the sample (i.e. Background was subtracted from control that contained all components (donor/acceptor) of the reaction except PatB). The initial velocity data for each of the donor concentrations were plotted and the K_m and k_{cat} values were calculated using nonlinear regression analysis. Each kinetic analysis was done in triplicates.

4.2.3.2 Analysis of Transferase Activity with Ellman's Reagent

PatB (1 μ M) was incubated with varying concentrations of donors in the presence of 1 mM (NAG)₃ to determine the acetyltransferase kinetics of the donors. For the SNAc donors, Ellman's reagent, DTNB, (1 mM) was added to the reaction mixture and the absorbance at 412 nm was monitored over time at room temp for the presence of a free thiol.⁵ The absorbance of controls (Buffer only, Buffer with DTNB, Buffer with DTNB and PatB, Buffer with DTNB and donors, Buffer with DTNB and (NAG)₃, Buffer with DTNB and PatB and donors, Buffer with DTNB and PatB and (NAG)₃, and Buffer with DTNB and donors with (NAG)₃) were plotted to obtain the

initial velocity of each control. The control with the highest initial velocity (Buffer with DTNB and donors with (NAG)₃) was subtracted from the samples (Buffer with DTNB and PatB and donors with (NAG)₃) prior to graphing the sample (ie. Background was subtracted from control that contained all components (donor/acceptor/DTNB) of the reaction except PatB). The initial velocity data for each of the donor concentrations were plotted and the K_m and k_{cat} values were calculated using nonlinear regression analysis. Each kinetic analysis was done in triplicates.

4.2.4 Peptidoglycan, the Natural Acceptor

4.2.4.1 Isolation of Peptidoglycan

PG was isolated as previously described.³ Briefly, Gram (+): Bacteria was grown overnight at 37°C in LB broth. The bacterial suspension was heated at 100°C for 20 min. The bacteria was sedimented by centrifugation (2,000 g, 4°C) and washed (2x saline, 1x water, 3x acetone) and air dried at 37°C. The bacterial powder was processed immediately by resuspension in water. Disruption of the cells was achieved with glass beads. The mixture of bacterial cells and glass beads was filtered. The filtrate was centrifuged for 10 min to remove any unbroken cells (1,500 g, 4°C). The supernatant was centrifuged for 30 min to sediment the cell wall (6,500 g, 4°C). The cell wall was resuspended in 50 mM phosphate buffer (pH 7.6) along with ribonuclease (100 µg/mL) and deoxyribonuclease (50 µg/mL) and toluene (0.25%) and incubated for 18 h at 37°C. Trypsin (200 µg/mL) was added and the solution was incubated for another 18 h at 37°C. The cell wall was sedimented via centrifugation (6,500 g, 4°C) for 30 min, washed 4x with water, and lyophilized. The purified cell wall was treated with 5% trichloroacetic acid for 18 h at 22°C to remove any wall

teichoic acids. The insoluble cell wall was sedimented via centrifugation (6,500 g, 4°C) for 30 min and washed (3x water and 3x acetone). The purified peptidoglycan was stored at -80°C until use.

Gram (-): Bacterial cells were harvested when growth had reached the mid exponential phase (OD ~0.5). The bacteria was pelleted by centrifugation (10,000 g, 4°C, 15 min) and resuspended in ice-cold water (0.2 g/mL). The bacterial suspension was added dropwise to an equal volume of boiling 8% SDS with stirring. The solution was stirred for 30 min and left to cool to room temperature overnight. The peptidoglycan was pelleted via ultracentrifugation (115,000 g, 20°C, 60 min). The pellet was resuspended in water and dialyzed against water at room temperature until SDS was completely removed. The peptidoglycan was pelleted by ultracentrifugation (115,000 g, 20°C, 60 min) and resuspended in solution (10 mM Tris-HCl, 10 mM NaCl, pH 7.0). The sample was sonicated until a smooth colloidal suspension was achieved. Imidazole (0.32 M) and α -amylase (100 μ g/mL) was added and the sample was incubated at 37°C for 2 h. Pretreated pronase (200 μ g/mL) was added and the sample was incubated at 60°C for 2 h. After pronase treatment, the sample was added dropwise to an equal volume of boiling 8% SDS. The solution was stirred for 15 min and cooled to room temperature. The sample was dialyzed against water until SDS was completely removed. The peptidoglycan was pelleted by ultracentrifugation (115,000 g, 20°C, 60 min). The peptidoglycan was washed with water 3x, then frozen and lyophilized to remove any remaining water. The purified peptidoglycan was stored at -80°C until use.

4.2.4.2 Confirmation of Peptidoglycan

4.2.4.2.1 Peptidoglycan Pull-Down Assay

Purified Nod2 (50 μ L) (Lauro 2017 Thesis) was added to the insoluble peptidoglycan isolated from *B. subtilis* in a Tris buffer (150 mM NaCl, 1 mM DTT, 1 mM EDTA, and pH 7 or 8.5). The mixture was incubated for 30 min at 37°C. The mixture was then centrifuged at 13,000 rpm for 5 min. The supernatant and pellet were separated. The pellet was resuspended in 50 μ L of 5X loading dye to equalize the two sample volumes. A 10 μ L aliquot of the supernatant and a 10 μ L aliquot of the resuspended pellet were run on a gel and analyzed for their Nod2 content.

4.2.4.2.2 Analysis of Peptidoglycan Fragments with MS

Isolated peptidoglycan (1 mg) from *B. subtilis* was digested with lysozyme (1 mg/mL) at 37°C overnight. Post incubation, the solution was centrifuged at 13,000 rpm for 5 min. The supernatant, which should contain small soluble fragments of the peptidoglycan, was filtered through a 3,000 molecular weight cut off (MWCO) filter to remove lysozyme. The filtrate was analyzed via high resolution mass spectrometry direct injection.

4.2.4.2.3 Nuclear Factor kappa-light-chain-enhancer of activated B cells (NF- κ B) Activation Assay

Two different cell lines were used. Cell line A (CMV) has no detectable level of Nod2, which is used as a control, and Cell line B over-expresses Nod2. Both cell lines contain the pRL Renilla luciferase reporter vector. Cells were incubated with 2 μ M MDP or the specified volume of peptidoglycan supernatant for 6 h. Following incubation, the lysates were collected and the Dual-Luciferase Reporter Assay

(Promega) was carried out according to the manufacturer's instructions. The results were normalized to Renilla activity.

4.2.4.2.4 Fluorescence-Assisted Carbohydrate Electrophoresis (FACE) Analysis

Isolated peptidoglycan (1 mg) from *B. subtilis* was digested with lysozyme (1 mg/mL) at 37°C overnight. Post incubation, the solution was centrifuged at 13,000 rpm for 5 min. The supernatant, which should contain small soluble fragments of the peptidoglycan, was filtered through a 3,000 MWCO filter to remove lysozyme. The filtrate was lyophilized down. Subsequently, 5 µL of 0.2 M 7-amino-1,3-naphthalenedisulfonic acid (ANDA) solution in acetic acid:water, 3:17 was added along with 5 µL of 1.0 M NaCNBH₃ solution in DMSO. The mixture was incubated at 37°C for 15 h. The labeled sample was run on a 35% polyacrylamide gel at 125 V for 5 h next to controls that were also labeled with ANDA.

A starch ladder was created to mimic a protein ladder used in protein gels. Starch (1 mg) was digested with α-amylase (1 mg/mL) for 8 min. The reaction was quenched with 1 N HCl. The sample was lyophilized, and labeled with ANDA to create a ladder for the carbohydrate gel. The resulting gel was analyzed on BioRad Gel Doc EZ Imager.

4.3 Results and Discussion

4.3.1 Analysis of PatB's Ability to Modify Mono- and Tri-saccharides

As shown in Table 4.1, PatB was not able to modify the monosaccharides tested: glucose (Glc), glucosamine (GlcN), NAG, and NAM (Table 4.1). PatB was also not able to modify the trisaccharide, tri-glucosamine (GlcN)₃. However we found that PatB was able to acetylate the trisaccharide, tri-*N*-acetyl-glucosamine (NAG)₃

(Figure 4.1) using both sets of donors as confirmed by high-resolution liquid chromatography mass spectrometry (HRLC/MS) (Table 4.2). Not surprisingly, this acceptor specificity is in agreement with previous work where it was demonstrated that PatB requires acceptors that are trisaccharides or longer and the acetylation of the amino group at the C2 position is crucial for PatB's activity.²

Table 4.1: No detection of modified products was observed by high-resolution mass spectrometry when PatB was incubated with *p*NP-Ac and SNAc donors with monosaccharides (Glc, GlcN, NAG and NAM) and trisaccharide (GlcN)₃.

Acceptor	Donor	Product	Calculated		Observed
			Exact Mass	[M+Na ⁺]	[M+Na ⁺]
Glc		Glc-Ac	222.07395	245.06317	N.D.
GlcN		GlcN-Ac	221.08994	244.07916	N.D.
NAG	<i>p</i> NP-Ac	NAG-Ac	263.10050	286.08972	N.D.
NAM		NAM-Ac	335.12163	358.11085	N.D.
(GlcN) ₃		(GlcN) ₃ -Ac	543.22755	566.21677	N.D.
Glc		Glc-Ac	222.07395	245.06317	N.D.
GlcN		GlcN-Ac	221.08994	244.07916	N.D.
NAG	SNAc	NAG-Ac	263.10050	286.08972	N.D.
NAM		NAM-Ac	335.12163	358.11085	N.D.
(GlcN) ₃		(GlcN) ₃ -Ac	543.22755	566.21677	N.D.

Table 4.2: Detection of modified (NAG)₃ products using PatB with *p*NP and SNAc donors by high-resolution mass spectrometry.

Donors	Product	Calculated		Observed
		Exact Mass	[M+Na ⁺]	[M+Na ⁺]
<i>p</i> NP-Ac	(GlcNAc) ₃ -Ac	669.25925	692.24847	692.24615
<i>p</i> NP-Ak	(GlcNAc) ₃ -Ak	679.24360	702.23282	702.23144
<i>p</i> NP-Az	(GlcNAc) ₃ -Az	710.26064	733.24987	733.24740
<i>p</i> NP-Bn	(GlcNAc) ₃ -Bn	731.27490	754.26412	754.26292
Acetyl-CoA	(GlcNAc) ₃ -Ac	669.25925	692.24847	692.24707
SNAc	(GlcNAc) ₃ -Ac	669.25925	692.24847	692.24614
SNAz	(GlcNAc) ₃ -Az	710.26064	733.24987	733.24688
SNAk	(GlcNAc) ₃ -Ak	707.27490	730.26412	730.26267

Emboldened by PatB's ability to install an alkynyl (SNAk) and azido (SNAz) handle, we attempted to attach a fluorophore to the modified acceptor via Copper catalyzed azide alkyne cycloaddition (CuAAC), also known as the click reaction.⁶ The product was confirmed by HRLC/MS (Figure 4.2).

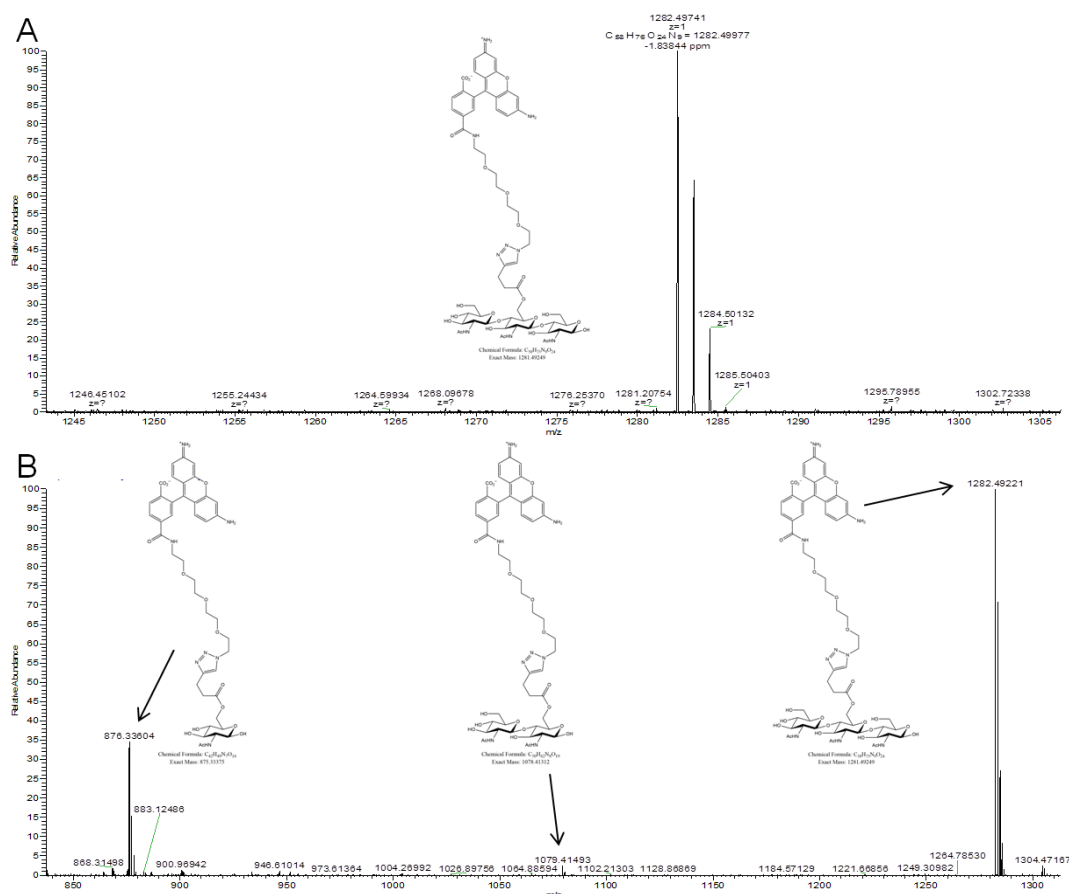


Figure 4.2: A) HRMS spectrum of Alexa Fluor 488 labeled (NAG)₃ via CUAAC. Exact mass of product: 1281.49249 Observed mass [M+H⁺]: 1282.49741. B) HRMS/MS spectrum of the fragmentation pattern of the click product showing the loss of one and two NAG molecules from the trisaccharide product. Loss of a NAG: exact mass: 1078.41312 Observed mass [M+H⁺]: 1079.41493. Loss of two NAG molecules: exact mass: 875.33375 Observed mass [M+H⁺]: 876.33604.

4.3.2 Analysis of Acetyltransferase Activity

The acetyltransferase activity of PatB utilizing the *pNP* and *SNAc* donors were assessed through the same assays used to determine PatB esterase activities (described in Chapter 2).^{4,5} The only difference is that (NAG)₃ is added to the solution for the determination of acetyltransferase activity. Otherwise, the assays were performed in

the same manner with the appropriate controls monitoring for presence of *p*NP (405 nm) or TNB (412 nm).

4.3.2.1 *p*-nitrophenyl acetate (*p*NP-Ac) Transferase Assay

The kinetic parameters of PatBs acetyltransferase activity using *p*NP donors were calculated at pH 6.5 in order to directly compare our results to that of Clarke. At pH 6.5, the overall K_{cat}/K_m values for *p*NP-Ac were approximately 50 times lower than previously reported (*p*NP-Ac: $K_{cat}/K_m = 280 \text{ M}^{-1} \text{ sec}^{-1}$) indicating that the PatB used in this study is not as efficient as the previously expressed SUMO-tagged PatB at utilizing *p*NP-Ac (Table 4.3).² Although the overall K_{cat}/K_m values for the other *p*NP donors are roughly three times higher than that of *p*NP-Ac, it is still approximately fifteen times lower than previously reported.

Table 4.3: Acetyltransferase activity of PatB (1 μM) with *p*NP donors and 1 mM (NAG)₃ at pH 6.5 (sodium phosphate buffer) as monitored at 405 nm.

	pH = 6.5		
	Acetyltransferase Activity		
Substrate	K_m (mM)	K_{cat} (sec^{-1})	K_{cat}/K_m ($\text{M}^{-1}\text{sec}^{-1}$)
<i>p</i> NP-Ac	0.00149	0.00000979	6.57
<i>p</i> NP-Ak	0.000683	0.0000119	17.57
<i>p</i> NP-Az	0.000921	0.0000173	18.75
<i>p</i> NP-Bn	0.000863	0.0000159	18.49

4.3.2.2 Analysis of Transferase Activity with Ellman's Reagent

The kinetic parameters of PatBs acetyltransferase activity using SNAc donors were calculated at pH 6.5 in order to directly compare the values to that of the *p*NP donors. At pH 6.5, the overall K_{cat}/K_m values for the SNAc donors were approximately three times higher than the *p*NP donors, but still five times lower than previously reported for the *p*NP-Ac ($K_{cat}/K_m = 280 \text{ M}^{-1} \text{ sec}^{-1}$) indicating that the PatB used in this study is not as efficient as the previously expressed SUMO-tagged PatB at pH 6.5 (Table 4.4).

However as we determined in Chapter 3 with the esterase activity assays, PatB has higher activity at a pH more representative of its natural environment. Therefore we repeated the kinetic analysis at pH 8.5, and the overall K_{cat}/K_m values for SNAc and SNAk are now approximately four times higher than that of the *p*NP donors (Table 4.4). The overall K_{cat}/K_m value for SNAz was twice as high as that of the *p*NP donors. Again we note that at either pH, PatB is not very efficient at transferring an acetyl group from acetyl-CoA. On the other hand, the K_{cat}/K_m value for PatBs acetyltransferase activity using acetyl-CoA at pH 8.5 is within the error range of the K_{cat}/K_m value for SUMO tagged PatBs acetyltransferase activity using *p*NP-Ac at pH 6.5. That is very surprising given the large size and charge disparity between the two donors.

Table 4.4: Acetyltransferase activity of PatB (1 μ M) with acetyl-CoA and SNAc donors and 1 mM (NAG)₃ at pH 6.5 (sodium phosphate buffer) and pH 8.5 (tris buffer) as monitored at 412 nm.

Substrate	Acetyltransferase Activity					
	pH = 6.5			pH = 8.5		
	K _m (mM)	K _{cat} (sec ⁻¹)	K _{cat} /K _m (M ⁻¹ sec ⁻¹)	K _m (mM)	K _{cat} (sec ⁻¹)	K _{cat} /K _m (M ⁻¹ sec ⁻¹)
Acetyl-CoA	0.204	0.00544	26.69	1.62	0.422	260.2
SNAc	0.327	0.0179	54.82	1.47	1.62	1,103
SNAz	0.661	0.0370	55.99	1.12	0.617	527.1
SNAk	0.531	0.0288	54.21	1.69	1.85	1,094

4.3.3 Peptidoglycan, the Natural Acceptor

Peptidoglycan was successfully isolated from Gram (+) (*B. subtilis*) and Gram (-) (*E. coli*, *V. parahaemolyticus*, and *P. putida*) species in order to test for PatB's ability to modified its natural acceptor with *p*NP and SNAc donors. The Gram (-) bacteria species were chosen in part due to their inability to acetylate their peptidoglycan.^{7,8} Furthermore a bacillus strain with the *O*-acetyltransferase (*Oat*) gene knocked out (*B. sub.* Δ *Oat*) was used to ensure that the isolated peptidoglycan would be devoid of any natural acetylation.

4.3.3.1 Isolation of Peptidoglycan

Peptidoglycan was successfully isolated following literature precedence.³ The peptidoglycan yield for Gram (+) bacterial species was ~1 mg/L and ~0.5 mg/L for Gram (-) bacterial species. This is not surprising as Gram (+) bacterial species have a

much thicker layer of peptidoglycan as compared to Gram (-) bacteria species. The isolated peptidoglycans have a similar white fluffy appearance and are insoluble in solution (Figure 4.3).

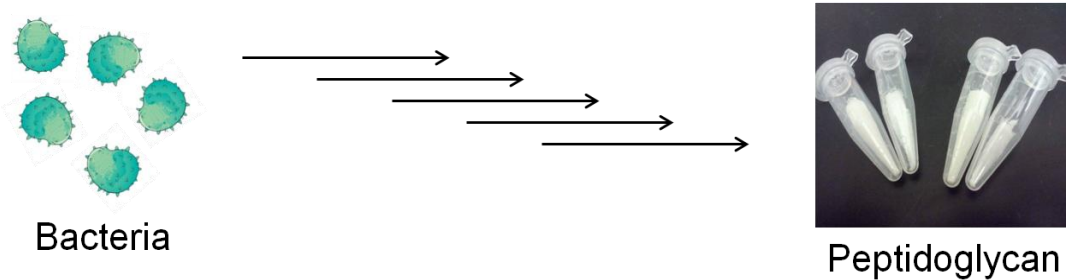


Figure 4.3: Peptidoglycan was isolated from various Gram (+) (*B. subtilis*) and Gram (-) (*E. coli*, *V. parahaemolyticus*, and *P. putida*) bacterial species following literature precedence with modifications.³

4.3.3.2 Confirmation of Peptidoglycan

To confirm that the isolated substance is indeed peptidoglycan, several assays that take advantage of peptidoglycan's structure and function were employed. First, we took advantage of the fact that Nod2 binds to components of the peptidoglycan.⁹ Thus isolated peptidoglycan was incubated with purified Nod2 (Lauro 2017 Thesis) to test if they are capable of binding to each other. Encouraged by the ability of the isolated peptidoglycan to pull down Nod2, we now aim to identify the components of the peptidoglycan that Nod2 binds. The second confirmation assay was done with mass spectrometry. The isolated peptidoglycan was digested with lysozyme to produce small fragments that were analyzed via high resolution mass spectrometry. Concurrently, we took advantage of the established NF- κ B assay to determine if the small fragments produced could activate the innate immune system. Lastly, we

wanted to visualize the fragments on a carbohydrate gel to ensure that peptidoglycan was indeed isolated.

4.3.3.2.1 Peptidoglycan Pull-Down Assay

The first step in confirming that peptidoglycan was successfully isolated was to test if it is capable of binding to Nod2. We took advantage of the insolubility of isolated peptidoglycan and the solubility of Nod2 and created a new peptidoglycan pull-down assay. Initially the Nod2 protein is present in the supernatant and not observed in the pellet (insoluble peptidoglycan) on a gel (Figure 4.4). However after incubation, the Nod2 protein can be found in the pellet as indicated by the presence of a Nod2 band in the protein gel. Given that Nod2 has specificity for peptidoglycan, this data supports that peptidoglycan is what was isolated. In addition, the support is further strengthened by that fact that the binding of Nod2 to the peptidoglycan is pH sensitive, binding in a pH regime of 5.0 to 7.0. If the incubation was carried out at pH 8.5, then no Nod2 is found in the pellet.

It is interesting to note that although we used this new assay to visualize the interaction between two known interacting partners, it can also be used as a method to identify new binding partners. To elaborate, the insoluble peptidoglycan is similar to a resin that would bind to proteins, and this would serve as the first step in the identification of new mammalian proteins that detect and bind peptidoglycan fragments.

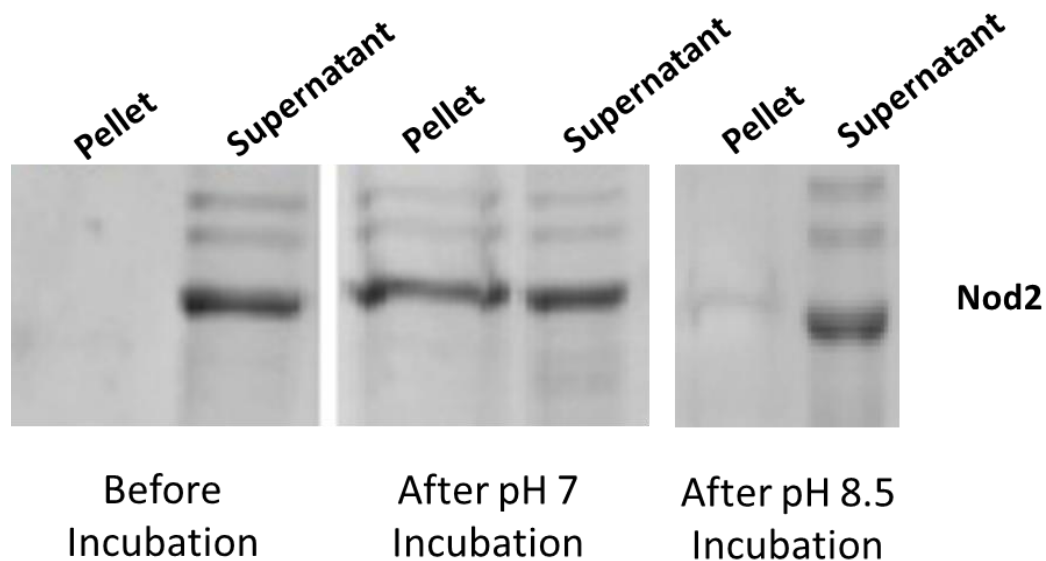


Figure 4.4: Prior to incubation with insoluble peptidoglycan (pellet), Nod2 was only found in the supernatant. Post incubation, Nod2 is observed in both lanes indicating that insoluble peptidoglycan was able to pull down Nod2. This binding was shown to be pH dependent as the pull down ability is lost at pH 8.5.

4.3.3.2.2 Analysis of Peptidoglycan Fragments with MS

The binding partner of Nod2 is believed to be MDP, a fragment of peptidoglycan.¹⁰ Thus we wanted to determine if it was possible to isolate and identify MDP in the isolated peptidoglycan sample. If so, that would support the binding of Nod2 to the isolated peptidoglycan observed in the pull-down assay. After lysozyme treatment, high-resolution mass spectrometry (HRMS) analysis resulted in the identification of two major masses. The structure of peptidoglycan was analyzed and two possible fragments were found as potential matches to the two identified masses: M4 and G-M4 (Figure 4.5). Although MDP was not directly observed, both of the fragments have MDP at a part of their structure. In order to isolate the MDP portion,

then a peptidase would need to be added in order to cleave the peptide stem. However that would require the discovery a new class of peptidases capable of cleaving a peptide bond between an L-amino acid and a D-amino acid. Unlike bacteria, human cells exclusively utilize L-amino acids, so peptidases that have been characterized can only cleave peptide bonds between two L-amino acids. We also noted that there are presumably more fragments in the supernatant, but these were the two fragments that were detected.

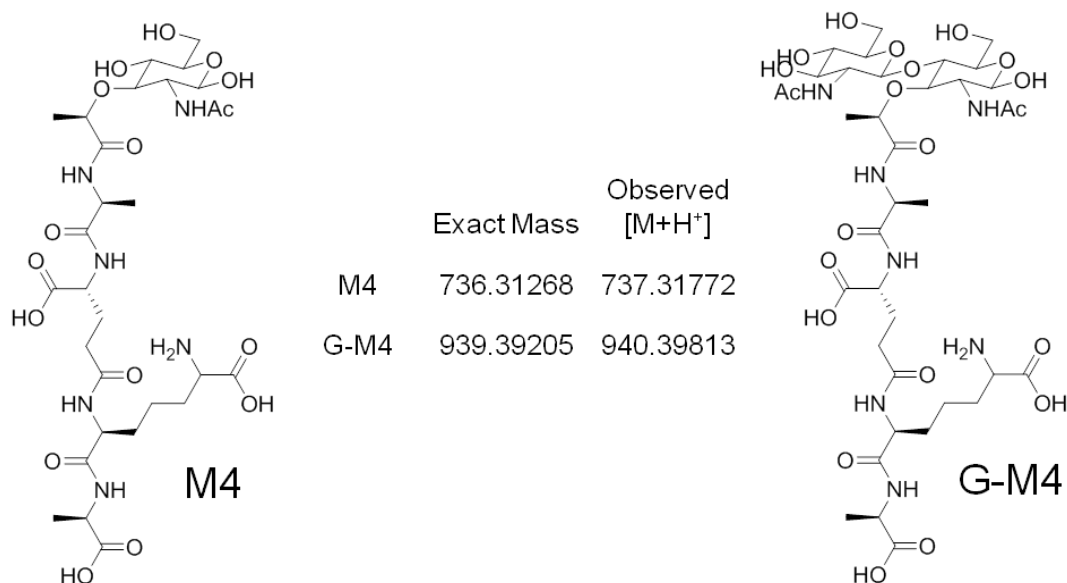


Figure 4.5: The structure of two proposed fragments of the peptidoglycan that corresponds with the two masses detected post lysozyme digestion via HRMS. M4: NAM with a tetrapeptide stem. G-M4: NAG-NAM with a tetrapeptide stem.

4.3.3.2.3 Nuclear Factor kappa-light-chain-enhancer of activated B cells (NF- κ B) Activation Assay

With the successful identification of two small peptidoglycan fragments in the supernatant post lysozyme digestion, we aimed to determine if the supernatant was

immunoactive through the NF- κ B activation assay. Normally, when small peptidoglycan fragments such as MDP bind to Nod2, it triggers a cascade of events through the NF- κ B pathway that results in the generation of cytokines and chemokines. In a NF- κ B activation assay, the luciferase gene is placed downstream of the NF- κ B binding site so that upon binding of MDP or other peptidoglycan fragments to Nod2, active luciferase is produced and the amount of luciferin generated as a product of luciferase's mechanism of action can be quantified (Figure 4.6).¹¹

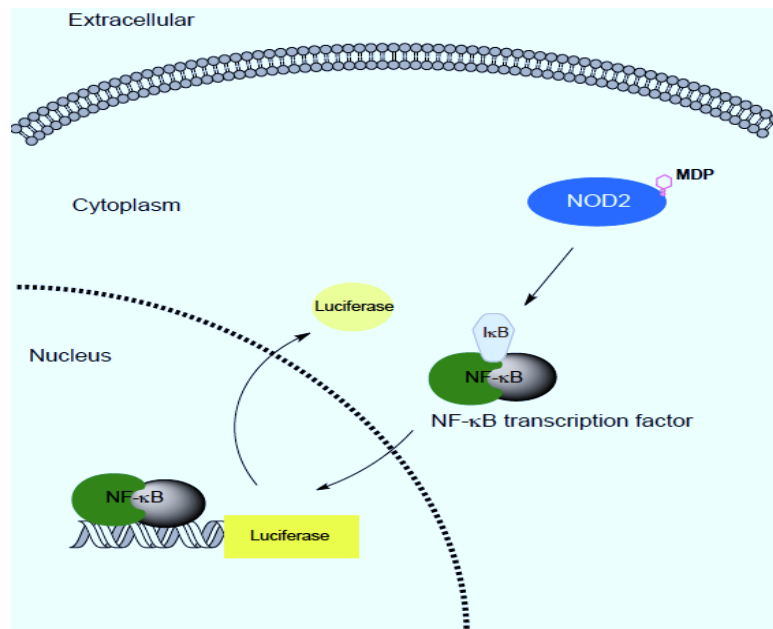


Figure 4.6: Upon binding of MDP or other peptidoglycan fragments to Nod2, the NF- κ B signaling pathway is activated. The NF- κ B transcription factor translocates from the cytoplasm to the nucleus. When the NF- κ B transcription factor binds to the promoter region of the DNA, it turns on the luciferase gene, which is placed downstream of the promoter. The activation level is quantified by measuring the production of luciferin.

As shown below, the supernatant obtained from the lysozyme digested peptidoglycan sample was able to activate the NF- κ B pathway. The gray bars represent a cell line that over-expressed Nod2 while the black bars represent a cell line that has basal level of Nod2 expression. In both cases, the addition of the supernatant resulted in a higher activation level as compared to the MDP control (Figure 4.7). It is interesting to note that the activation level seems to reach a plateau with the addition of 50 μ L of the supernatant. One drawback to this strategy is the inability to compare the MDP control and sample directly. The amount of soluble peptidoglycan fragments present in the supernatant is unknown. Therefore the exact concentration of the sample can not be calculated, so a direct comparison to the MDP control cannot be made. It is only possible to say that from the results, the supernatant does contain small components of the peptidoglycan that are able to activate the innate immune system through the NF- κ B pathway. Furthermore the increase in activation in the CMV control indicates that the peptidoglycan fragments present in the supernatant are capable of activating the NF- κ B pathway by binding to proteins other than Nod2. The activation could be a result of the binding of iE-DAP to Nod1.

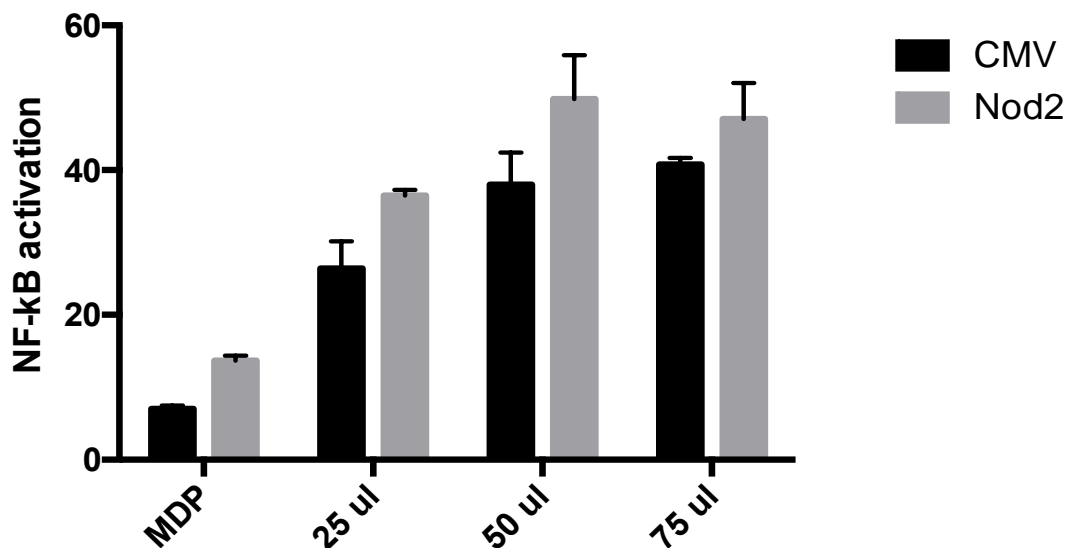


Figure 4.7: The supernatant of lysozyme digested peptidoglycan is able to activate the NF- κ B pathway. CMV: control no Nod2. Nod2: over-expresses Nod2. Data is not statistically significant as the experiments were done in duplicates. However, the goal was to employ the NF- κ B assay as a qualitative method to verify peptidoglycan.

4.3.3.2.4 Fluorescence-Assisted Carbohydrate Electrophoresis (FACE) Analysis

Although the supernatant was immunoactive, the composition of its peptidoglycan fragments remained elusive except the two fragments observed via HRMS. Thus we set out to find another method that would allow us to visualize the fragment composition present in the supernatant.

There has been literature precedence using fluorescence-assisted carbohydrate electrophoresis (FACE) to analyzed carbohydrates on a gel.¹² Given that the peptidoglycan has a carbohydrate backbone, we reasoned that FACE may yield insights regarding the fragment composition. A carbohydrate gel is larger (14x16 cm) and contains a higher percentage of polyacrylamide (35%) as compared to a standard

protein gel (8x5.8 cm; 4-15%). As a result, a carbohydrate gel needs to be run at a lower voltage for a longer period of time in order for the sugars to separate.

The carbohydrate portion of peptidoglycan fragments were labeled with ANDA via reductive amination (Figure 4.8).¹³ Subsequently, the sample was analyzed on a carbohydrate gel along with ANDA labeled controls (NAG, Mal, and Glc). A starch ladder was created to mimic a protein ladder. The controls were also loaded in the same column to mimic a ladder effect. Several bands were observed in the peptidoglycan sample indicating that there were other fragments present in addition to the two observed via HRMS (Figure 4.9). Some of the bands appear to line up with the control bands, but given the unevenness of the gel, it's difficult to make any definitive conclusions about the molecular weight of these fragments. Attempts have been made to extract and purify the separated fragments out of the gel, but to no avail. Another approach being considered is to take advantage of the ANDA tag and separate the peptidoglycan fragments via high-performance liquid chromatography (HPLC)/MS.

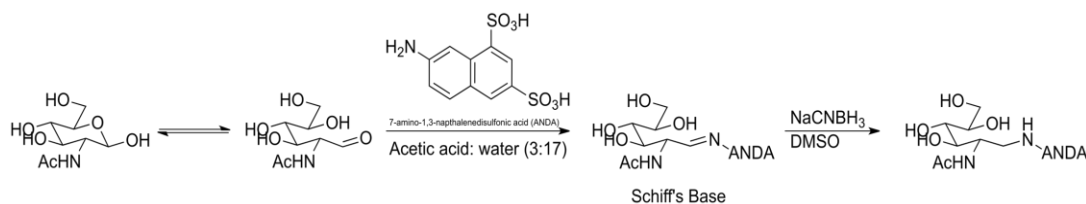


Figure 4.8: Scheme of carbohydrate labeling via reductive amination with ANDA.

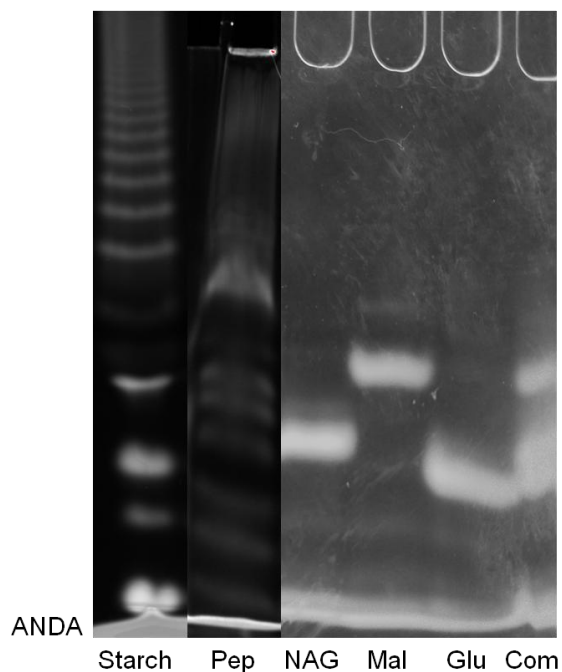


Figure 4.9: Fluorescent detection of ANDA labeled peptidoglycan fragments (Pep) on a carbohydrate gel along with a homemade starch ladder (Starch) and reference controls (NAG, Mal (maltose), Glc, and Com (combined sample containing NAG, Mal and Glc)).

4.4 Conclusions

This chapter detailed the exploration of acceptors for PatB. Our findings show that PatB prefers to modify an acceptor that is minimally three sugar units in length and the acetylation of the amino group at C2 position is necessary. These results are in agreement with literature data.² Using (NAG)₃ as the acceptor, the kinetic parameters of PatBs acetyltransferase activity was calculated. It was shown that PatB has higher acetyltransferase activity at pH 8.5 rather than pH 6.5, which we attribute once again to the facts that our PatB does not have a large tag attached and pH 8.5 more close resembles the environment PatB prefers. We were also able to employ CuAAC to attach an Alex Fluorophore to the alkynyl handle installed on (NAG)₃ by PatB.

Furthermore, we isolated the natural acceptor, peptidoglycan, from a number of bacterial species. A new pull-down assay was also developed to confirm the identity of the peptidoglycan. The new assay also has the potential to be a very valuable tool in identifying other mammalian proteins that bind to peptidoglycan. Now that we have acceptors and donors for PatB, we aimed to get a better understanding of PatBs mechanism of action both *in vitro* and *in vivo*.

REFERENCES

1. Vollmer, W.; Blanot, D.; de Pedro, MA. Peptidoglycan structure and architecture. *FEMS Microbiol. Rev.*, **2008**, 32 (2), 149-167. doi: 10.1111/j.1574-6976.2007.00094.
2. Moynihan, PJ.; Clarke, AJ. Substrate specificity and kinetic characterization of peptidoglycan *O*-acetyltransferase B from *Neisseria gonorrhoeae*. *J. Biol. Chem.*, **2014**, 289 (24), 16748-16760. doi: 10.1074/jbc.M114.567388.
3. Young, KD. Techniques for analysis of peptidoglycans. *Methods in Microbiol.* **1998**, 27, 277-286. doi: 10.1016/S0580-9517(08)70290-3.
4. Huggins, C. & Lapides, J. Chromogenic substrates: IV. Acyl esters of *p*-nitrophenol as substrates for the colorimetric determination of esterase. (1947). *J. Biol. Chem.*, **1947**, 170, 467-482.
5. Riddles, PW.; Blakeley, RL.; Zenner, B. Ellman's reagent: 5,5'-dithiobis(2-nitrobenzoic acid)-a reexamination. *Anal. Biochem.*, **1979**, 94 (1), 75-81. doi: 10.1016/0003-2697(79)90792-9.
6. Kolb, HC.; Finn, MG.; Sharpless, KB. Click chemistry: diverse chemical function from a few good reactions. *Angew. Chem. Int. Ed. Engl.* **2001**, 40 (11), 2004-2021. doi: 10.1002/1521-3773(20010601)40:11.
7. Vollmer, W. Structural variation in the glycan strands of bacterial peptidoglycan. *FEMS Microbiol. Rev.*, **2008**, 32 (2), 287-306. doi: 10.1111/j.1574-6976.2007.00088.
8. Clarke, AJ.; Dupont, C. *O*-acetylated peptidoglycan: its occurrence, pathobiological significance, and biosynthesis. *Can. J. Microbiol.*, **1992**, 38 (2), 85-91. doi: 10.1139/m92-104.
9. Girardin, SE.; Boneca, IG.; Viala, J.; Chamailard, M.; Labigne, A.; Thomas, G.; Philpott, DJ.; Sansonetti, PJ. Nod2 is a general sensor of peptidoglycan through muramyl dipeptide (MDP) detection. *J. Biol. Chem.*, **2003**, 278 (11), 8869-8872. doi: 10.1074/jbc.C200651200.

10. Mo, J.; Boyle, JP.; Howard, CB.; Monie, TP.; Davis, BK.; Duncan, JA. Pathogen sensing by Nucleotide-binding Oligomerization Domain-containing Protein 2 (NOD2) is mediated by direct binding to muramyl dipeptide and ATP. *J. Biol. Chem.*, **2012**, 287, 23057-23067. doi: 10.1074/jbc.M112.344283.
11. Mohanan, V.; Grimes, CL. Hsp70 binds to and stabilizes Nod2, an innate immune receptor involved in Crohn's disease. *J. Biol. Chem.*, **2014**, 289 (27), 18987-18998. doi: 10.1074/jbc.M114.557686.
12. Young, KD. A simple gel electrophoretic method for analyzing the muropeptide composition of bacterial peptidoglycan. *J. Bacteriol.*, **1996**, 178 (13), 3962-3966. doi: 10.1128/jb.178.13.3962-3966.1996.
13. Jackson, P. The use of polyacrylamide-gel electrophoresis for the high-resolution separation of reducing saccharides labeled with the Fluorophore 8-aminonaphthalene-1,3,6-trisulphonic acid. Detection of picomolar quantities by an imaging system based on a cooled charge-coupled device. *J. Biochem.*, **1990**, 270 (3), 705-713. PMID: PMC1131789.

Chapter 5

IN VITRO AND IN VIVO APPLICATIONS OF PATB

5.1 Introduction

At last, we have functional PatB, natural acceptor, peptidoglycan, from various sources, and a set of SNAc donors. We set forth to study possible applications of PatB both *in vitro* and *in vivo*.

As discussed in Chapters 1 and 2, *O*-acetylation of the peptidoglycan by PatB is a defense mechanism of bacteria to protect against degradation by exogenous autolysins such as lysozyme and mutanolysin.^{1,2} We aimed to determine if in fact, our PatB is able to confer the same resistance to isolated peptidoglycan. To do so, we took advantage of the fact that isolated peptidoglycan is insoluble, so it has a high turbidity which can be monitored by measuring the absorbance at OD₆₀₀. The absorbance of unmodified peptidoglycan digested with lysozyme will lead to a decrease in absorbance over time as smaller soluble fragments are generated. On the other hand, if the peptidoglycan is modified with PatB and SNAc donors, then the resulting peptidoglycan would be resistant to lysozyme degradation and the absorbance would not decrease over time (Figure 5.1).

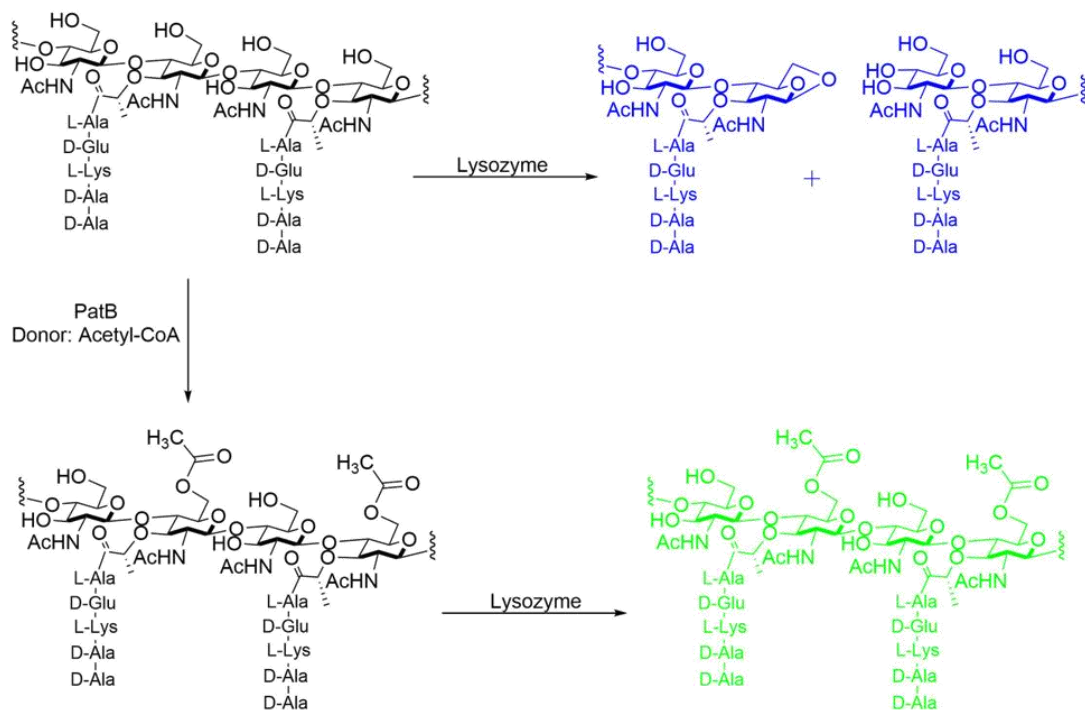


Figure 5.1: Unmodified peptidoglycan is susceptible to lysozyme degradation (top), forming a 1,6-anhydro-NAM product. However if the peptidoglycan is modified by PatB prior to lysozyme treatment, then the peptidoglycan is protected against lysozyme degradation.

Intrigued by the ability of the bioorthogonal SNAc donors to modify isolated peptidoglycan, *in vivo* labeling of Gram (+) bacterial cells using PatB was pursued. Inspiration to tag the peptidoglycan polymer was based on previous strategies used to label either the peptide stems³⁻¹⁰ or carbohydrate core^{11,12} of peptidoglycan. While these methods rely on metabolic incorporation of unnatural peptidoglycan building blocks, PatB assisted labeling would be a complimentary method that does not rely on the peptidoglycan biosynthetic pathway, but rather Nature's ability to post-synthetically modify peptidoglycan to install bioorthogonal functionality on the carbohydrate portion of mature peptidoglycan, more specifically the 6-OH of NAM,

which to date remains an unexplored peptidoglycan labeling target. Similar enzymatic approaches have been employed by the Spiegel lab to use sortase A (SrtA) as a tool for incorporating molecular handles onto the cell wall of *Staphylococcus aureus*¹³ and by Liu and Tam to label *E. coli* cell surfaces through a butelase-mediated ligation method to a transmembrane protein.¹⁴

5.2 Materials and Methods

5.2.1 Materials and Instrumentation

All chemicals were purchased from Sigma and ThermoFisher Scientific and used without further purification unless otherwise noted. All absorbance spectra were taken with Eppendorf BioSpectrometer.

5.2.2 Peptidoglycan Degradation Assay (*in vitro*)

Isolated peptidoglycan (1 mg) from *B. subtilis*, *E. coli*, *V. parahaemolyticus*, and *P. putida* (see Chapter 4 for procedure) was incubated with the **1**, **6**, **7**, or **8** donor (4 mM) in the presence and absence of PatB (1 μ M) for 2 h. The modified peptidoglycan was pelleted at 21,000 g for 5 min to remove PatB and any remaining donor. The modified peptidoglycan was then resuspended and lysozyme (100 μ g/mL) was added to cleave the glycosidic bonds. The sample was incubated at 37°C with shaking and the OD was monitored over time as indicated.

5.2.3 Bacterial Cell Labeling (*in vivo*)

Cells were grown from overnight culture until OD₆₀₀ of 0.5 (Erythromycin (20 μ g/mL) was added for Δ Oat strain). The bacterial culture was centrifuged at 11,000 g for 5 min. The cells were resuspended in M9 minimal media with PatB (1 μ M) and **6**

or **8** (250 µg/mL) and incubated at 37°C for the specified duration. The cells were spun down at 11,000 g for 2.5 min and the pellet was washed with M9 minimal media (2x) and water (2x). The cells were resuspended in water and CuSO₄ (0.1 mM), TBTA (128 µM), sodium ascorbate (1.2 mM), and Alexa-Fluor 488 (20 µM) was added and incubated at room temp for 30 min in the dark. The cells were spun down at 11,000 g for 2.5 min and the pellet was washed 3x with 1xPBS. The cells were fixed with 4% paraformaldehyde for 30 min in the dark at room temp. The cells were spun down at 11,000 g for 2.5 min and the pellet was washed 3x with PBS. The cells were resuspended in water and tetramethylrhodamine Wheat Germ Agglutinin (WGA; 5 µg/mL) conjugate was added and incubated for 15 min at room temp in the dark. The dual labeled cells were spun down at 11,000 g for 2.5 min and the pellet was washed 3x with 1xPBS. The cells were resuspended in 1xPBS and a small drop was added to the center of a 18 mm x 18 mm cover glass (Zeiss) (pre-treated with 0.1 mg/mL poly-L-lysine (Sigma P1274)). The rest of the cells were stored at -20°C with 10% glycerol. The coverslip rested for 30 min in the dark before it was placed on top of a drop of Prolong Diamond Antifade Mountants on microscope slide. The slide rested in the dark overnight at room temp. The sides of the coverslip were sealed with nail polish and stored at -20°C until imaging.

Prepared slides were imaged with Structured Illumination Microscopy (SIM) on a Zeiss Elyra PS.1 microscope with Plan-Apochromat 63x/1.4 Oil DIC M27 objective. The fluorophore of Alexa-Fluor 488 and tetra-rhodamine WGA conjugate were excited with 488 nm and 561 nm laser excitations, respectively. The camera exposure time was 100.0 ms, the raw data images which contain 5 rotations are in Z-stack mode with 0.110 µm as the stack interval. The software of Carl Zeiss ZEN 2012

was used to process the raw data to yield SIM images and the processing settings were kept constant. 2D maximum intensity projection images were generated from SIM images with ZEN 2012 software. Scale bars were made in ZEN 2012 with the line measurement tool function.

5.3 Results and Discussion

5.3.1 Peptidoglycan Degradation Assay (*in vitro*)

To evaluate the *in vitro* application of using PatB as a tool to confer lysozyme resistance to isolated peptidoglycan. The insoluble peptidoglycan isolated from *B. sub. ΔOat* was subjected to lysozyme degradation in the presence and absence of PatB with **1, 6-8**; the optical density was measured over time to monitor the increase or decrease of peptidoglycan degradation process.¹⁵ The optical density of the insoluble peptidoglycan control remained stable over the course of the experiment (Figure 5.2 and 5.3). However the optical density of unmodified peptidoglycan decreased over time with lysozyme treatment, indicating that the peptidoglycan was being digested into soluble fragments from lysozyme treatment (Figure 5.2 and 5.3). In contrast, if the peptidoglycan was pre-treated with PatB and **1, 6, 7** or **8**, then the polymer was protected against lysozyme degradation (Figure 5.2 and 5.3).

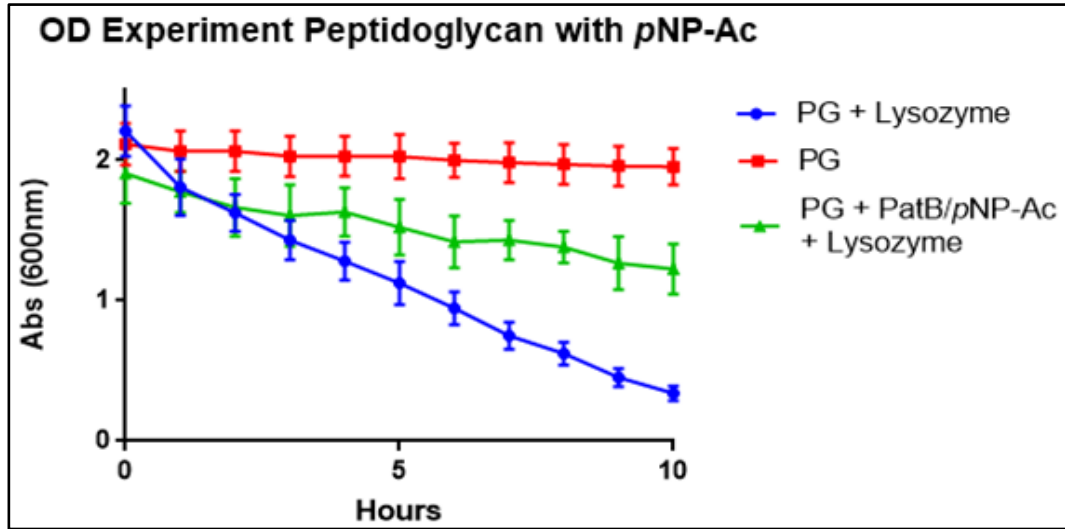


Figure 5.2: PatB-modified PG, with *pNP-Ac*, from *B. subtilis* Δ Oat (green) was protected against lysozyme degradation as compared to no modification (blue) and no lysozyme control (red). Values plotted are average of three independent experiments as the mean \pm S.D.

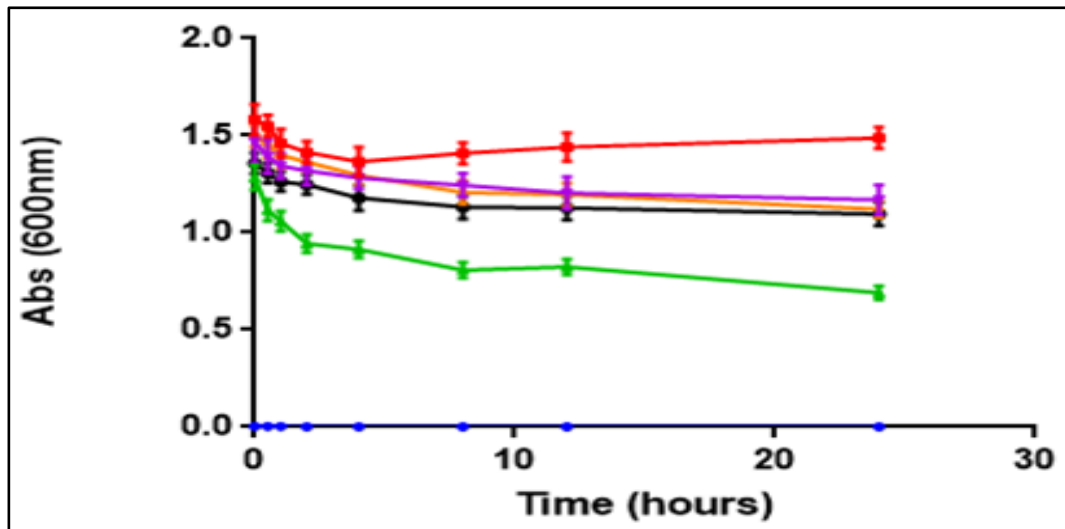


Figure 5.3: PatB-modified PG, with **6** (purple), **7** (black) or **8** (orange), from *B. subtilis* Δ Oat was protected against lysozyme degradation. Unmodified peptidoglycan (green). Blank (blue). Peptidoglycan without lysozyme (red). Values plotted are average of three independent experiments as the mean \pm S.D.

Encouraged by these results, peptidoglycan was isolated from other bacterial species: *E. coli*, *V. parahaemolyticus*, and *P. putida*; as these species have not been shown to *O*-acetylate their peptidoglycan.^{16,17} The isolated peptidoglycan was again subjected to lysozyme treatment with and without modification by PatB and similar results were obtained. PatB conferred lysozyme resistance to the isolated peptidoglycan from all of the bacterial strains tested (Figure 5.4, 5.5 and 5.6) using all of the SNAc donors. It seems that the functional group is irrelevant as long as the 6-OH group of NAM is capped. Also expected, some degradation of the acetylated peptidoglycan was observed, as PatB may not be able to modify every NAM residue in the peptidoglycan.¹⁸ Overall, these data demonstrate that PatB is capable of modifying small and large fragments of peptidoglycan with bioorthogonal functionality.

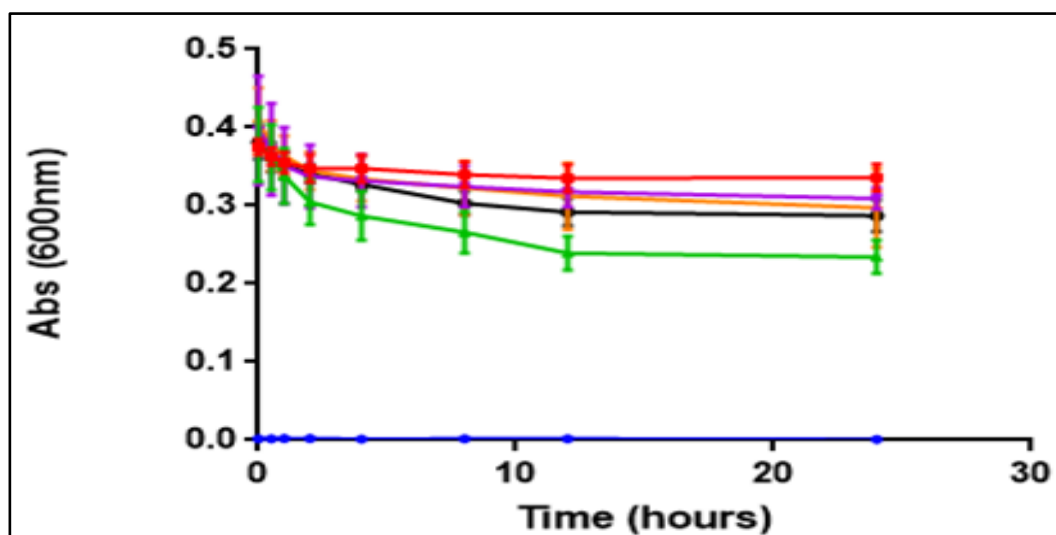


Figure 5.4: PatB-modified PG, with **6** (purple), **7** (black) or **8** (orange), from *E. coli* was protected against lysozyme degradation. Unmodified peptidoglycan (green). Blank (blue). Peptidoglycan without lysozyme (red). Values plotted are average of three independent experiments as the mean \pm S.D.

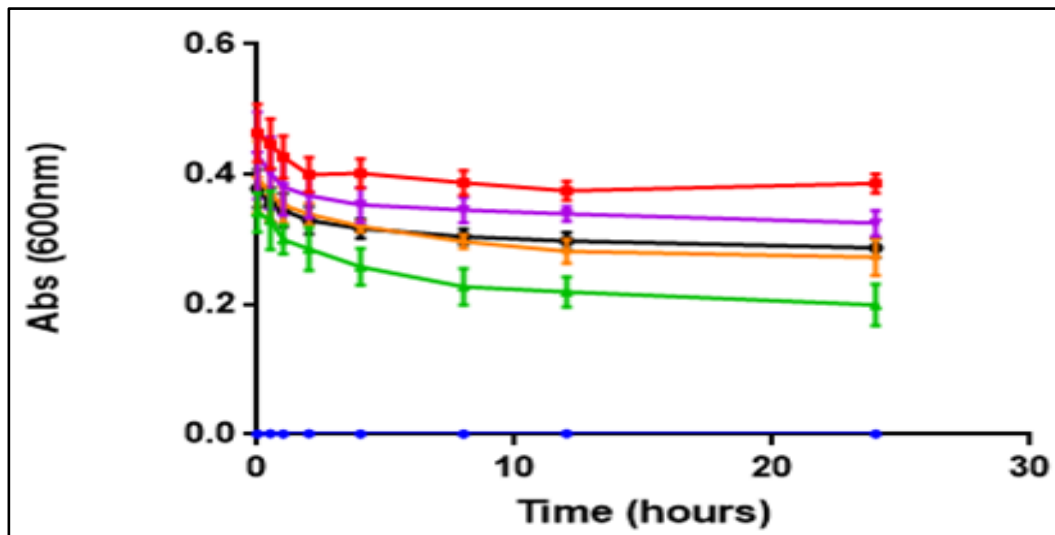


Figure 5.5: PatB-modified PG, with **6** (purple), **7** (black) or **8** (orange), from *P. putida* was protected against lysozyme degradation. Unmodified peptidoglycan (green). Blank (blue). Peptidoglycan without lysozyme (red). Values plotted are average of three independent experiments as the mean \pm S.D.

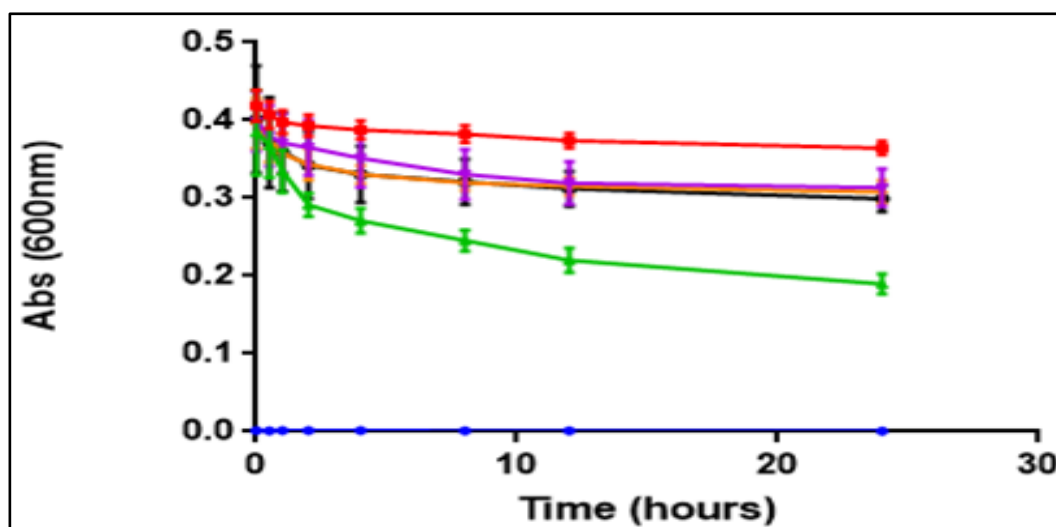


Figure 5.6: PatB-modified PG, with **6** (purple), **7** (black) or **8** (orange), from *V. parahaemolyticus* was protected against lysozyme degradation. Unmodified peptidoglycan (green). Blank (blue). Peptidoglycan without lysozyme (red). Values plotted are average of three independent experiments as the mean \pm S.D.

These results indicate that PatB is able to utilize the donors to modified not only a small peptidoglycan mimic, (NAG)₃, but also the natural acceptor, isolated peptidoglycan, from both Gram (+) and Gram (-) bacterial species. The modification does indeed protect the isolated peptidoglycan from lysozyme degradation.

5.3.2 Bacterial Cell Labeling (*in vivo*)

B. subtilis ΔOat and wild type cells were harvested during their exponential phase, treated with PatB and donor, SNAc or SNAc-Ak. CuAAC was implemented to label the cells with Alexa Fluor 488-Az and subsequently imaged via superresolution Structured Illumination Microscopy (SIM).¹⁹ Multiple incubation time points were observed, and it was determined that optimal labeling was achieved at 240 min (Figure 5.7 and 5.8).

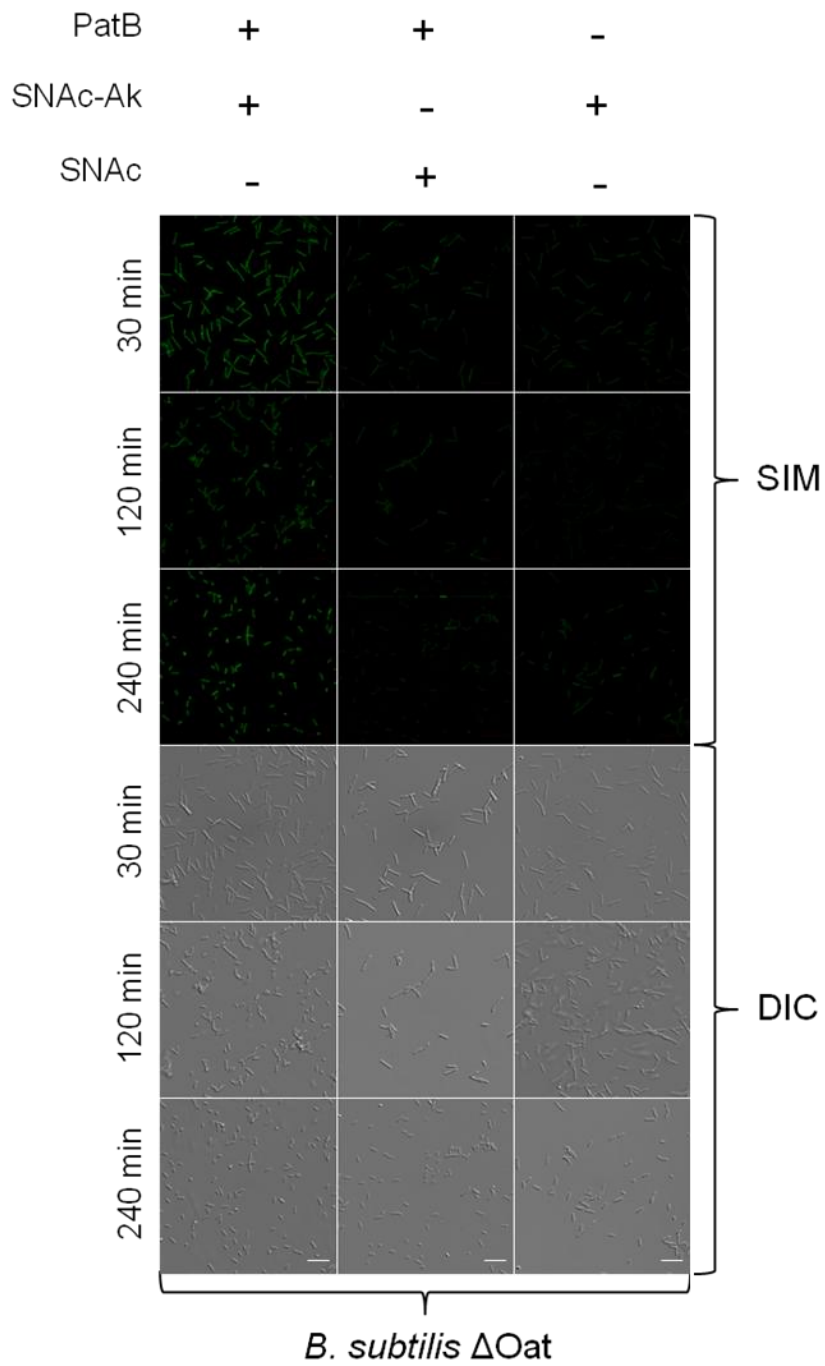


Figure 5.7: SIM and corresponding DIC images of Alexa-Fluor 488 labeled *B. subtilis* Δ Oat cells post modification by PatB and SNAk, PatB and SNAc, or SNAk alone at the various time points indicated. Scale bar denotes 10 μ m.

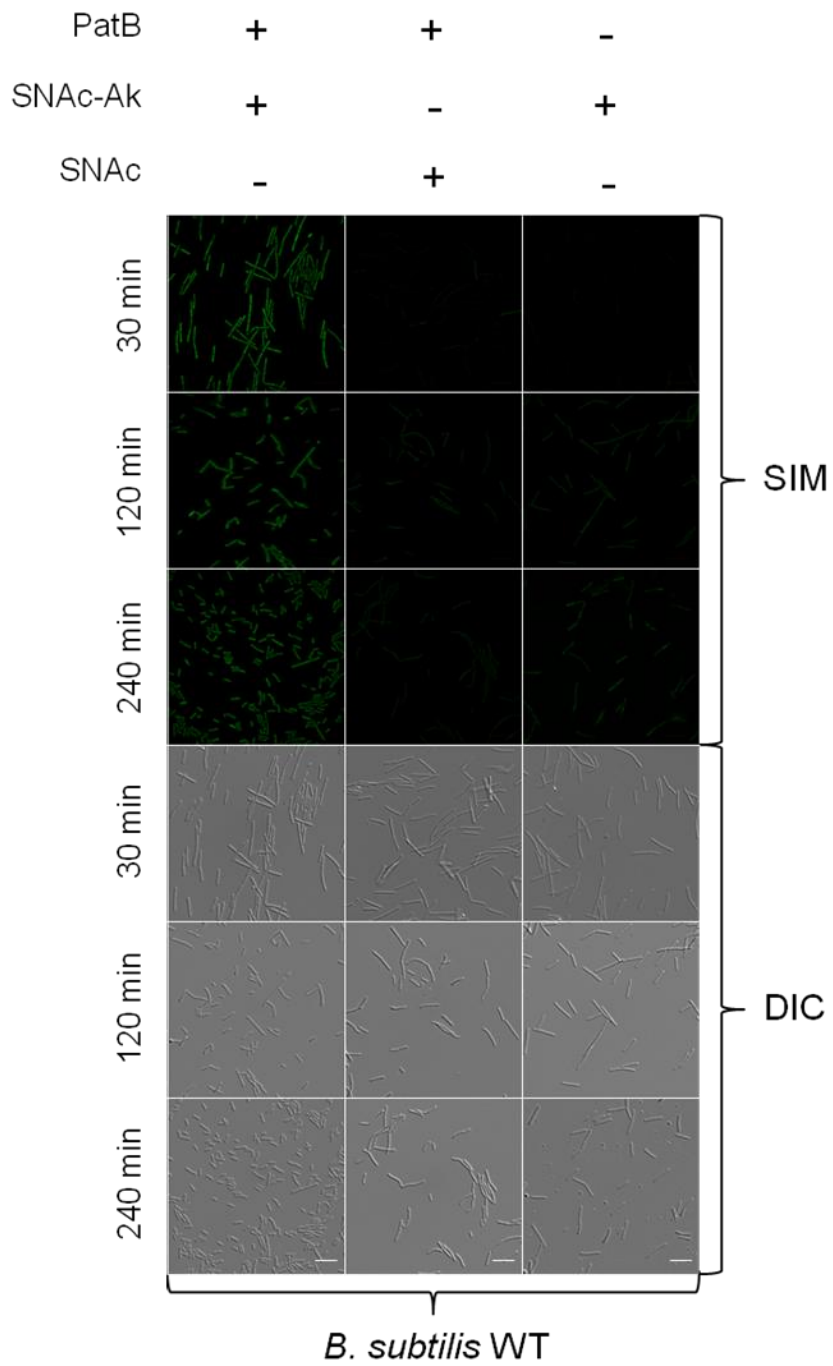


Figure 5.8: SIM and corresponding DIC images of Alexa-Fluor 488 labeled *B. subtilis* WT cells post modification by PatB and SNAk, PatB and SNAc, or SNAk alone at the various time points indicated. Scale bar denotes 10 μm .

In both *B. subtilis* Δ Oat and wild type strains, the cells displayed a higher fluorescence signal intensity when treated with PatB and SNAc-Ak as compared to treatment with SNAc-Ak alone or PatB with SNAc, both of which showed only background auto-fluorescence (Figure 5.9 and 5.10). These results indicate that PatB is necessary for efficient labeling of bacterial cells using SNAc derivatives. Moreover, we note that the fluorescence seen in the WT *B. subtilis* cells treated with only SNAc-Ak could be attributed to the wild type OatA present in these cells as the fluorescence is absent when *B. subtilis* Δ Oat is treated with only SNAc-Ak (Figure 5.11 and 5.12).

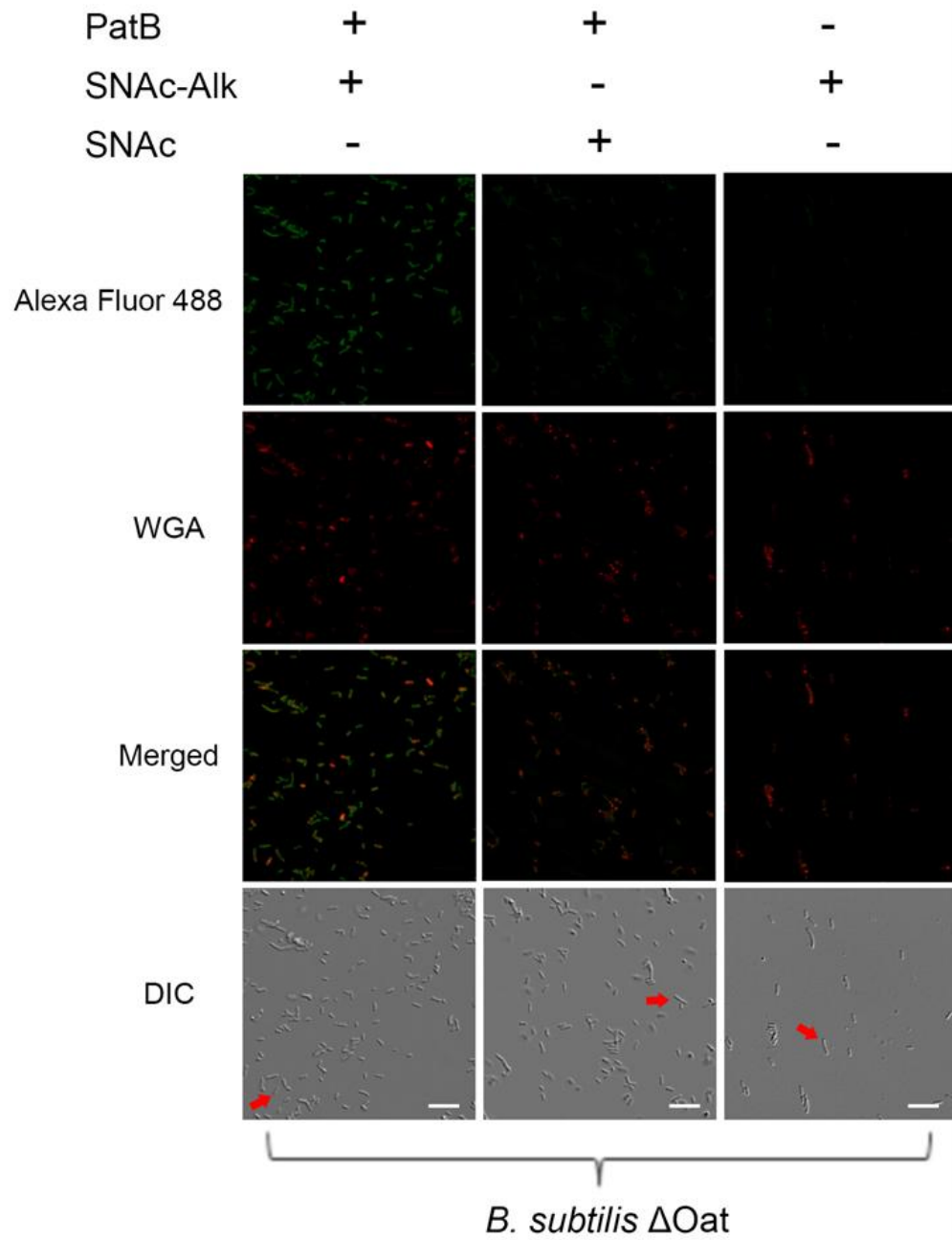


Figure 5.9: Large field SIM and corresponding DIC images of Figure 5.11. Red arrows indicate the cells that are shown in Figure 5.11. Scale bar denotes 10 μ m.

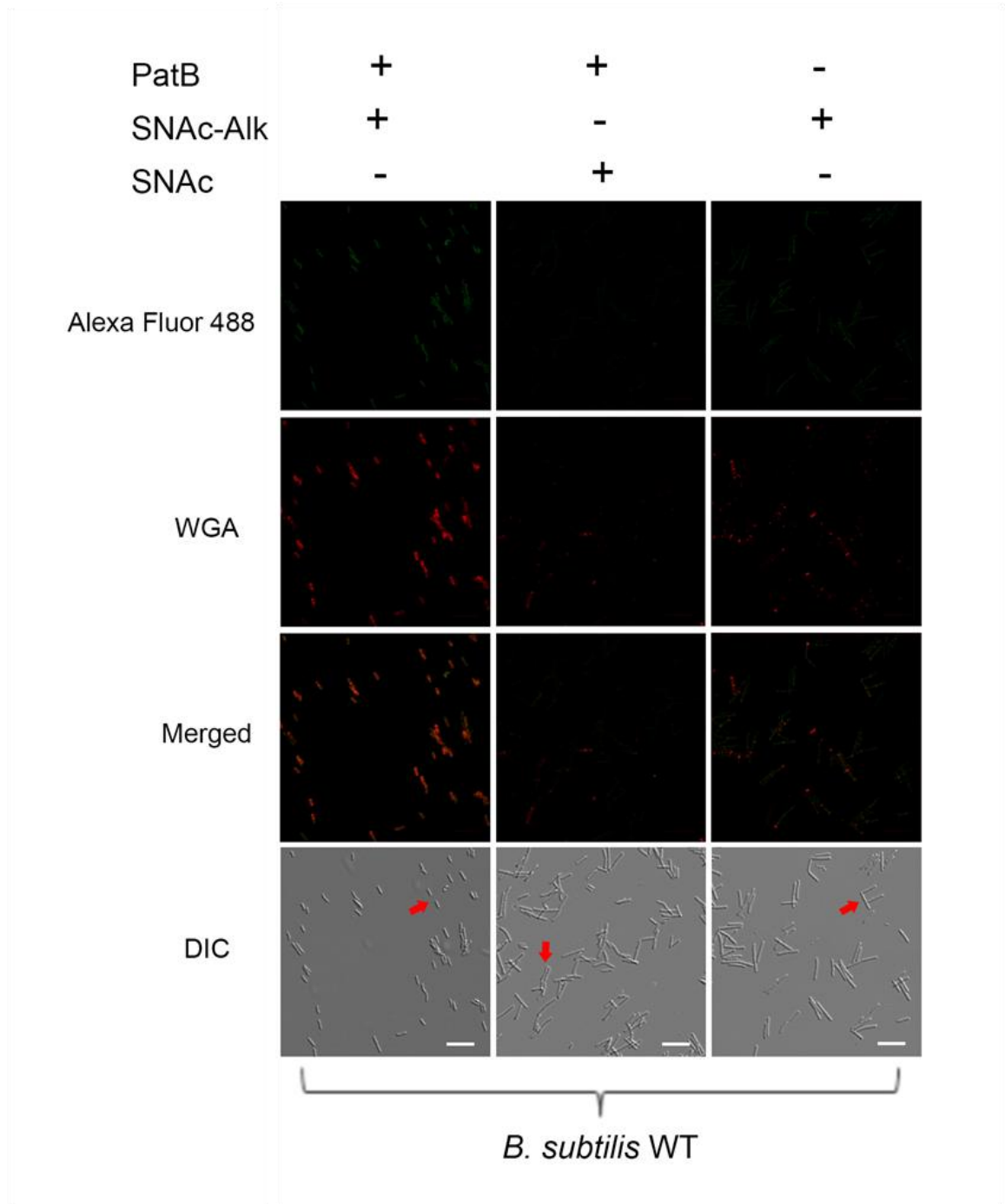


Figure 5.10: Large field SIM and corresponding DIC images of Figure 5.12. Red arrows indicate the cells that are shown in Figure 5.12. Scale bar denotes 10 μ m.

To verify that the labeling is specific to the peptidoglycan, the cells were stained with a tetramethylrhodamine conjugate of wheat germ agglutinin (WGA), which binds to NAG.^{20,21} This verification approach was chosen rather than a mass spectrometry based assay due to the fact that the acetylated peptidoglycan is resistant to lysozyme degradation²² making isolation of detectable fragments extremely difficult. Moreover, the fragile acetyl modification is lost during the harsh peptidoglycan isolation.²³ The co-localization of Alexa Fluor 488 and tetramethylrhodamine-WGA in the samples treated with PatB and SNAc-Ak suggest that the labeling was specific to the peptidoglycan (Figure 5.11 and 5.12). The Δ Oat cells have a higher fluorescence signal as compared to the wild type, which can be attributed to the fact that there are more sites available for PatB modification in the Δ Oat cells. It is also interesting to note that the fluorescence signal appears to be localized around an area referred to as the septal division ring.²⁴ Nascent peptidoglycan is proposed to be formed at this ring during bacterial division.²⁵ Thus it is plausible that PatB is more likely to target the unmodified peptidoglycan found in this area. We propose that the labeling methodology presented here was successful and specific in labeling peptidoglycan as a Gram-positive organism was studied, therefore PatB did not have to pass through the outer membrane to reach its extracellular peptidoglycan target. Moreover, very little cytoplasmic labeling was observed as the SNAc derivative would most likely be destroyed due to the high concentration of glutathione within the cell.^{26,27}

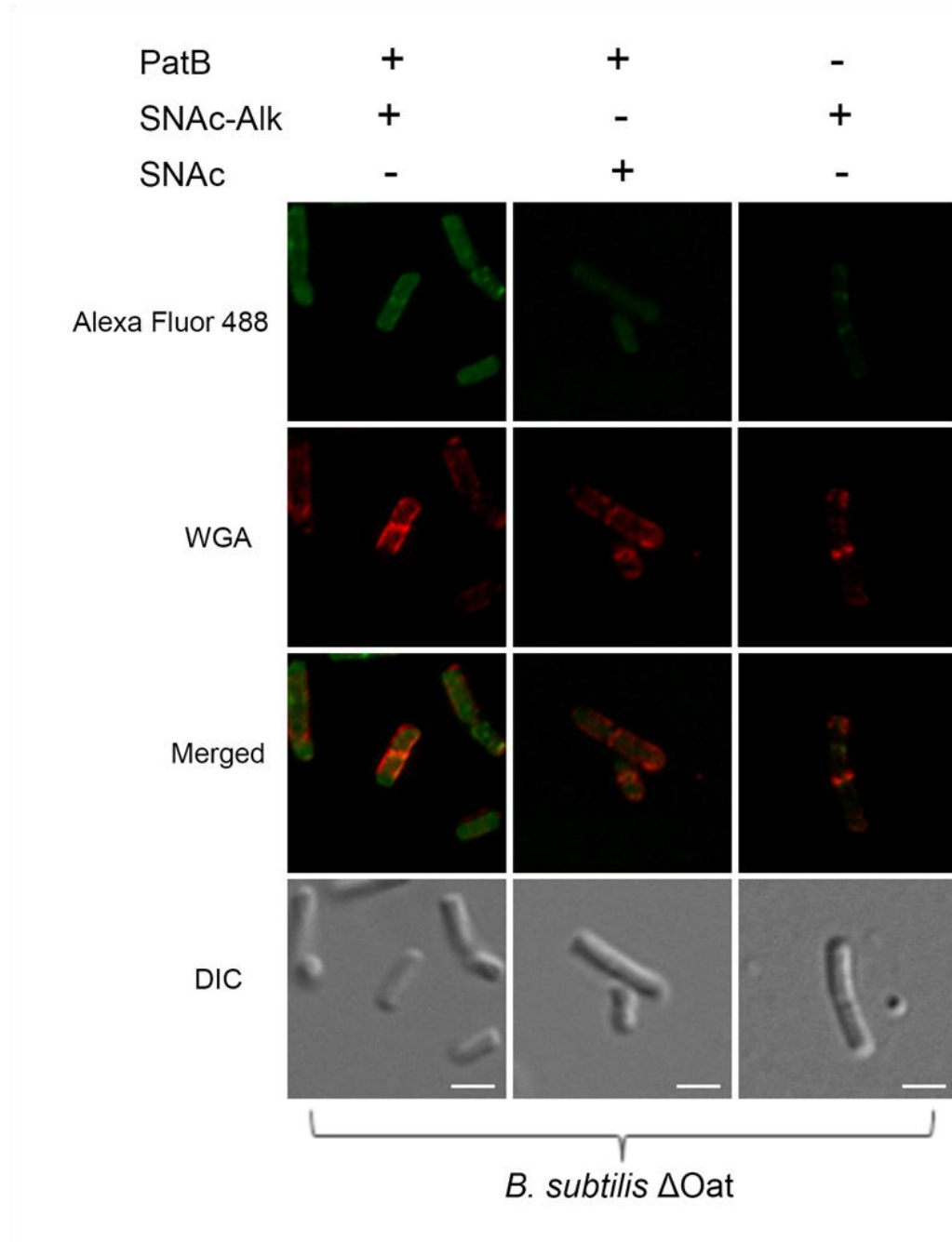


Figure 5.11: SIM and corresponding DIC images of *B. subtilis* ΔOat cells labeled with Alexa-Fluor 488 (top row) post modification by PatB and SNAc-Ak, PatB and SNAc, or SNAc-Ak alone for 240 min. The cell wall was also stained with a tetramethylrhodamine WGA conjugate (second row) to show colocalization of the fluorophores (third row). Images are representative of three biological replicates. Scale bar denotes 2 μm.

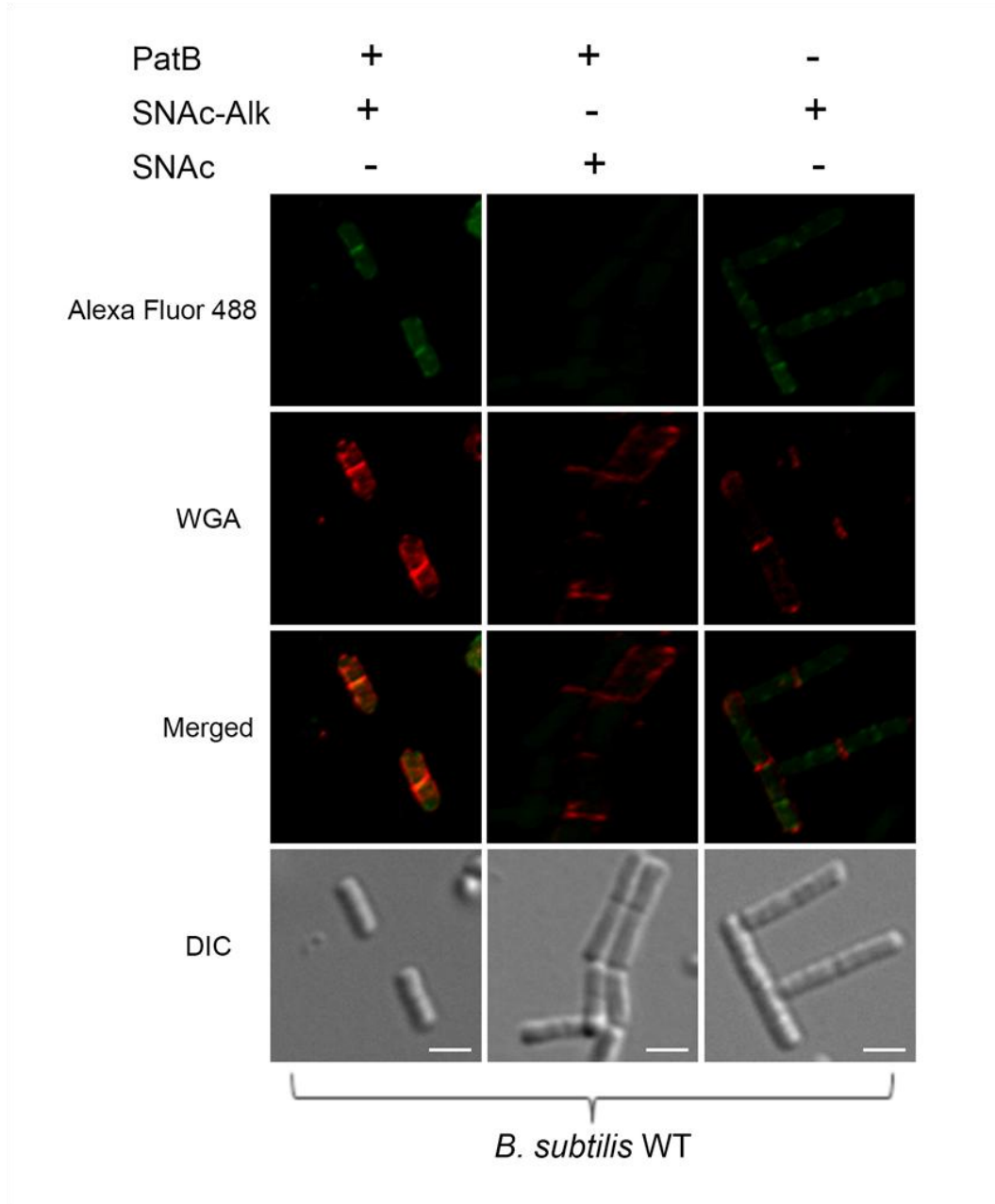


Figure 5.12: SIM and corresponding DIC images of *B. subtilis* WT cells labeled with Alexa-Fluor 488 (top row) post modification by PatB and SNAc-Ak, PatB and SNAc, or SNAc-Ak alone for 240 min. The cell wall was also stained with a tetramethylrhodamine WGA conjugate (second row) to show colocalization of the fluorophores (third row). Images are representative of three biological replicates. Scale bar denotes 2 μ m.

5.4 Conclusions

This chapter detailed two applications of PatB with SNAc donors. *In vitro*, it was determined that post PatB modification, the isolated peptidoglycan from multiple bacterial species was protected against lysozyme degradation. The results presented show that PatB is able to modify the isolated peptidoglycan at the 6-OH position of NAM to block lysozyme regardless of the bacterial species. This is very exciting because the SNAc donors could be further fine tuned to install other handles on peptidoglycan fragments, which could assist in the identification of specie-specific peptidoglycan fragment generated as a result of the interactions between the microbiome and the innate immune system.

In addition we show that the PatB/SNAc system can be employed to label whole bacterial cells specifically at the peptidoglycan level. This new labeling strategy is complimentary to existing methods as it labels a different position of the carbohydrate backbone without having to rely on the peptidoglycan biosynthetic pathway. The PatB/SNAc system also seems to have some specificity to the septal ring area of the peptidoglycan. This could afford us the opportunity to study peptidoglycan turnover in detail by labeling nascent peptidoglycan and tracking it as the cell grow and divide.

REFERENCES

1. Chung, W.; Hancock, REW. Action of lysozyme and nisin mixtures against lactic acid bacteria. *Intl. J. Food Microbiol.*, **2000**, *60* (1), 25-32. doi: 10.1016/S0168-1605(00)00330-5.
2. Pushkaran, AC.; Nataraj, N.; Nair, N.; Gotz, F.; Biswas, R.; Mohan, CG. Understanding the structure-function relationship of lysozyme resistance in *Staphylococcus aureus* by peptidoglycan *O*-acetylation using molecular docking, dynamics, and lysis assay. *J. Chem. Inf. Model.*, **2015**, *55* (4), 760-770. doi: 10.1021/ci500734k.
3. Sadamoto, R.; Niikura, K.; Sears, PS.; Liu, H.; Wong, CH.; Suksomcheep, A.; Tomita, F.; Monde, K.; Nishimura, S. Cell-wall engineering of living bacteria. *J. Am. Chem. Soc.*, **2002**, *124* (31), 9018-9019. doi: 10.1021/ja026133x.
4. Liechti, GW.; Kuru, E.; Hall, E.; Kalinda, A.; Brun, YV.; VanNieuwenhze, M.; Maurelli, AT. A new metabolic cell-wall labeling method reveals peptidoglycan in *Chlamydia trachomatis*. *Nature*, **2014**, *506*, 507-510. doi: 10.1038/nature12892.
5. Siegrist, MS.; Whiteside, S.; Jewett, JC.; Aditham, A.; Cava, F.; Bertozzi, CR. D-amino acid chemical reporters reveal peptidoglycan dynamics of an intracellular pathogen. *ACS Chem. Biol.*, **2013**, *8*, 500-505. doi: 10.1021/cb3004995.
6. Shieh, P.; Siegrist, MS.; Cullen, AJ.; Bertozzi, CR. Imaging bacterial peptidoglycan with near-infrared fluorogenic azide probes. *Proc. Natl. Acad. Sci. USA*, **2014**, *111* (15), 5456-5461. doi: 10.1073/pnas.1322727111.
7. Kuru, E.; Hughes, HV.; Brown, PJ.; Hall, E.; Tekkam, S.; Cava, F.; de Pedro, MA.; Brun, YV.; VanNieuwenhze, MS. In situ probing of newly synthesized peptidoglycan in live bacteria with fluorescent D-amino acids. *Angew. Chem. Int. Ed. Engl.*, **2012**, *51*, 12519-12523. doi: 10.1002/anie.201206749.

8. Lebar, MD.; May, JM.; Meeske, AJ.; Leiman, SA.; Lupoli, TJ.; Tsukamoto, H.; Losick, R.; Rudner, DZ.; Walker, S.; Kahne, D. Reconstitution of peptidoglycan cross-linking leads to improved fluorescent probes of cell wall synthesis. *J. Am. Chem. Soc.*, **2014**, *136*, 10874-10877. doi: 10.1021/ja505668f.
9. Daniel, RA.; Errington, J. Control of cell morphogenesis in bacteria: two distinct ways to make a rod-shaped cell. *Cell*, **2003**, *113*, 767-776. PMID: PMC12809607.
10. Tiyanont, K.; Doan, T.; Lazarus, MB.; Fang, X.; Rudner, D.; Walker, S. Imaging peptidoglycan biosynthesis in *Bacillus subtilis* with fluorescent antibiotics. *Proc. Natl. Acad. Sci. USA*, **2006**, *103*, 11033-11038. doi: 10.1073/pnas.0600829103.
11. Sadamoto, R.; Matsubayashi, T.; Shimizu, M.; Ueda, T.; Koshida, S.; Koda, T.; Nishimura, S. Bacterial surface engineering utilizing glucosamine phosphate derivatives as cell wall precursor surrogates. *Chemistry*, **2008**, *14*, 10192-10195. doi: 10.1002/chem..200801734.
12. Liang, H.; DeMeester, KE.; Hou, C.; Parent, MA.; Caplan, JL.; Grimes, CL. Metabolic labeling of the carbohydrate core in bacterial peptidoglycan and its applications. *Nat. Commun.*, **2017**, *8*, 15015. doi: 10.1038/ncomms15015.
13. Nelson, JW.; Chamessian, AG.; McEnaney, PJ.; Murelli, RP.; Kazmierczak, BI.; Spiegel, DA. A biosynthetic strategy for re-engineering the *Staphylococcus aureus* cell wall with non-native small molecules. *ACS Chem. Biol.*, **2010**, *5* (12), 1147-1155. doi: 10.1021/cb100195d.
14. Bi, X.; Yin, J.; Nguyen, G.; Rao, C.; Halim, N.; Hemu, X.; Tam, JP.; Liu, C. Enzymatic engineering of live bacterial cell surfaces using Butelase 1. *Angew. Chem. Int. Ed. Engl.*, **2017**, *129* (27), 7930-7933. doi: 10.1002/ange.201703317.
15. Barbosa, M.; Yang, G.; Fang, J.; Kurilla, MG.; Pompliano, DL. Development of a whole-cell assay for peptidoglycan biosynthesis inhibitors. *Antimicrob. Agents. Chemother.*, **2002**, *46* (4), 943-946. doi: 10.1128/AAC.46.4.943-946.2002.
16. Vollmer, W. Structural variation in the glycan strands of bacterial peptidoglycan. *FEMS Microbiol. Rev.*, **2008**, *32* (2), 287-306. doi: 10.1111/j.1574-6976.2007.00088.

17. Clarke, AJ.; Dupont, C. *O*-acetylated peptidoglycan: its occurrence, pathobiological significance, and biosynthesis. *Can. J. Microbiol.*, **1992**, 38 (2), 85-91. doi: 10.1139/m92-104.
18. Brown, S.; Santa Maria, JP.; Walker, S. Wall teichoic acids of Gram-positive bacteria. *Annu. Rev. Microbiol.*, **2013**, 67, 313-336. doi: 10.1146/annurev-micro-092412-155620.
19. Gustafsson MG.; Shao, L.; Carlton, PM.; Wang, CJ.; Golubovskaya, IN.; Cande, WZ.; Agard, DA.; Sedat, JW. Three-dimensional resolution doubling in wide-field fluorescence microscopy by structured illumination. *J. Biophys.*, **2008**, 94 (12), 4957-4970. doi: 10.1529/biophysj.107.120345.
20. Yoshida, M.; Stadler, J.; Bertholdt, G.; Gerisch, G. Wheat germ agglutinin binds to the contact site A glycoprotein of *Dictyostelium discoideum* and inhibits EDTA-stable cell adhesion. *EMBO J.*, **1984**, 3 (11), 2663-2670. PMID: PMC557747.
21. Ursell, TS.; Nguyen, J.; Monds, RD.; Colavin, A.; Billings, G.; Ouzounov, N.; Gitai, Z.; Shaevitz, JW.; Huang, KC. Rod-like bacterial shape is maintained by feedback between cell curvature and cytoskeletal localization. *Proc. Natl. Acad. Sci. USA*, **2014**, 111 (11), E1025-1034. doi: 10.1073/pnas.1317174111.
22. Davis, KM.; Weiser, JN. Modifications to the peptidoglycan backbone help bacteria to establish infection. *Infection and Immunity*, **2011**, 79 (2), 562-570. doi: 10.1128/IAI.00651-10.
23. Young, KD. Techniques for analysis of peptidoglycans. *Methods in Microbiol.*, **1998**, 27, 277-286. doi: 10.1016/S0580-9517(08)70290-3.
24. Weiss, DS. Bacterial cell division and the septal ring. *Mol. Microbiol.*, **2004**, 54 (3), 588-597. doi: 10.1111/j.1365-2958.2004.04283.
25. Bisson-Filho, AW.; Hsu, Y.; Squyres, GR.; Kuru, E.; Wu, F.; Jukes, C.; Sun, Y.; Dekker, C.; Holden, S.; VanNieuwenhze, MS.; Brun, YV.; Garner, EC. Treadmilling by FtsZ filaments drives peptidoglycan synthesis and bacterial cell division. *Science*, **2017**, 355 (6326), 739-743. doi: 10.1126/science.aak9973.
26. Sidenius, U.; Skonberg, C.; Olsen, J.; Hansen, SH. In vitro reactivity of carboxylic acid-CoA thioesters with glutathione. *Chem. Res. Toxicol.*, **2004**, 17 (1), 75-81. doi: 10.1021/tx034127o.

27. Lushchak, VI. Glutathione homeostasis and functions: potential targets for medical interventions. *J. Amino Acids*, **2011**, 2012, 1-26. doi: 10.1155/2012/736837.

Chapter 6

CONCLUSIONS AND FUTURE DIRECTIONS

6.1 Conclusions

6.1.1 Purification and Characterization of PatB Expression from an *E. coli* System

This dissertation aimed to improve the current understanding of PatB, an important enzyme in bacterial survival. Previous to this work, limited biochemical information regarding PatB was obtained with a SUMO-tagged PatB.¹ To further our understanding of PatB, we developed a new expression and purification system for a dual tagged PatB in an *E. coli* system. The dual tag system improved the stability of the protein and yielded PatB that is >95% pure. The purified protein was also characterized using a diverse array of biochemical and bio-analytical techniques to confirm proper folding and function.

6.1.2 Donor and Acceptor Promiscuity of PatB

This dissertation work has shown that PatB has lax substrate specificity for both *p*NP and SNAc donors, allowing for the covalent attachment of bioorthogonal functionality directly onto a small molecule peptidoglycan fragment mimic, isolated peptidoglycan from *B. subtilis*, *E. coli*, *V. parahaemolyticus*, and *P. putida*, and intact *B. subtilis* cells post-synthetically. In addition, it was determined that wild type PatB has an optimal catalytic efficiency at basic pH, which reflects its natural environment.^{2,3}

6.1.3 Applications of the PatB/SNAc System

This dissertation explored two possible applications of PatB. *In vitro*, it was shown that PatB modifications protected the isolated peptidoglycans against lysozyme degradation mirroring bacteria's ability to post-synthetically modify peptidoglycan to protect it from lytic enzymes, aiding in cell survival. Furthermore, PatB's utility was explored as a tool to incorporate fluorescent tags via click chemistry on the peptidoglycan both *in vitro* and in whole cells allowing for fluorescent visualization of bacterial cells. PatB proves to be a useful tool in understanding the acetylation modification of peptidoglycan and its resistance mechanisms.

6.2 Future Directions

The PatB/SNAc system presented in this dissertation has many implications. One implication is that the SNAc derivatives employed here shed light on the mechanism of action of PatA, the proposed acetyl carrier. It is currently unknown how PatA translocates the acetate moiety of acetyl-CoA from the cytosol to the periplasmic space. However given that PatB prefers SNAc donors, which contain a thio-ester bond, it seems to suggest that the acetyl group of acetyl-CoA is possibly linked to a cysteine residue of PatA. This dissertation work also has many potential future directions.

6.2.1 Crystallization of PatB

The first possible future direction is the crystallization of PatB. No crystal structure of PatB has been reported to date, but Clarke has predicted a three-dimensional homology model of PatB based on its sequence similarly to an esterase from *Sacchomyces cerevisiae*.⁴ Although this dissertation work has expanded the knowledge of PatB's molecular mechanism, a crystal structure would provide some

vital information regarding the active site of PatB. With a closer examination of the active site, more efficient donors could be designed to be utilized with PatB. In addition, a better understanding of the active site could lead to the design and synthesis of potent inhibitors of PatB. Inhibition of PatB would render the bacteria more susceptible to lysozyme degradation.

The purified PatB in this study contains a His₆ tag that has been shown to aid in the crystallization process.⁵ Therefore we attempted to crystallize PatB. The initial buffer screening process yielded hits for the potential crystals (Figure 6.1). However the crystals were too small to diffract via X-ray. Therefore further optimization is necessary to obtain larger crystals that are more suitable for diffraction. In addition, the SNAc donors could be added to the buffer conditions to explore the possibility of obtaining a co-crystal with PatB.



Figure 6.1: Small crystals were observed during initial crystal screening conditions. However further optimizations are required to obtain a crystal suitable for X-ray diffraction. Due to instrumentation errors, no error bar is shown.

6.2.2 Labeling of *B. subtilis* Spores

When conditions are not favorable for growth and reproduction, some Gram (+) bacteria such as *Bacillus* triggers a sporulation event.⁶ The bacteria enter a metabolically dormant state and wait until the conditions become more favorable. The

spore state allows the bacteria to withstand severe chemical and physical conditions. During the course of our labeling experiments, we used various media solutions. When we attempted to label *B. subtilis* cells in PBS buffer, which is devoid of nutrients, we observed the presence of spores that were surprising fluorescently labeled (Figure 6.2). This was very exciting because currently in literature, labeling of spores has been achieved through a membrane localizing fluorescent dye (FM-4-64) or a genetically engineering fluorescent membrane protein.^{7,8} Preliminary data shows that the PatB/SNAc system has the potential to be a new method to label the peptidoglycan of spores directly.

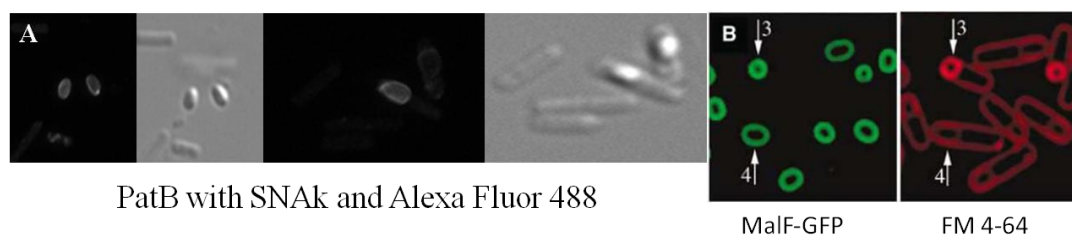


Figure 6.2: A) *B. subtilis* spores were labeled with Alexa Fluor 488 after being modified by PatB with SNAc in PBS buffer. B) *B. subtilis* spores labeled with MalF-GFP and FM-4-64. Figure (part B) adapted from Rubio and Pogliano (2004).⁷

6.2.3 Direct Fluorophore Attachment

In Chapter 5, we detailed the application of the PatB/SNAc system to fluorescently label the carbohydrate backbone of peptidoglycan. Labeling was accomplished by installing an alkynyl tag with SNAc, then employing CuAAC to fluorescently label the peptidoglycan. Although CuAAC has been utilized many times to fluorescently tag the peptidoglycan,^{9,10,11} a downside to the method is that copper is toxic to cells.¹² It has been demonstrated in this dissertation that PatB has lax substrate

specificity. Therefore the possibility of attaching a fluorophore directly to the peptidoglycan using PatB and a modified SNAc donor was explored. To that extent, SNAc-Bodipy was synthesized and assessed for its compatibility with PatB. PatB was able to fluorescently tag (NAG)₃ using SNAc-Bodipy (Figure 6.3).

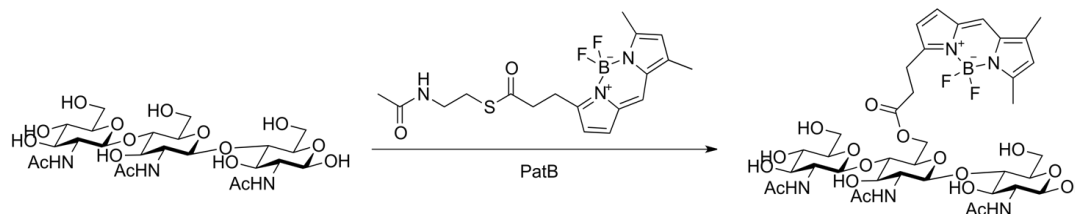


Figure 6.3: SNAc-Bodipy was synthesized and installed onto (NAG)₃ by PatB.

Upon treatment with PatB and SNAc-Bodipy, the Δ Oat cells appear to be labeled, but the labeling seems to be non-specific as the whole cell is green (Figure 6.4). In contrast, the WT cells appear to have more localized areas of labeling throughout the cells, and the fluorescence signal intensity is similar in the presence or absence of PatB (Figure 6.5). It is interesting to note that the labeling does not appear to be localized at the septal ring area, which is different than the labeling that was observed in Figure 5.11 and 5.12. In the absence of PatB, similar labeling patterns were observed in the Δ Oat and WT cells. In addition, the cells were also stained with WGA, but the signal does not appear to be localized in all four samples (Figure 6.4 and 6.5). Ongoing work is aimed at optimizing this direct labeling strategy. Preliminary data is hopeful that the PatB/SNAc system could be employed to directly attach a fluorophore onto the peptidoglycan of bacterial cells.

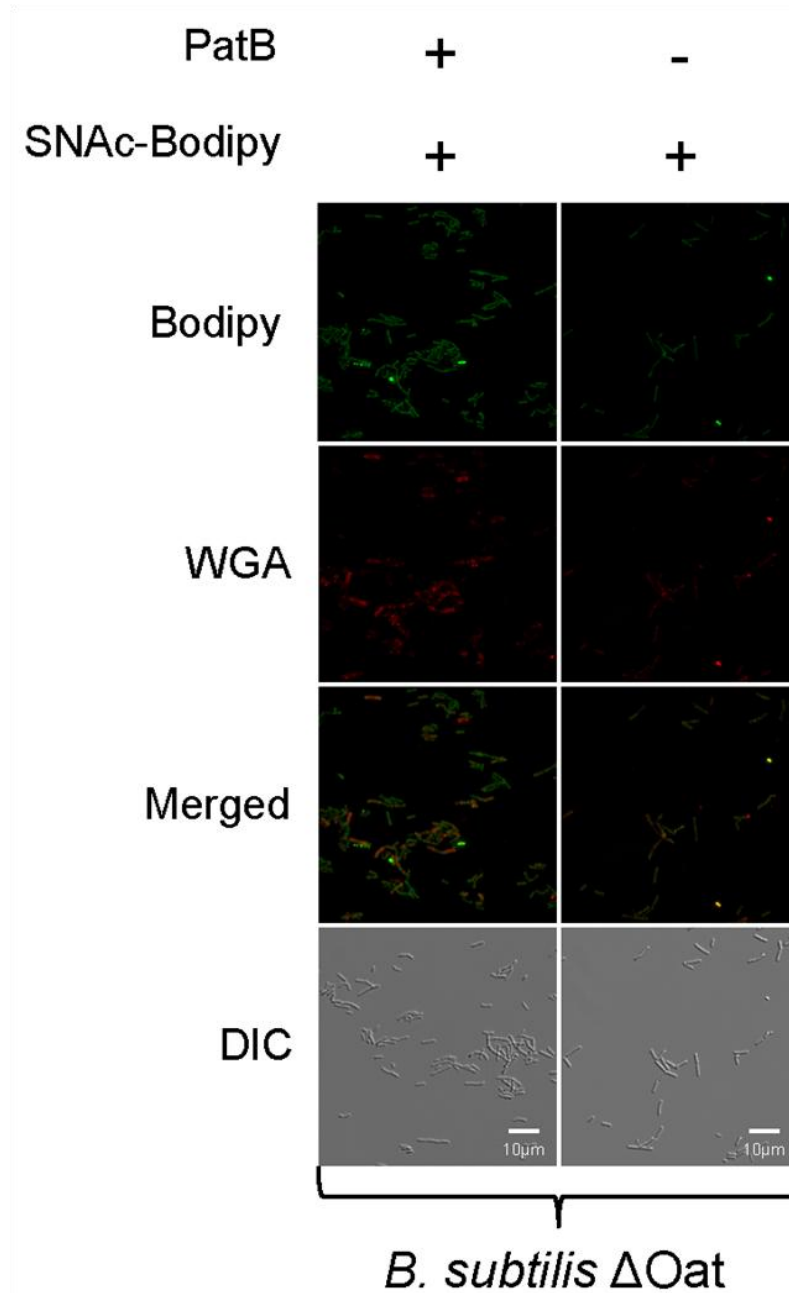


Figure 6.4: SIM and corresponding DIC images of *B. subtilis* Δ Oat cells labeled with SNAc-Bodipy by PatB for 240mins (first row). The cell wall was also stained with a tetramethylrhodamine WGA conjugate (second row) to show colocalization of the fluorophores (third row). Images are representative of three biological replicates.

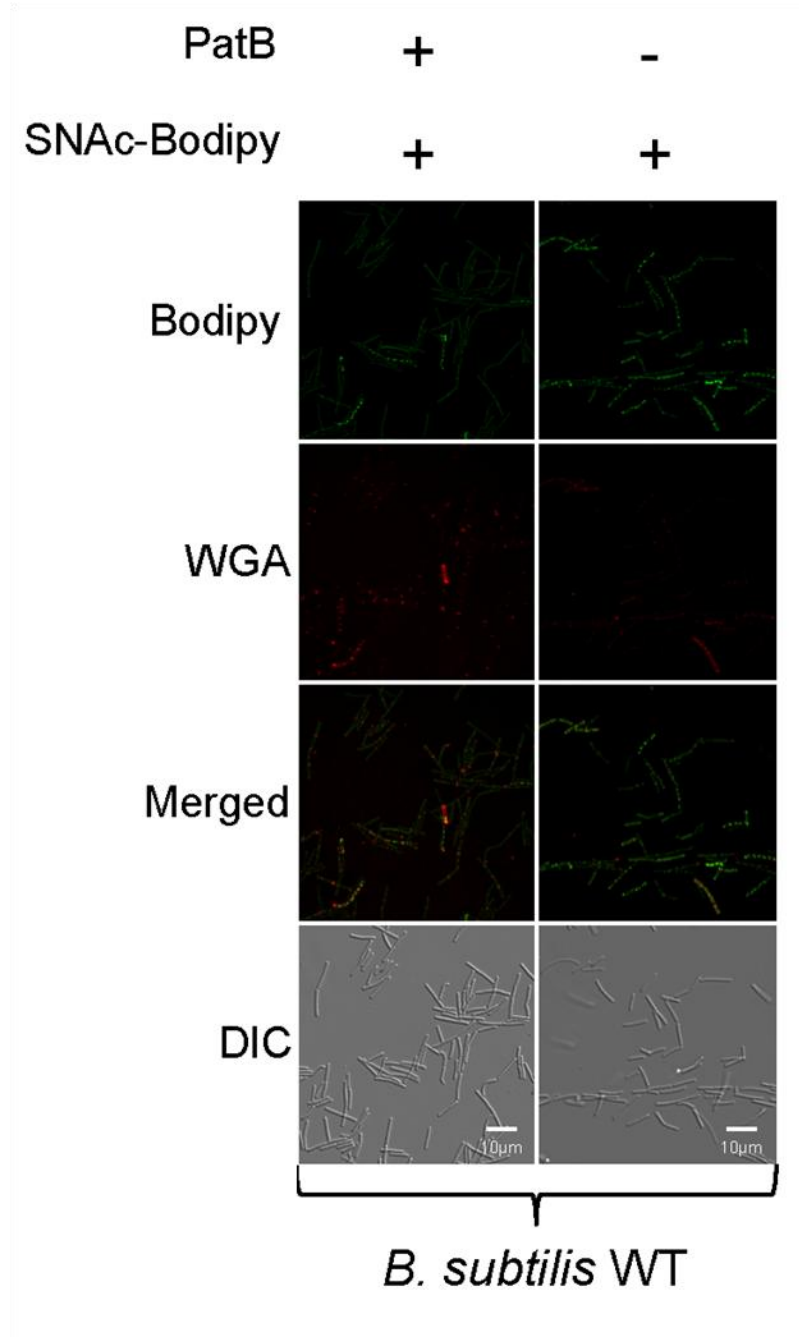


Figure 6.5: SIM and corresponding DIC images of *B. subtilis* WT cells labeled with SNAc-Bodipy by PatB for 240mins (first row). The cell wall was also stained with a tetramethylrhodamine WGA conjugate (second row) to show colocalization of the fluorophores (third row). Images are representative of three biological replicates.

6.2.4 Bacteria and Peptidoglycan as Educational Tools

I have long aspired to join the faculty ranks, and during the course of this dissertation, I have had numerous opportunities to pursue my passion of teaching. I was also very fortunate that two of the teaching projects directly connect with this dissertation through their emphasis of utilizing the bacteria and peptidoglycan as educational tools.

The first project was an introductory course to biochemistry (Chem342) taught to sophomore level biochemistry majors prior to the traditional biochemistry I/II sequences the students would take in their junior year of college. The course was developed by Dr. Harold B. White, III at the University of Delaware.¹³ The course has a very different format (PBL) than most introductory courses. In lieu of a textbook, the students dissect primary literature articles to examine a central topic over time. For example, in recent years the class, “Beer, Bugs & Drugs,” has been taught by Dr. Catherine Leimkuhler Grimes with an emphasis on the understanding of bacteria and antibiotics over time (Figure 6.6).¹³

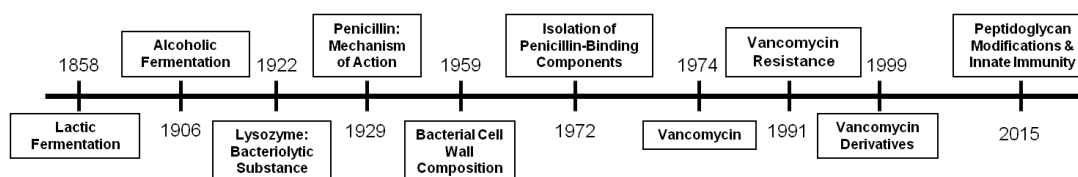


Figure 6.6: Timeline of the ten primary literature articles that students in Chem342 Beer, Bugs & Drugs, will examine over the course of the semester.

After reading each article, the students are responsible for compiling a list of learning issues (generally focused on techniques, materials, methods and/or concepts presented in the paper), and exploring those issues further on their own. This approach

gives the students the opportunity to pursue the specific concepts that interests them. When they are in class, the students work in groups to share and discuss their learning issues with each other to gain a better understanding of the paper. Students will often have different learning issues, and this allows the students to see the paper from a different perspective. In addition, by having the students explain their learning issues to each other, the students gain a more concrete understanding of the concepts themselves. The process of explaining concepts/techniques to each other also serves to boost students' confidence. As a part of my duties, I performed demonstrations such as the iodine-starch dialysis experiment during class. Since the class is taken by sophomore students, many of them are not familiar with laboratory practices. The demonstrations help the students visualize the techniques presented in the articles. In addition, I helped the students build a timeline of historical events corresponding to the timeline of the articles to give them the perspective of how current issues could impact science. With Dr. Grimes' guidance, I also co-developed a POGIL activity on amino acids that served as an introduction to the topic for the students. Even though the format of the class is different than that of a traditional survey course, the students are still exposed to a wide variety of biochemical concepts and techniques through their examination of the articles (Table 6.1).

Table 6.1: A selection of biochemical topics, concepts and techniques that students encounter in the articles they read for Chem342 Beer, Bugs & Drugs.

Biochemical Topics, Concepts and Techniques		
-pH/pKa	-Amino acids	-Crystal structures
-Equilibrium	-Enzymes	-Hydrogen bonding
-Coupled equations	-Glycolysis	-Spectroscopy
-Aerobic Fermentation	-Radioactive assays	-Affinity chromatography
-Anaerobic Fermentation	-Azotometer	-Antibiotics
-Henderson-Hasselbalch equation	-Fisher, Newman, and Haworth projection	-Minimal Inhibitory Concentration
-Sterile techniques	-Continuous assays	-Resistance
-Bacterial cultures	-Non-continuous assays	-ADP coupled assay
-Enantiomers and diastereomers	-Bacterial cell wall biosynthesis	-Innate immune activation
-Balanced equations	- K_m/K_{cat}	-Ninhydrin staining
-Chirality and optical rotation	-Ion exchange chromatography	-Size exclusion chromatography
-Solubility	-SDS page gel	-Cofactors
-Dialysis	- K_d/K_a	Etc...

The class described here is not only unique, but also effective. A brief biochemistry quiz is administered on the first and last day of class to assess students' growth during the semester. On average, the students' scores improved ~10-20% on the post quiz from the pre quiz, which correlates to a normalized gain of 0.321.¹³ Moreover, the course is also distinctively flexible. Professors can tailor the class to their liking by altering the articles or changing the topic all together.

The second project, STEM Early Education Kinship (SEEK), is in collaboration with Dr. Jennifer Gallo-Fox in the Department of Human Development and Family Studies at the University of Delaware. Many early childhood educators do not have a strong science background, and thus tend to shy away from teaching

science in their classrooms. One of the goals of the project was to connect Dr. Gallo-Fox's early childhood educators in HDFS413 with the budding biochemists in Dr. Grimes' Chem342 class. The hope is that these connections will last beyond their time at UD providing a forum to facilitate the sharing and discussion of science teaching ideas and scientific concepts. A poster session was organized to help promote the formation of these connections. The Chem342 students were responsible for presenting a poster (edited by Dr. Grimes and me) on a concept they learned from an article of their choice, and the HDFS413 students were responsible for bringing a possible science teaching idea to review with the Chem342 students. In addition, a group was created on LinkedIn to help foster and sustain the growth of this network. The group has 85 members to date.

A second aim of the SEEK project was the development of a suitable activity for early childhood educators to use in their classrooms as an introduction to bacteria. In a laboratory setting, scientists typically grow bacteria on agar plates supplemented with Lysogeny Broth (LB) medium.¹⁴ Both the LB medium and agar could be difficult for an early childhood educator to obtain, thus we sought to create a similar "plate" with more readily accessible ingredients. To that end, alternative "plates" suitable for bacterial growth were constructed using gelatin and chicken bouillons. The gelatin serves as the solidifying agent while the chicken bouillons provide the nutrients. The new "plates" were evaluated for their ability to grow bacteria. The alternative "plates" were able to grow bacteria after an overnight incubation at 37°C, and the growth is comparable to that observed with a traditional LB-agar plate (Figure 6.7).



LB-agar Plate

Alternative Plate

Figure 6.7: Comparison of bacterial growth on a traditional LB-agar plate (left) and an alternative plate made with gelatin and chicken bouillon (right).

These alternative plates are a great tool for early childhood educators to use to help children visualize the presence of bacteria in their lives. As a part of the introductory lesson, the children could swab various areas and items to determine what items or which area harbors the most bacteria. The lesson could further be expanded to include a discussion on why children should clean their hands with soap or purell frequently. Subsequent lessons could explore the various types of bacteria and their purposes.

The experiences I have gained from these two educational projects have helped me grow and develop tremendously. As a researcher, my ability to articulate my research improved greatly as a result of the projects. In addition, I acquired numerous teaching tools that will aid me in my journey to become a better instructor, and I greatly look forward to implementing all that I have learned in my future classrooms. This dissertation has provided me with a strong platform to tackle my next career step.

REFERENCES

1. Moynihan, PJ.; Clarke, AJ. Substrate specificity and kinetic characterization of peptidoglycan *O*-acetyltransferase B from *Neisseria gonorrhoeae*. *J. Biol. Chem.*, **2014**, 289 (24), 16748-16760. doi: 10.1074/jbc.M114.567388.
2. Brookes, R.; Sikyta, B. Influence of pH on the growth characteristics of *Neisseria gonorrhoeae* in continuous culture. *Appl. Microbiol.*, **1967**, 15 (2), 224-227. PMID: PMC546882.
3. Morse, SA.; Hebel, BH. Effect of pH on the growth and glucose metabolism of *Neisseria gonorrhoeae*. *Infect. Immun.* **1978**, 21 (1), 87-95. PMID: PMC421961.
4. Moynihan, PJ.; Clarke, AJ. Mechanism of action of peptidoglycan *O*-acetyltransferase B involves a Ser-His-Asp catalytic triad. *Biochemistry* **2014**, 53, 6243-6251. doi: 10.1021/bi501002d.
5. Carson, M.; Johnson, DH.; McDonald, H.; Brouillette, C.; DeLucas, LJ. His-tag impact on structure. *Acta. Cryst.*, **2007**, D63, 295-301. doi: 10.1107/S0907444906052024.
6. Tocheva, EI.; Ortega, DR.; Jensen, GJ. Sporulation, bacterial cell envelopes and the origin of life. *Nature Rev. Microbiol.*, **2016**, 14, 535-542. doi: 10.1038/nrmicro.2016.85.
7. Rubio, A.; Pogliano, K. Septal localization of forespore membrane proteins during engulfment in *Bacillus subtilis*. *EMBO J.*, **2004**, 23 (7), 1636-1646. doi:10.1038/sj.emboj.7600171.
8. Doan, T.; Morlot, C.; Meisner, J.; Serrano, M.; Henriques, AO.; Moran, CP. Jr.; Rudner, DZ. Novel secretion apparatus maintains spore integrity and developmental gene expression in *Bacillus subtilis*. *PLoS*, **2009**, 5 (7), e1000566. doi: 10.1371/journal.pgen.1000566.

9. Liechti, GW.; Kuru, E.; Hall, E.; Kalinda, A.; Brun, YV.; VanNieuwenhze, M.; Maurelli, AT. A new metabolic cell-wall labeling method reveals peptidoglycan in *Chlamydia trachomatis*. *Nature*, **2014**, *506*, 507-510. doi: 10.1038/nature12892.
10. Siegrist, MS.; Whiteside, S.; Jewett, JC.; Aditham, A.; Cava, F.; Bertozzi, CR. D-amino acid chemical reporters reveal peptidoglycan dynamics of an intracellular pathogen. *ACS Chem. Biol.*, **2013**, *8*, 500-505. doi: 10.1021/cb3004995.
11. Liang, H.; DeMeester, KE.; Hou, C.; Parent, MA.; Caplan, JL.; Grimes, CL. Metabolic labeling of the carbohydrate core in bacterial peptidoglycan and its applications. *Nat. Commun.*, **2017**, *8*, 15015. doi: 10.1038/ncomms15015.
12. Liang, L.; Astruc, D. The copper(I)-catalyzed alkyne-azide cycloaddition (CuAAC) “click” reaction and its applications. An overview. *Coord. Chem. Rev.*, **2011**, *255* (23-24), 2933-2945. doi: 10.1016/j.ccr.2011.06.028.
13. Grimes, C.L.; White, H.B. III Passing the baton: mentoring for adoption of active-learning pedagogies by research-active junior faculty. *Biochem. & Mol. Biol. Edu.*, **2015**, *43* (5), 345-357. doi: 10.1002/bmb.20885.
14. Sanders, ER. Aseptic laboratory techniques: plating methods. *J. Vis. Exp.*, **2012**, *63*, 3064-3082. doi: 10.3791/3064.

Appendix
SPECTROSCOPIC DATA

A.1 NMR

A.1.1 NMR of *p*NP Derivatives

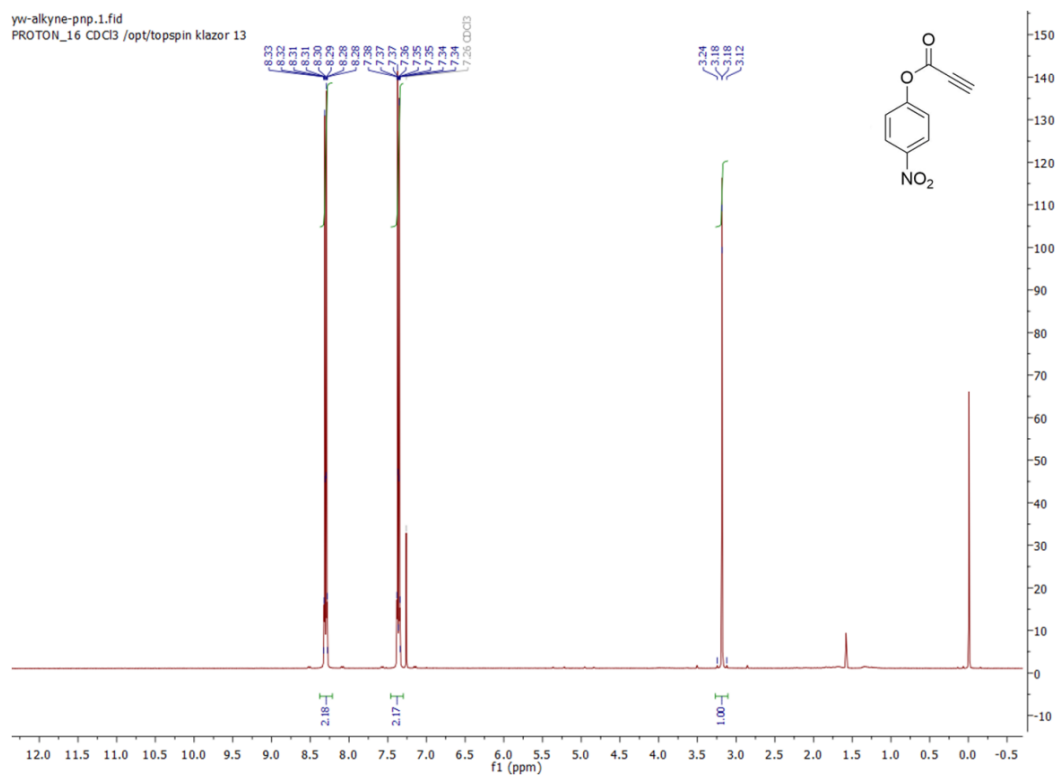


Figure A.1: ^1H NMR Spectra (CDCl_3) of *p*NP-Ak Compound (**2**). ^1H NMR (400 MHz, Chloroform-*d*) δ 8.31 (d, 2H, benzyl), 7.36 (d, 2H, benzyl), 1.55 (s, 1H, CCH).

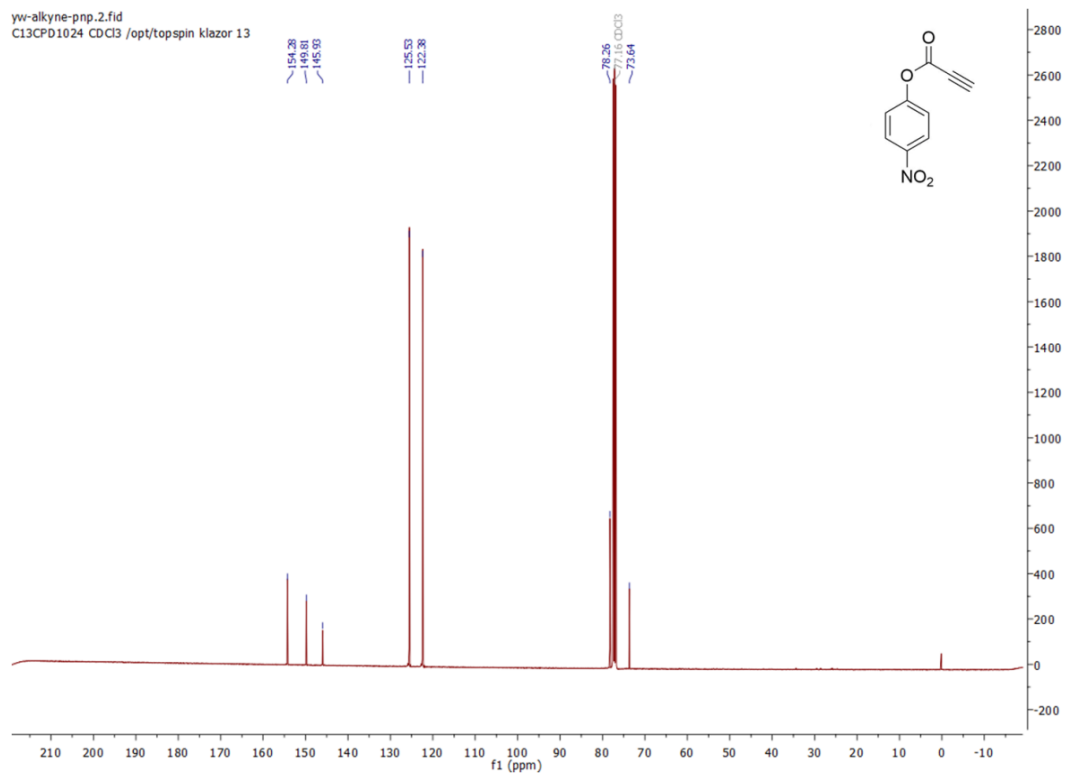


Figure A.2: ^{13}C NMR Spectra (CDCl_3) of *p*NP-Ak Compound (2). ^{13}C NMR (151 MHz, Chloroform-*d*) δ 154.38, 149.81, 145.93, 125.53, 122.38, 78.26, 73.64.

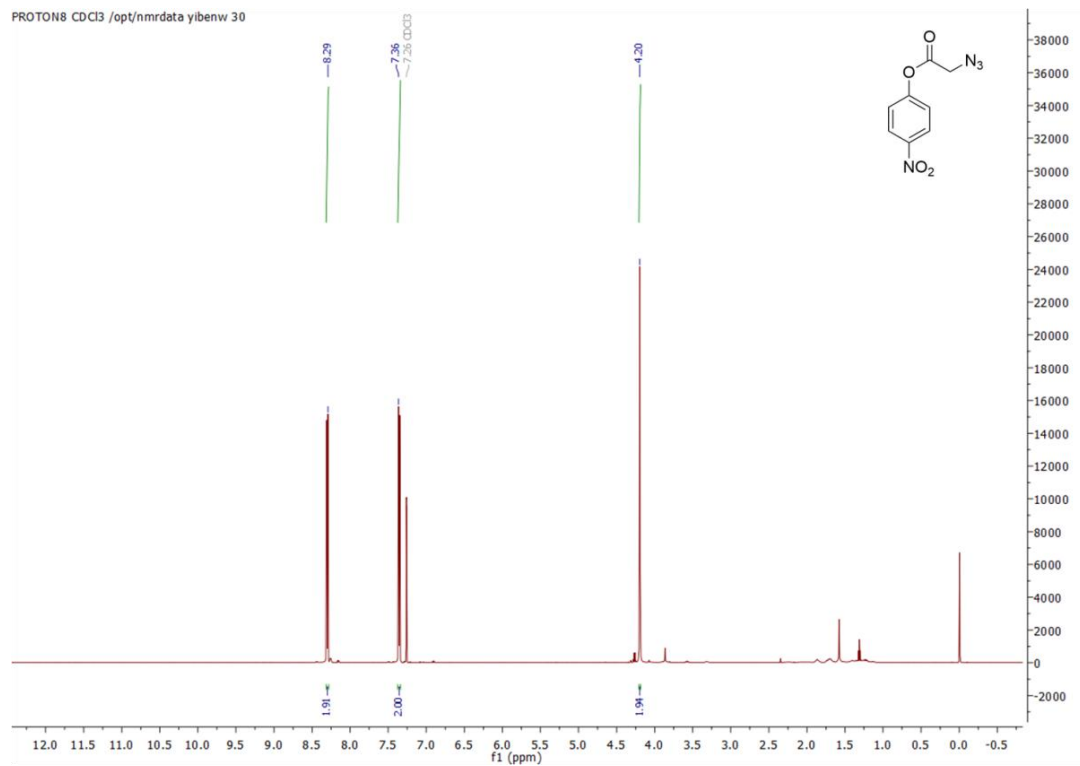


Figure A.3: ^1H NMR Spectra (CDCl_3) of *p*NP-Az Compound (**3**). ^1H NMR (400 MHz, Chloroform-*d*) δ 8.31 (d, 2H, benzyl), 7.36 (d, 2H, benzyl), 4.20 (s, 2H, CH_2N_3).

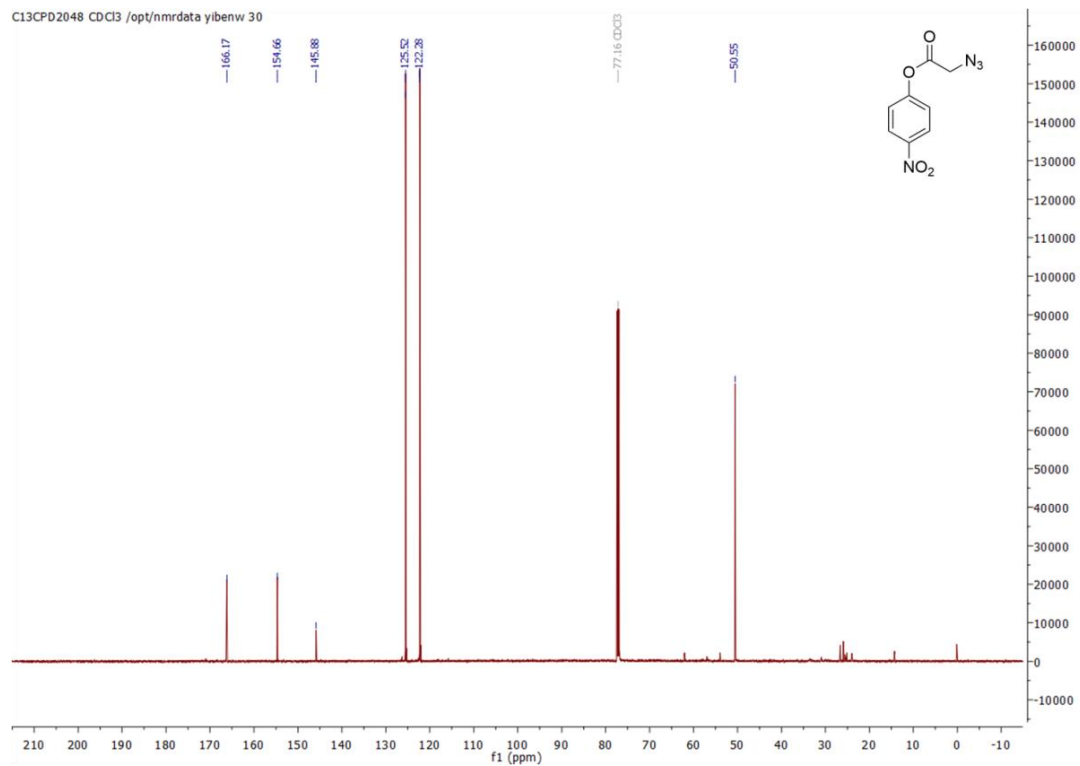


Figure A.4: ^{13}C NMR Spectra (CDCl_3) of *p*NP-Az Compound (**3**). ^{13}C NMR (151 MHz, Chloroform-*d*) δ 166.17, 154.66, 145.88, 125.52, 122.28, 50.55.

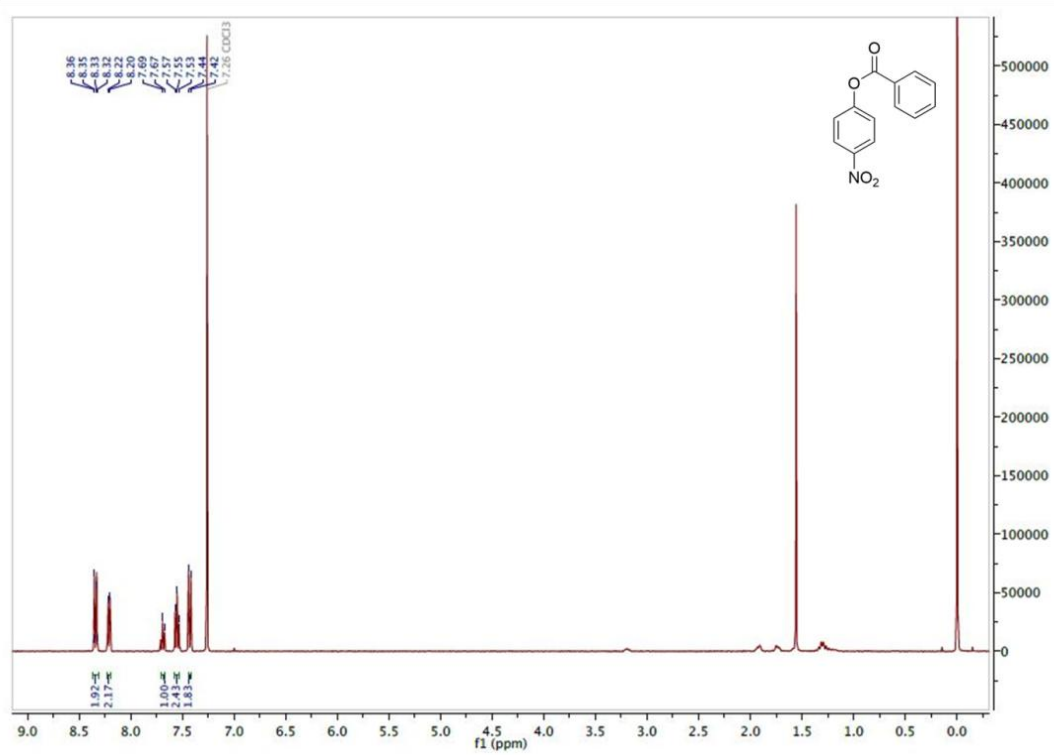


Figure A.5: ^1H NMR Spectra (CDCl_3) of *p*NP-Bn Compound (4). ^1H NMR (400 MHz, Chloroform-*d*) δ 8.35 (d, 2H, benzyl), 8.21 (d, 2H, benzyl), 7.68 (t, 1H, benzyl), 7.55 (t, 2H, benzyl), 7.43 (d, 2H, benzyl).

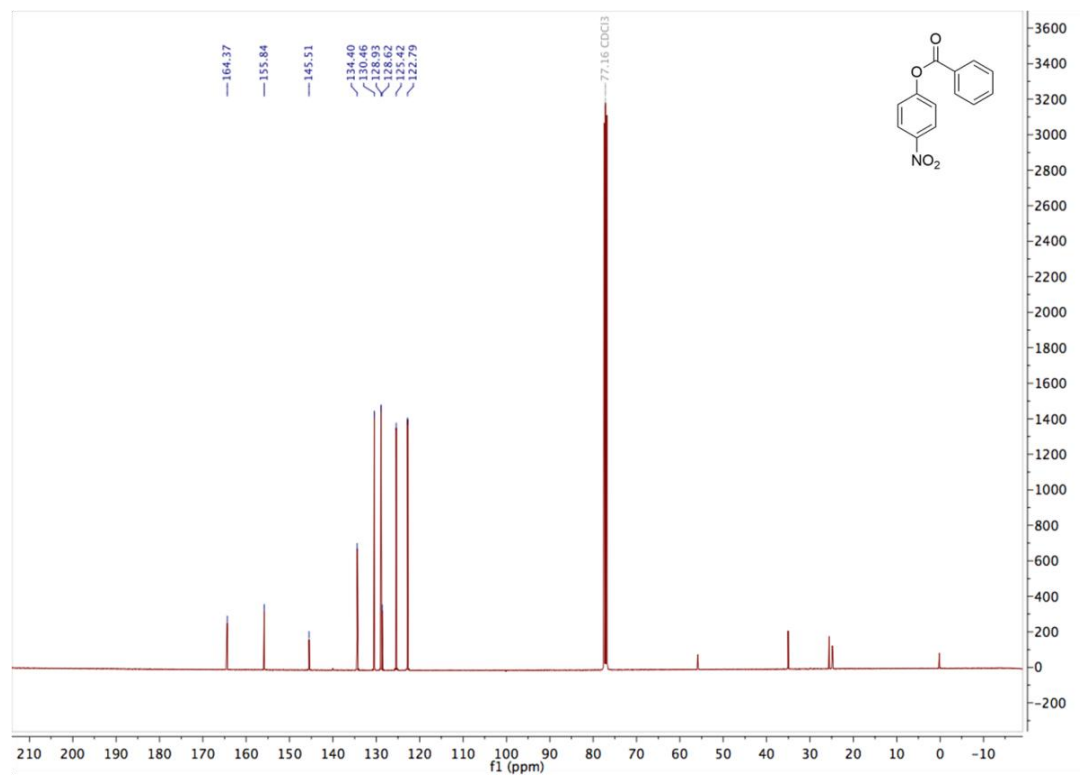


Figure A.6: ^{13}C NMR Spectra (CDCl_3) of *p*NP-Bn Compound (4). ^{13}C NMR (151 MHz, Chloroform-*d*) δ 164.37, 155.84, 145.51, 134.40, 130.46, 128.93, 128.62, 125.42, 122.79.

A.1.2 NMR of SNAc Derivatives

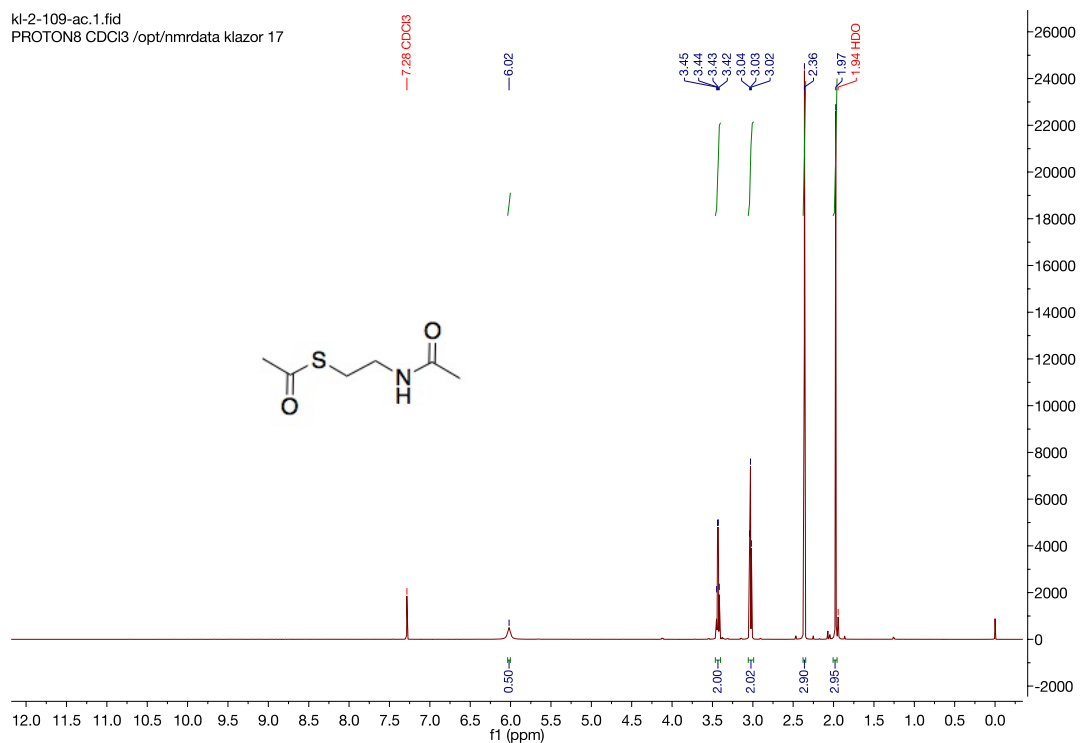


Figure A.7: ¹H NMR Spectra (CDCl₃) of SNAc Compound (6). ¹H NMR (600 MHz, Chloroform-*d*) δ 6.02 (s, 1H, NH), 3.43 (q, *J* = 6.3 Hz, 2H, CH₂NH), 3.03 (t, *J* = 6.5 Hz, 2H, CH₂S), 2.36 (s, 3H, acetyl), 1.97 (s, 3H, acetyl).

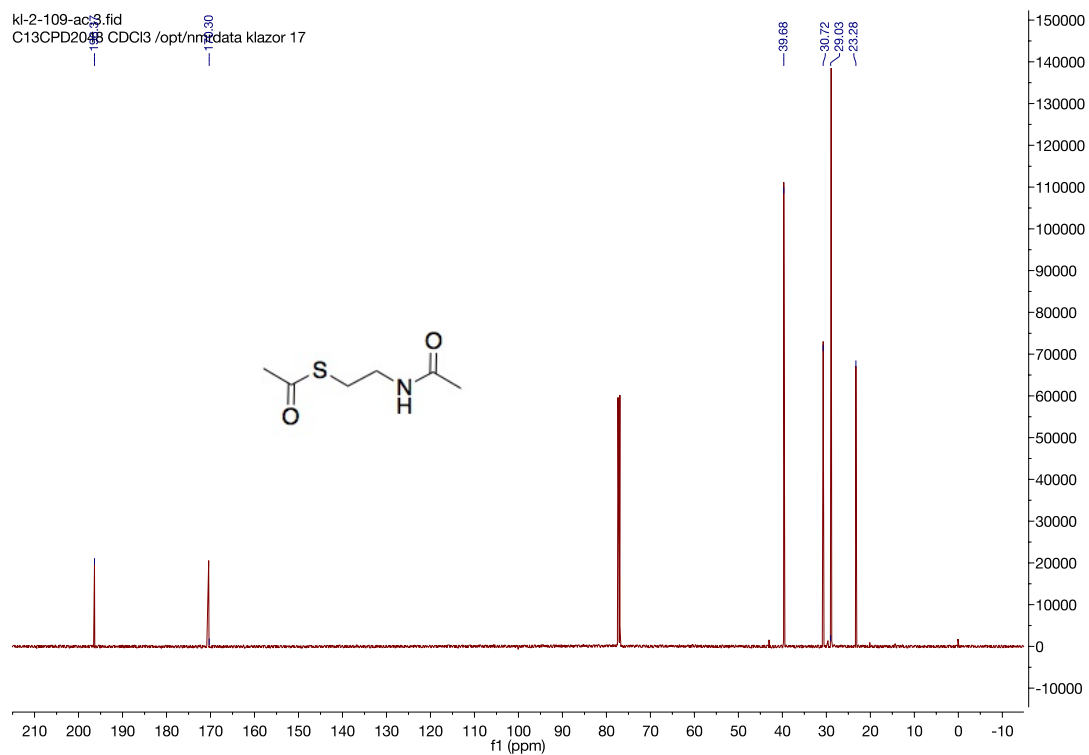


Figure A.8: ^{13}C NMR Spectra (CDCl_3) of SNAc Compound (**6**). ^{13}C NMR (151 MHz, Chloroform-*d*) δ 196.37, 170.30, 39.68, 30.72, 29.03, 23.28.

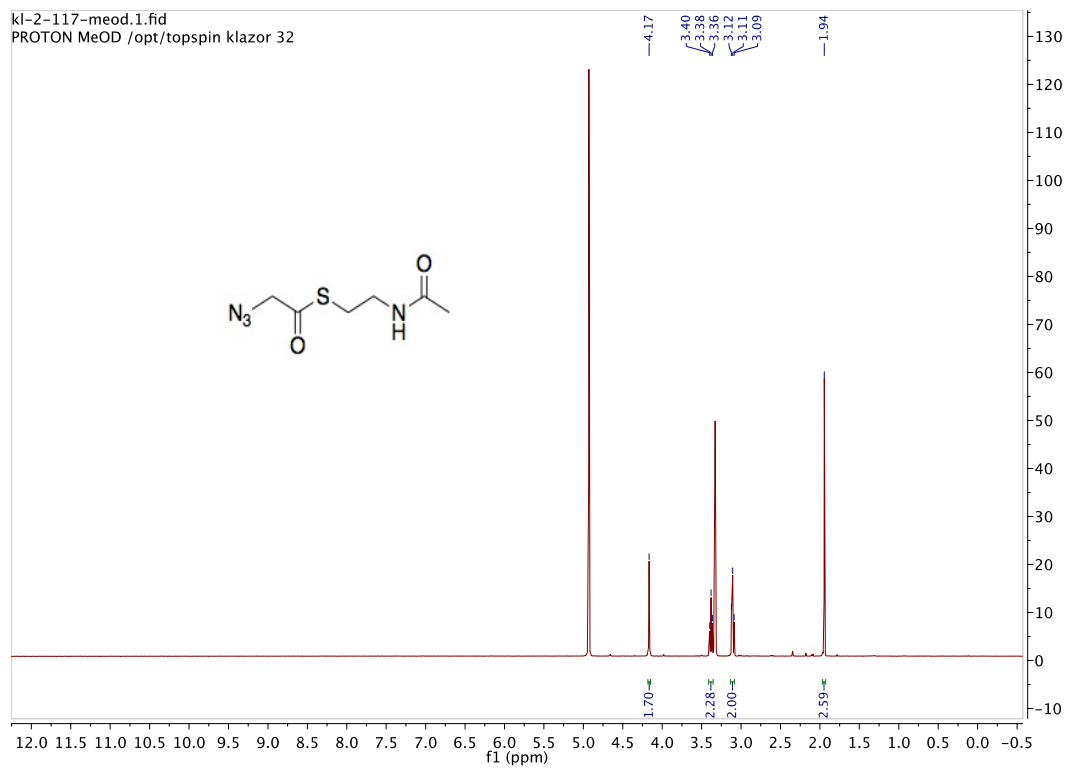


Figure A.9: ¹H NMR Spectra (MeOD) of SNaz Compound (7). ¹H NMR (400 MHz, Methanol-d₄) δ 4.15 (s, 2H, CH₂N₃), 3.37 (t, J = 6.6 Hz, 2H, HNCH₂CH₂S), 3.09 (t, J = 6.6 Hz, 2H, HNCH₂CH₂S), 1.93 (s, 3H, acetyl).

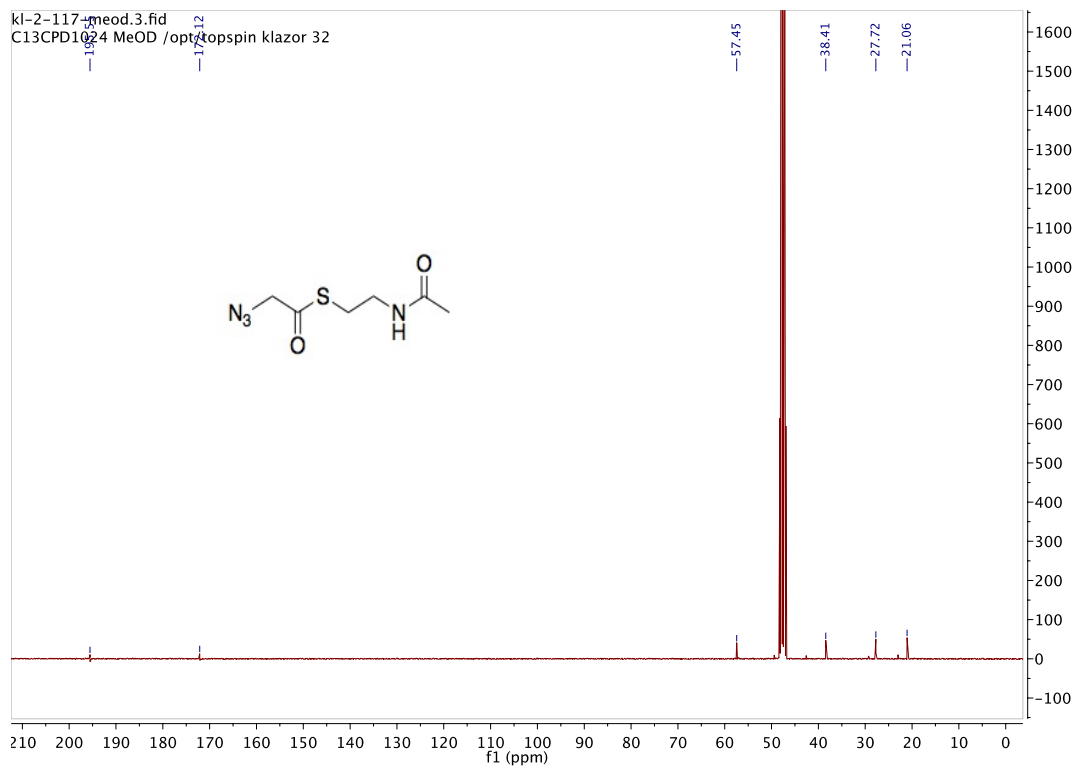


Figure A.10: ^{13}C NMR Spectra (CDCl_3) of SNAz Compound (7). ^{13}C NMR (101 MHz, Methanol- d_4) δ 195.55, 172.12, 57.45, 38.41, 27.72, 21.06.

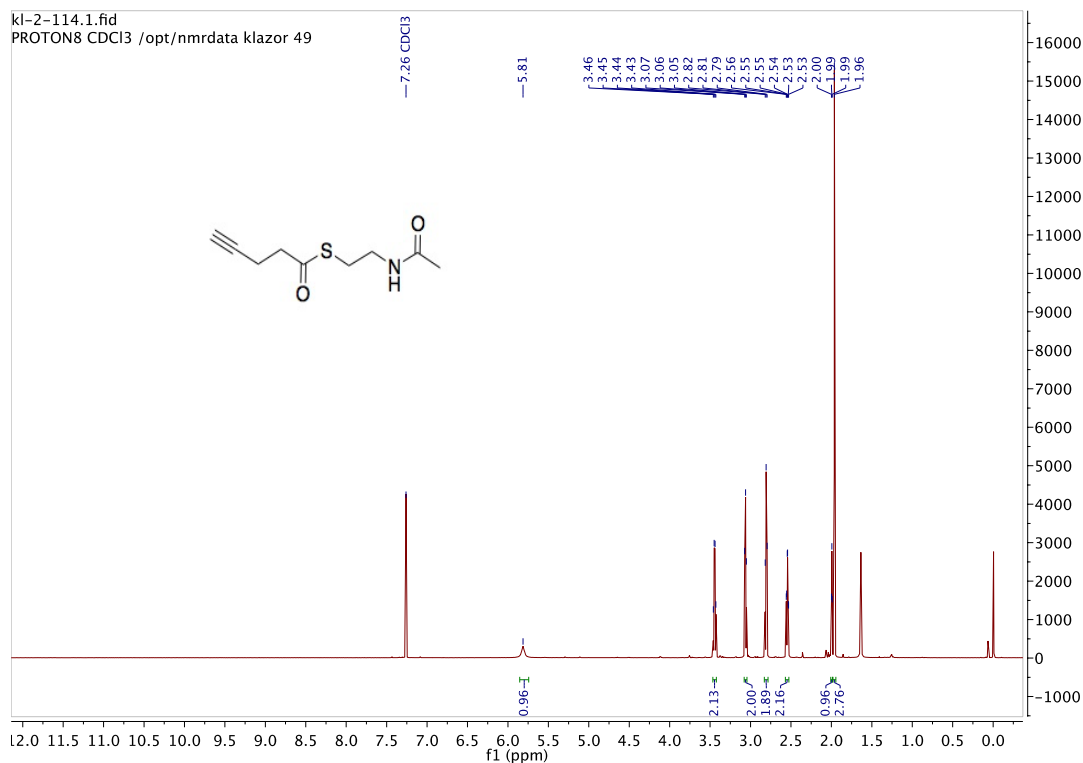


Figure A.11: ¹H NMR Spectra (CDCl₃) of SNak Compound (**8**). ¹H NMR (600 MHz, Chloroform-d) δ 5.81 (s, 1H, NH), 3.44 (q, J = 6.1 Hz, 2H, HNCH₂CH₂S), 3.06 (t, J = 6.4 Hz, 2H, HNCH₂CH₂S), 2.81 (t, J = 7.2 Hz, 2H, CH₂CH₂CCH), 2.54 (td, J = 7.2, 2.6 Hz, 2H, CH₂CH₂CCH), 1.99 (t, J = 2.6 Hz, 1H, CH₂CH₂CCH), 1.96 (s, 3H, acetyl).

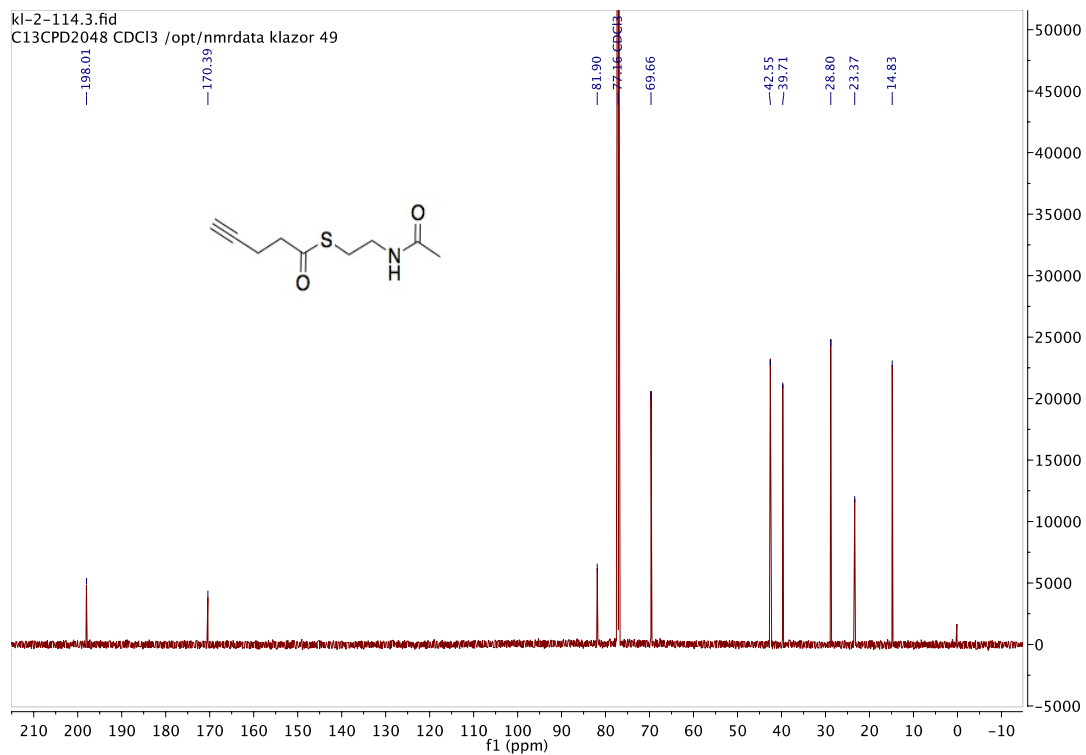


Figure A.12: ¹³C NMR Spectra (CDCl₃) of SNak Compound (8). ¹³C NMR (151 MHz, Chloroform-d) δ 198.01, 170.39, 81.90, 69.66, 42.55, 39.71, 28.80, 23.37, 14.83.

A.2 HRMS

A.2.1 HRMS of *p*NP Derivatives

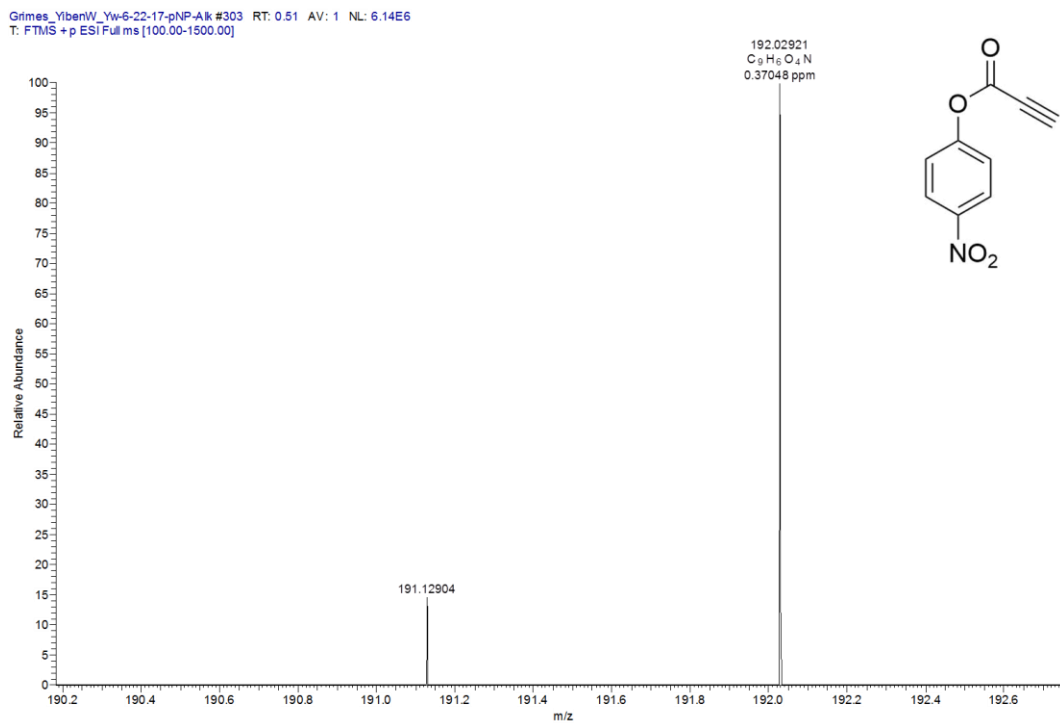


Figure A.13: HRMS Spectra of *p*NP-Ak Compound (**2**). HRMS (ESI-pos) for C₉H₆NO₄⁺ [M+H]⁺: calculated 192.02913, observed 192.02921.

Grimes_YibenW_Yw-6-22-17-pNP-Az #270 RT: 0.45 AV: 1 NL: 3.40E6
T: FTMS + p ESI Full ms [100.00-1500.00]

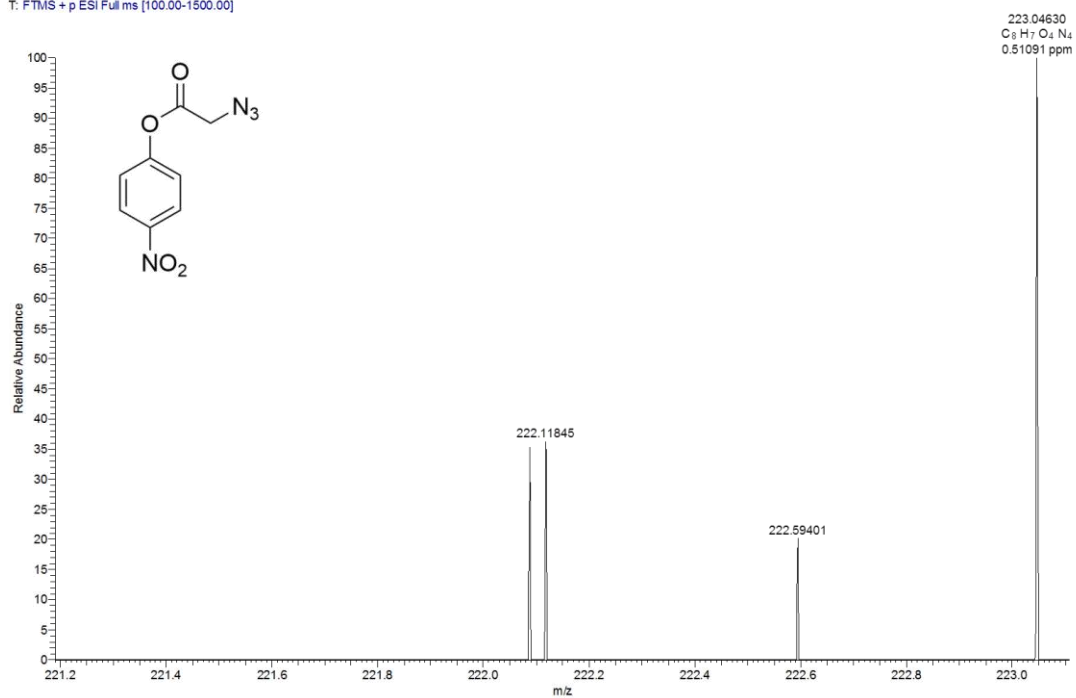


Figure A.14: HRMS Spectra of *p*NP-Az Compound (**3**). HRMS (ESI-pos) for C₈H₇N₄O₄⁺ [M+H]⁺: calculated 223.04618, observed 223.04630.

Grimes_YibenW_Yw-6-22-17-pNP-Bn#206 RT: 0.35 AV: 1 NL: 2.16E7
T: FTMS +p ESI Full ms [100.00-1500.00]

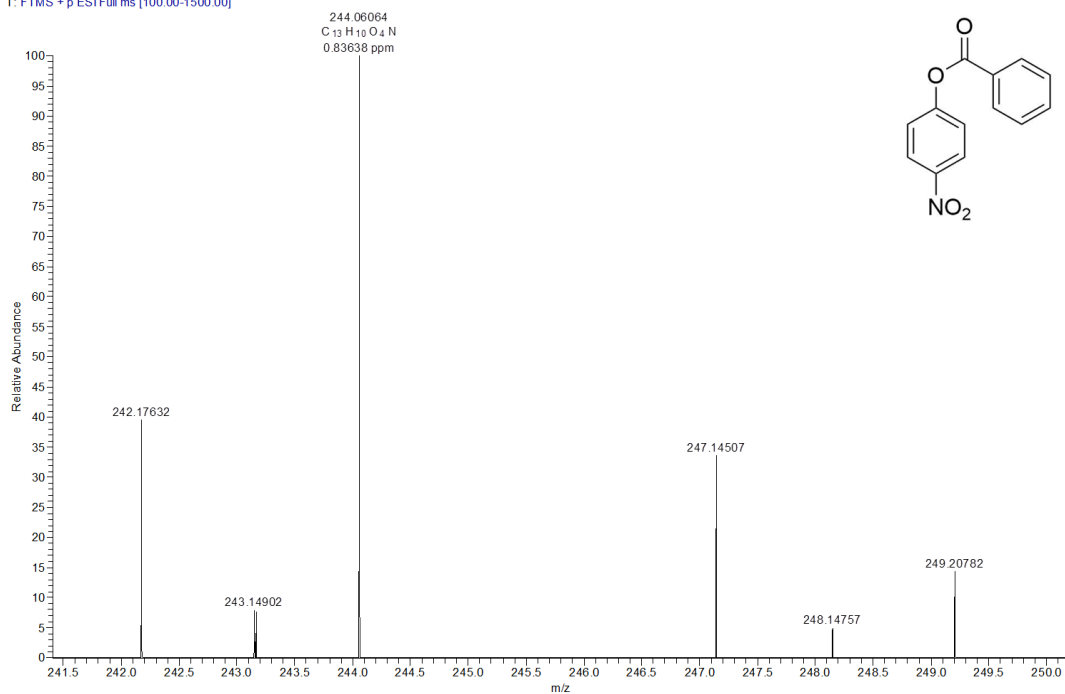


Figure A.15: HRMS Spectra of *p*NP-Bn Compound (**4**). HRMS (ESI-pos) for C₁₃H₁₀NO₄⁺ [M+H]⁺: calculated 244.06043, observed 244.06064.

A.2.2 HRMS of SNAc Derivatives

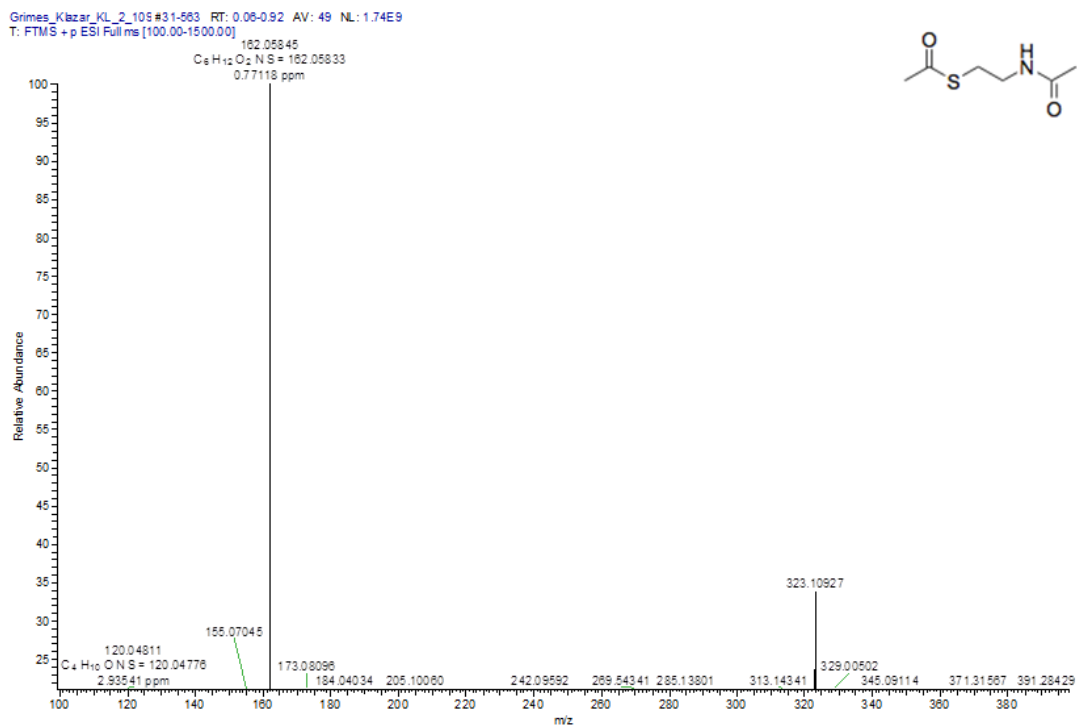


Figure A.16: HRMS of SNAc Compound (6). HRMS (ESI-pos) for $C_6H_{12}NO_2S^+$ $[M+H]^+$: calculated 162.05833, observed 162.05845.

Grimes Klare S 160826141922 #58-135 RT: 0.26-0.60 AV: 78 NL: 5.83E7
T: FTMS + p ESI/Fullms [100.00-1500.00]

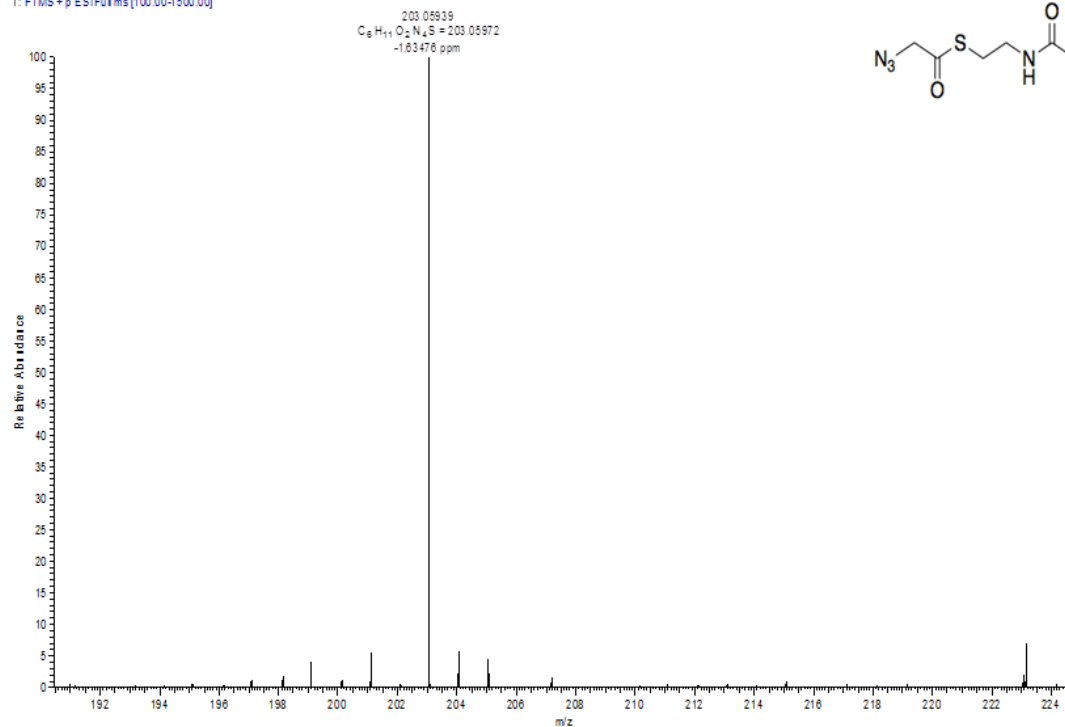


Figure A.17: HRMS Spectra of SNaz Compound (7). HRMS (ESI-pos) for C₆H₁₁N₄O₂S⁺ [M+H]⁺: calculated 203.05972, observed 203.05939.

Grimes_Klazar_XL_2_114#184-203 RT: 0.29-0.35 AV: 4 NL: 3.76E9
T: FTMS +p ESI/Full.ms [100.00-1500.00]

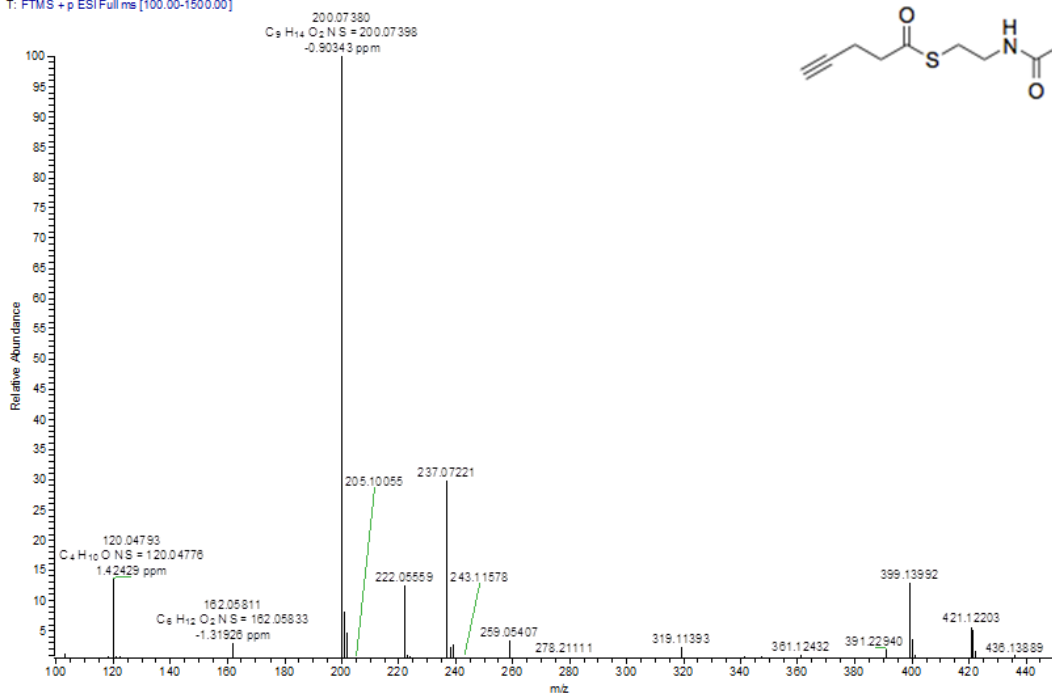
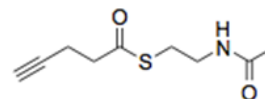


Figure A.18: HRMS Spectra of SNAk Compound (**8**). HRMS (ESI-pos) for C₉H₁₄NO₂S⁺ [M+H]⁺: calculated 200.07398, observed 200.07380.

A.3 IR

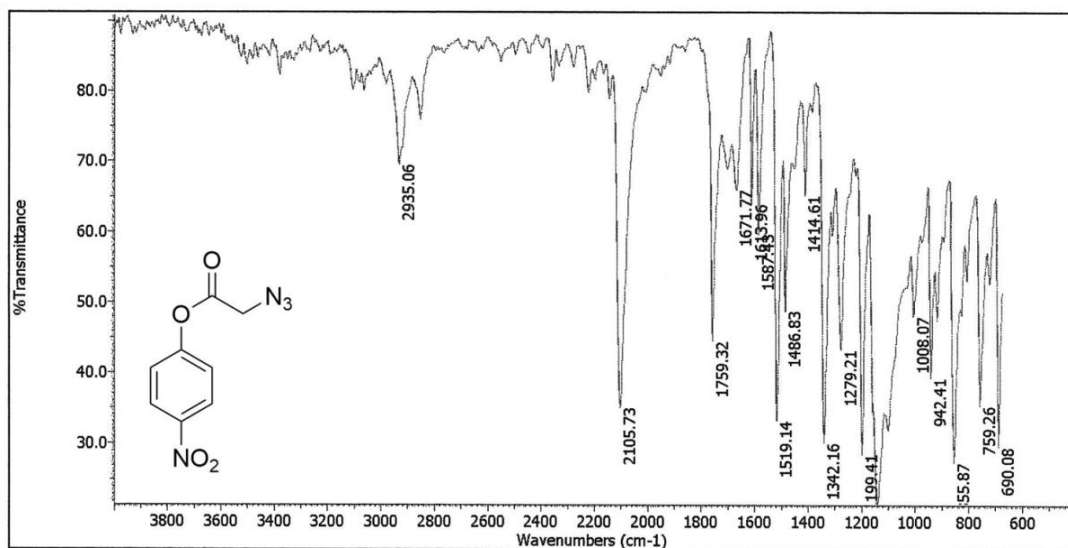


Figure A.19: IR Spectra of *p*NP-Az Compound (3). IR shift: 2105.73cm⁻¹ (Azide).

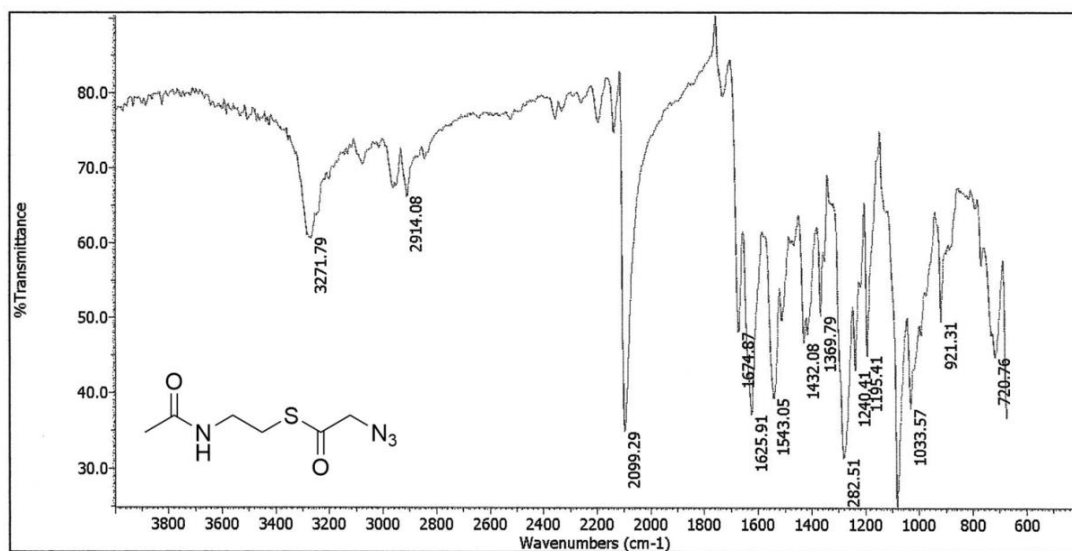


Figure A.20: IR Spectra of SNAz Compound (7). IR shift: 2099.29cm⁻¹ (Azide).